

**UNDERSTANDING THE RELATIONSHIP BETWEEN CLOT CONTRACTION  
AND PLATELET BIOLOGY UNDER HEMODYNAMIC CONDITIONS**

Kevin Timothy Trigani

A DISSERTATION

in

Chemical & Biomolecular Engineering

Presented to the Faculties of the University of Pennsylvania

in

Partial Fulfillment of the Requirements for the

Degree of Doctor of Philosophy

2022

**Supervisor of Dissertation**

Scott L. Diamond

Professor, Department of Chemical & Biomolecular Engineering

**Graduate Group Chairperson**

John C. Crocker

Professor, Department of Chemical & Biomolecular Engineering

**Dissertation Committee**

Lawrence F. Brass, Professor, Department of Medicine

Bomyi Lim, Professor, Department of Chemical & Biomolecular Engineering

Talid R. Sinno, Professor, Department of Chemical & Biomolecular Engineering

**UNDERSTANDING THE RELATIONSHIP BETWEEN CLOT CONTRACTION  
AND PLATELET BIOLOGY UNDER HEMODYNAMIC CONDITIONS**

**COPYRIGHT**

**2022**

**Kevin Timothy Trigani**



## ACKNOWLEDGMENTS

I would first like to acknowledge the invaluable contributions of my advisor, Scott Diamond. Dr. Diamond has been immensely helpful and instructive in guiding me to become a better thinker, problem solver, and scientist. His assistance and input were incredibly important to this work, and would not be possible without him. I would next like to acknowledge past and present lab members for their help over the years: Dr. Xinren Yu, Dr. Chris Verni, Dr. Jason Rossi, Dr. Jason Chen, Michael DeCortin, Yiyuan Zhang, Jennifer Crossen, and Yue Liu. I would also like to thank our lab's phlebotomist, Huiyan Jing, for assisting me in phlebotomy for all data gathered. I would like to thank my committee members as well: Dr. Lawrence Brass, Dr. Bomyi Lim, and Dr. Talid Sinno. Thank you all for your insightful comments and questions throughout this process. I would like to thank my fellow CBE classmates here at Penn and ChemBE classmates from Hopkins, for all their help along the way. Lastly, I would like to thank my friends and family, especially my parents, for their continuous support over the years. I would not have made it this far without them.

## ABSTRACT

### UNDERSTANDING THE RELATIONSHIP BETWEEN CLOT CONTRACTION AND PLATELET BIOLOGY UNDER HEMODYNAMIC CONDITIONS

Kevin Timothy Trigani

Scott L. Diamond

As thrombosis proceeds, platelets in a clot can expose phosphatidylserine (PS), providing a negatively charged surface for thrombin generation. These PS<sup>+</sup> platelets have been shown to sort to the perimeter of platelet masses via platelet contraction. However, it remains unclear how thrombin and fibrin affect PS<sup>+</sup> platelet sorting within a clot. We used an 8-channel microfluidic device to perfuse blood over collagen/TF to evaluate temporal and spatial PS<sup>+</sup> platelet sorting. We found that thrombin inhibition, fibrin polymerization inhibition, or fibrinolysis each increased clot contraction and PS sorting. Fibrin attenuated clot contraction and PS sorting. Clots without fibrin had a 3.6-times greater contraction than clots with fibrin. Based on these results, we wanted to study contraction further. We tested the effect of inhibitors of ADP and/or thromboxane A<sub>2</sub> (TXA<sub>2</sub>) signaling on clot contraction. We developed two automated imaging methods to score fluorescent platelet percent contraction: (1) “global” measurement of clot length, and (2) “local” changes in surface area coverage of platelet aggregates within the clot. Total platelet fluorescence and global aggregate contraction were highly correlated ( $R^2 = 0.87$ ). Local aggregate contraction was more pronounced than global aggregate contraction across all inhibition conditions. Conditions with TXA<sub>2</sub> inhibition were shown to significantly reduce local aggregate contraction relative to conditions without TXA<sub>2</sub>,

unlike conditions with ADP inhibition. Lastly, we recently obtained a glycoprotein VI (GPVI) inhibitor. GPVI is a collagen receptor on platelets that drives platelet activation; however, its role at later stages in clotting remains unclear. We tested the effect of anti-GPVI Fab on PS exposure, which occurs at later stages of platelet activation. On collagen/TF, Fab present at  $t=0$ s reduced PS exposure, but had no effect when added 30 or 90 seconds later. Thrombin generated via PS exposure had an important role in driving platelet deposition when Fab was present, since inhibition of PS via annexin V binding in the presence of Fab significantly inhibited platelet deposition. Our results from these studies help elucidate the relationship between platelet activation, PS exposure, fibrin, and clot contraction.

## TABLE OF CONTENTS

<b>ACKNOWLEDGMENTS.....</b>	<b>iii</b>
<b>ABSTRACT.....</b>	<b>iv</b>
<b>TABLE OF CONTENTS .....</b>	<b>vi</b>
<b>LIST OF FIGURES .....</b>	<b>viii</b>
<b>CHAPTER 1: INTRODUCTION.....</b>	<b>1</b>
1.1 Hemostasis and Thrombosis .....	1
1.2 Clot Contraction.....	2
1.3 Phosphatidylserine Exposure.....	2
1.4 Microfluidics .....	3
<b>CHAPTER 2: FIBRIN ATTENUATES PHOSPHATIDYLSERINE SORTING .....</b>	<b>4</b>
2.1 Introduction .....	4
2.2 Materials and Methods .....	7
2.3 Results .....	10
2.4 Discussion .....	24
<b>CHAPTER 3: THE ROLE OF ADP AND TXA2 IN LIMITING CONTRACTION .....</b>	<b>29</b>
3.1 Introduction .....	29
3.2 Materials and Methods .....	32
3.3 Results .....	37
3.4 Discussion .....	46
<b>CHAPTER 4: THE EFFECT OF ANTI-GPVI FAB E12 ON PLATELET DEPOSITION AND PHOSPHATIDYLSERINE EXPOSURE .....</b>	<b>51</b>

<b>4.1</b>	<b>Introduction .....</b>	<b>51</b>
<b>4.2</b>	<b>Materials and Methods .....</b>	<b>54</b>
<b>4.3</b>	<b>Results .....</b>	<b>58</b>
<b>4.4</b>	<b>Discussion .....</b>	<b>70</b>
<b>CHAPTER 5: FUTURE WORK .....</b>		<b>74</b>
<b>5.1</b>	<b>Further investigation of PS<sup>+</sup> platelet sorting in clot development .....</b>	<b>74</b>
<b>5.2</b>	<b>Evaluating the effects of secondary platelet inhibition on clot contraction.....</b>	<b>77</b>
<b>5.3</b>	<b>Further evaluation of anti-GPVI Fab E12 and the role of PS exposure in propagating platelet deposition.....</b>	<b>79</b>
<b>APPENDICES .....</b>		<b>87</b>
<b>Appendix A: Chapter 2.....</b>		<b>87</b>
<b>Appendix B: Chapter 3.....</b>		<b>99</b>
<b>Appendix C: Chapter 4.....</b>		<b>102</b>
<b>BIBLIOGRAPHY .....</b>		<b>107</b>

## LIST OF FIGURES

Figure 2-1. Inhibition of thrombin enhances PS sorting. ....	11
Figure 2-2. Inhibition of fibrin polymerization enhances PS exposure and sorting. ....	13
Figure 2-3. Fibrinolysis enhances PS sorting. ....	15
Figure 2-4. PS sorting is enhanced in the absence of procoagulant conditions (no TF)...	17
Figure 2-5. PS sorting correlates with contraction, and correlates inversely with fibrin FI. .....	19
Figure 2-6. Extent of PS sorting and % contraction is consistent across similar fibrin conditions. ....	20
Figure 2-7. Pearson correlation coefficient measures PS temporal sorting and autocorrelation metric measures PS spatial sorting. ....	22
Figure 3-1. ASA, 2-MeSAMP, and MRS-2179 have an additive effect on limiting platelet deposition, but do not have an additive effect on limiting P-selectin display. ....	37
Figure 3-2. Quantitative fluorescence data from Figure 3-1. ....	38
Figure 3-3. P-selectin+ platelets have limited global and local contraction; ASA, 2- MeSAMP, and MRS-2179 have a limiting effect on global platelet contraction, while only ASA limits local platelet contraction. ....	40
Figure 3-4. Platelet fluorescence correlates with global contraction. ....	43
Figure 3-5. ASA limits local platelet contraction, while 2-MeSAMP and MRS-2179 have no effect. ....	45
Figure 3-6. Schematic of clot development and contractile processes under control conditions (A) and with ADP/TXA2 inhibitors present (B). ....	46
Figure 4-1. Inhibition of GPVI shows significant decrease in PS exposure. ....	58
Figure 4-2. Decrease in annexin V in the presence of anti-GPVI is due from anti-GPVI, not limited platelet deposition or fibrin polymerization. ....	60
Figure 4-3. Effects of anti-GPVI Fab require its presence from the initiation of clot development in the presence of thrombin. ....	62
Figure 4-4. Effects of anti-GPVI Fab on clot development are reversible. ....	64
Figure 4-5. Annexin V and anti-GPVI Fab have additive effect on limiting platelet deposition. ....	67

Figure 4-6. Representative 3D images of clot end point.....	69
Figure 5-1. Pearson correlation coefficients of annexin V fluorescence between final clot image (at 15 minutes) and clot image at varying time points among all conditions tested. ....	75
Figure 5-2. Time-sequential inhibition of thrombin demonstrated varying anti-GPVI potency on platelet deposition and fibrin deposition. ....	79
Figure 5-3. Time-sequential addition of annexin V in the presence of anti-GPVI had little effect on platelet deposition or PS exposure, but a minimal effect on fibrin deposition. .	83
Figure 5-4. Annexin V has a slight inhibitory effect on fibrin deposition. ....	85

## **CHAPTER 1: INTRODUCTION**

### **1.1 Hemostasis and Thrombosis**

When a blood vessel in the body is disrupted, hemostasis occurs to prevent blood loss. Hemostasis involves a number of elements, including platelets, fibrin, fibrinogen, von Willebrand factor (vWF), and thrombin, among others. Collagen becomes exposed when the endothelial layer of a vessel is disrupted. This initial collagen exposure triggers platelets in a nascent state to become activated near the site of injury, where they can begin to bind. As platelets bind to collagen, they can send signals to other nearby platelets to begin to activate and bind as well, causing a platelet plug to form.

As platelets become activated and aggregate, coagulation also begins to occur. Coagulation is the process by which fibrin forms. There are two pathways by which fibrin can form: (1) intrinsic/contact activation pathway, or (2) extrinsic/tissue factor pathway. With intrinsic pathway coagulation, Factor XII can be activated through contact with a variety of different negatively charged surfaces or molecules, which leads to a cascade of reactions that results in the conversion of prothrombin to thrombin. Upon thrombin formation, soluble fibrinogen is converted to insoluble fibrin, which then becomes cross-linked to form polymerized fibrin. Another pathway exists to form fibrin, whereby exposure to tissue factor (TF) leads to activation of Factor X, which converts prothrombin to thrombin, eventually leading to fibrin polymerization. Together, platelets and fibrin limit blood loss from a disrupted or injured vessel.



Under normal conditions, hemostasis allows for the correct balance of pro-coagulant and anti-coagulant forces. This balance allows for blood loss to be limited when a blood vessel is injured or disrupted; it also helps to prevent unwanted or excessive blood clotting. When hemostasis is no longer maintained due from excessive pro-coagulant forces, thrombosis occurs. Thrombosis leads to increased clot embolization and vessel occlusion, which can result in a number of clinical complications, including myocardial infarction or ischemic stroke. Gaining a deeper understanding of this delicate balance in blood clotting is important to better treat different complex clinical conditions.

## **1.2 Clot Contraction**

In the final stages of hemostasis, aggregated platelets and polymerized fibrin in the clot begin to contract. The process of clot contraction is quite complex and involves a number of components within the blood clot: platelets, fibrinogen, fibrin, red blood cells (RBCs), vWF, among others. Contraction reduces the physical space and gaps within a blood clot, preventing blood loss and allowing for the restoration of blood flow [1–5]. Contraction ultimately leads to clot resolution, which ensures that normal blood flow is restored in the vessel. In cases where contraction is limited or does not occur properly, there can be an increased risk of bleeding [6].

## **1.3 Phosphatidylserine Exposure**

When platelets bind to collagen, they begin to activate and change in a number of different ways: physical shape change, integrin activation, granule secretion, and exposure of phospholipids [7]. One such phospholipid that can be exposed upon platelet

activation is phosphatidylserine (PS). At rest, PS is normally found on the inside of the platelet membrane, but upon activation, PS can be exposed to the outer membrane surface [8]. An enzyme called TMEM16F facilitates the externalization of PS, where it provides a negatively charged surface for tenase and prothrombinase complexes to assemble to assist in the formation of Factor X and thrombin, respectively [9]. When there is a mutation in TMEM16F, a condition called Scott Syndrome can occur, which can lead to mild bleeding [9–11].

#### **1.4 Microfluidics**

Blood clotting is often studied under static conditions, and studies can use an altered blood composition (e.g. platelet-rich plasma, platelet-poor plasma, etc.) to evaluate hemostatic or thrombotic behavior. While these studies can be insightful, they do not seek to mimic conditions present in the body; and while in vivo mice experiments can provide useful insight into the in vivo dynamics of blood clotting, mouse blood clotting components are not identical to human clotting components [12]. Our lab has designed an 8-channel microfluidic device that can evaluate 8 independent conditions in human whole blood clotting under shear flow [13,14]. We can control for extrinsic or intrinsic coagulation by patterning collagen  $\pm$  TF. We can run experiments at a wide range of shear rates, including arterial or venous shear rates. Fluorophores can be added to blood to study different components (e.g. platelets, fibrin, P-selectin, etc.), where we use epifluorescence microscopy to record images at different time points throughout the experiment.

## CHAPTER 2: FIBRIN ATTENUATES PHOSPHATIDYLSERINE SORTING

### 2.1 Introduction

Platelet adhesion and deposition are primary hemostatic events that allow engagement of the coagulation cascade (secondary hemostasis). Upon adhering to collagen, platelet activation via GPVI signaling drives ADP release, thromboxane synthesis, and integrin  $\alpha_{IIb}\beta_3$  activation. Tissue factor (TF) can drive thrombin and fibrin generation via the extrinsic pathway, which is propagated by coagulation factors that are bound to phosphatidylserine-positive (PS<sup>+</sup>) platelets [15]. Continued clot growth requires fibrinogen- $\alpha_{IIb}\beta_3$  cross bridging of platelets.

Platelets in clots can display heterogeneous traits during clot development, as detected by P-selectin display in the core/shell model of hemostasis [16–18]. PS exposure is also a differentiating factor between platelet subpopulations [17]. In procoagulant platelets experiencing sustained calcium mobilization, PS is externalized from the inner leaflet of the platelet membrane to the outer leaflet via scramblases. PS provides a surface for thrombin generation that is supportive of thrombosis [19,20]. PS<sup>+</sup> platelets have been shown to exhibit ballooning and procoagulant spreading [21], as well as colocalization of coagulation factors that promote a rapid increase in thrombin formation [22,23].

Once platelets are activated, enzymes like TMEM16F induce the externalization of PS from the inner leaflet to the outer leaflet of the platelet membrane [9]. Externalization of PS is significantly decreased in Scott syndrome patients, as a result of a mutation in TMEM16F [9–11]. Patients with Scott syndrome experience a mild

bleeding phenotype, which points to the importance of PS exposure in helping to facilitate coagulation. Baig, et al. [10] used a TMEM16F knockout mouse model to show that TMEM16F is critical for PS exposure, although residual PS on knockout platelets suggested there may be other mechanisms for PS exposure. Activated platelets are less efficient at externalizing PS under static conditions, suggesting shear forces play an important role in PS exposure [19,24]. PS-exposing platelets display low levels of  $\alpha_{IIb}\beta_3$  in the activated conformation [25]. Upon initial stimulation by GPVI,  $\alpha_{IIb}\beta_3$  is activated in platelets, but only PS-exposing platelets display pronounced inactivation of  $\alpha_{IIb}\beta_3$  [25–27].

Understanding the distribution of PS on platelets in a growing thrombus has been a subject of several studies. Munnix, et al. [27] first demonstrated a ring of PS<sup>+</sup> platelets at the base of a platelet deposit. They found human blood perfused at 1000 s<sup>-1</sup> over collagen in the presence of TF/CaCl<sub>2</sub> resulted in a heterogeneous distribution of annexin V around the periphery of CD61<sup>+</sup> platelets from the initial phases of thrombus formation, although it remained unclear the mechanism for this ring-like structure. To elucidate this phenomenon, Nechipurenko, et al. [28] showed that procoagulant platelets, rich in PS, formed a ring-like structure around contracted thrombi and often colocalized with fibrin. They used non-muscle myosin-deficient mouse blood to show that when contraction is inhibited, a ring of PS<sup>+</sup> platelets does not form around the platelet mass, concluding that contraction drives PS<sup>+</sup> platelets to the periphery of clots.

Although fibrin contributes to contraction through its interaction with platelets, fibrin's physical limitation on contraction has been supported by recent in vitro and in

vivo studies. Chen, et al. [29] developed a microfluidic system to evaluate dynamics of thrombus formation under shear flow. One of their findings was that while fibrin contributes to clot formation and stabilization, clot contraction is due primarily from contractile forces generated by activated platelets and transmitted between platelets and collagen. Samson, et al. [30] found that blocking endogenous fibrinolysis in vivo reduced clot contraction. In their model, fibrin contributes to clot rigidity; fibrinolysis decreases the amount of fibrin polymers and thus decreases rigidity, resulting in enhanced clot contraction.

Here, we investigated how inhibition of the coagulation cascade in several different conditions alters PS exposure and distribution in clot formation. We used a microfluidic device to perfuse whole blood (WB) at physiological shear rates to evaluate PS distribution during clot development. In this assay, we refer to a clot as the entire area covered by the collagen strip, which subsequently includes numerous platelet masses. Temporal and spatial sorting of PS<sup>+</sup> platelets were evaluated using a Pearson correlation coefficient and an autocorrelation metric, respectively. We found that the absence of fibrin within a clot enhanced PS<sup>+</sup> platelet sorting (also referred to as PS sorting) to the periphery of platelet masses. Conversely, the presence of fibrin attenuated PS sorting, as the PS distribution within the clot was more homogeneous by comparison. These findings demonstrate that fibrin attenuates contraction and reduces the spatial sorting of PS<sup>+</sup> platelets during human WB clotting under flow.

## **2.2 Materials and Methods**

### **Reagents and materials, blood collection, and preparation of collagen/TF on glass slides**

See Supplemental Methods for reagents and materials. Blood collection and collagen/TF preparation has been previously described [13,14]. Blood collection protocol and preparation of collagen/TF on glass slides are included in the Supplemental Methods.

### **8-channel microfluidic device experiments**

After collagen/TF was patterned, an 8-channel device was placed over the collagen strip and vacuum-sealed. Each channel in the device had a width of 250  $\mu\text{m}$  and a height of 120  $\mu\text{m}$ . Then 35  $\mu\text{L}$  of 0.5% bovine serum albumin (BSA) was added to each of the 8 wells and perfused through each of the corresponding channels. After blood collection, fluorophores were added: CD61 (platelets), fluorescent fibrinogen (fibrin), and annexin V (PS). In control studies, we found that annexin V had a slightly inhibitory effect on fibrin formation, but significant fibrin formation still occurred when annexin V was present (Supp. Fig. S2-1). Then any agonists or controls were added (controls in each experiment were 0.5% BSA of the same volume as the agonist); blood was then loaded to each of the wells. A syringe with a fixed rate perfused the blood through the channels to induce blood flow through the device. The syringes used were 1000  $\mu\text{L}$  syringes (Hamilton Co., Reno, Nevada), and the syringe pump (Harvard PHD 2000; Harvard Apparatus, Holliston, MA) was set to 24  $\mu\text{L}/\text{min}$  for experiments done at venous shear rate ( $100 \text{ s}^{-1}$ ). Blood was perfused through the device for 15 minutes. The epifluorescence

microscope (Olympus Ix81; Olympus America Inc, Central Valley, PA) captured individual time frames at chosen locations with chosen wavelengths.

### **Contraction measurements**

Contraction was measured as a percent based on clot length during the course of an experiment (Supp. Fig. S2-2). The clot length was measured by drawing a line (parallel to the direction of flow) down the center of the clot. Initial clot lengths were measured at 9 minutes and final clot lengths were measured at 15 minutes. Percent contraction was calculated as the difference between the initial and final clot lengths divided by the initial clot length. Percent contraction measurements were made for multiple clots for each condition, and the average was taken as the percent contraction.

### **Autocorrelation metric calculations for PS spatial sorting**

To evaluate the differences in spatial distribution of PS at the end of experiments, we developed an autocorrelation metric to quantify the extent of sorting of annexin V fluorescence. Using the Matlab function “xcorr2,” we calculated the 2D autocorrelation of an annexin V image of a clot. For an input matrix of size  $n \times n$ , the “xcorr2” function output an autocorrelation matrix of size  $(2n-1) \times (2n-1)$ . In order to calculate each of the values in the autocorrelation matrix, the matrix was overlaid with itself in all possible orientations. The elements of the overlaid matrices were then multiplied element by element and the summation was input into the autocorrelation matrix in the corresponding location to the matrix overlay. Thus, the center of the autocorrelation matrix had the highest value because the center corresponds to a perfect overlay of the

matrix with itself. The autocorrelation matrix was then normalized to 1 by dividing every matrix element by the maximum value in the matrix in order to eliminate any effects from differences in fluorescence intensity (FI) between images. Next, since the meaningful autocorrelation data was close to the center of the autocorrelation matrix, we truncated the autocorrelation matrix to 20 pixels in each direction from the center pixel, resulting in a 41 x 41 matrix. Truncating or cropping are commonly used in image correlation spectroscopy when evaluating 2D autocorrelation matrices in order to better fit the autocorrelation data to a Gaussian function [31–34]. Supplemental Figure S2-3 illustrates this matrix truncation. Lastly, the absolute value of the elements of this final matrix were summed to give the autocorrelation metric. Example images (synthetic and real) with corresponding autocorrelation metric values are illustrated in Supplemental Figure S2-4.

### **Pearson correlation coefficient calculations for PS temporal sorting**

To evaluate temporal changes in PS distribution, Pearson correlation coefficients were calculated for annexin V images at 9 minutes and 15 minutes. The Pearson correlation coefficient is commonly used to measure the degree of correlation between two images by comparing them pixel by pixel [27,35,36]. We wanted to compare the annexin V distribution between an early time point and the final time point of 15 minutes. For the early time point, we chose 9 minutes as an intermediary time point that was not too early for insufficient annexin V fluorescence, but not too late that the comparison to the 15-minute image would be similar regardless of the condition. Supplemental Figure S2-5 provides example images (synthetic and real) with corresponding Pearson



correlation coefficients. Images were first transferred into Matlab as pixel values in a matrix. The Matlab function “corr2” was used to calculate the Pearson correlation coefficient between the two matrices of pixel values, given by the following equation:

$$R = \frac{\sum_{i=1}^n (x_i - \bar{x})(y_i - \bar{y})}{\sqrt{\sum_{i=1}^n (x_i - \bar{x})^2} \sqrt{\sum_{i=1}^n (y_i - \bar{y})^2}}$$

Where  $x_i$  and  $y_i$  are pixel values at location  $i$  for annexin V images at 9 minutes and 15 minutes, respectively, and  $\bar{x}$  and  $\bar{y}$  are the average FIs for images at 9 minutes and 15 minutes, respectively.

## 2.3 Results

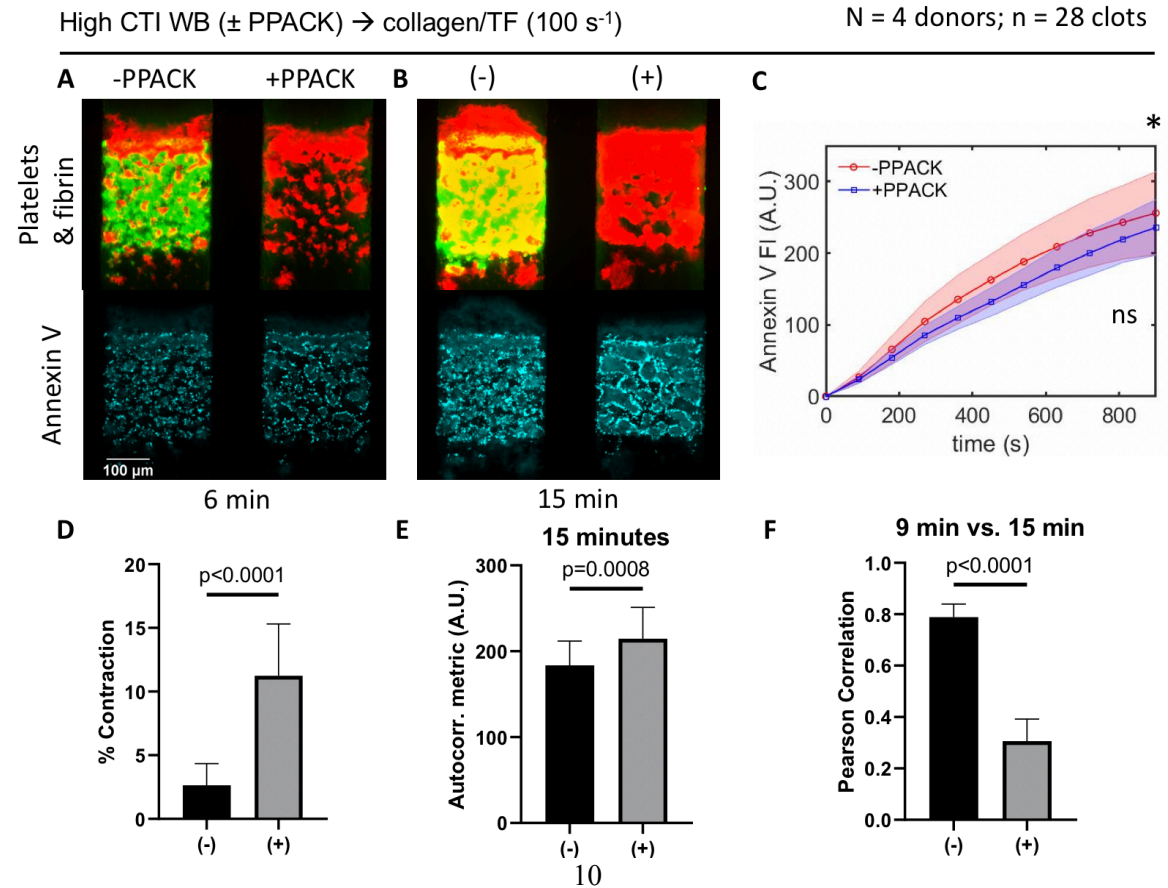


**Figure 2-1. Inhibition of thrombin enhances PS sorting.**

High CTI WB was perfused with and without PPACK over collagen/TF at an initial shear rate of  $100\text{s}^{-1}$ . CD61, fluorescent fibrinogen, and annexin V were added to stain for platelets, fibrin, and PS, respectively. Images of clots were taken in 90-second intervals for 15 minutes; example images are illustrated at 6 minutes (A) and 15 minutes (B) of CD61 (red), fluorescent fibrinogen (green), and annexin V (cyan). Annexin V FI was measured during the course of the experiment as average FI  $\pm$  standard deviation (C). Contraction was measured as % contraction between 9 and 15 minutes in clots (D). An autocorrelation metric was calculated for the final (15-minute) annexin V image for each clot as a measure of PS spatial sorting (E). The Pearson correlation coefficient was calculated between 9- and 15-minute annexin V images for each clot as a measure of PS temporal sorting (F). Data are from 4 different donors (N=4) and 28 individual clots (n=28). A.U. = arbitrary units

**Inhibition of thrombin enhances PS sorting**

We evaluated PS distribution in CTI-treated whole blood (WB)  $\pm$  PPACK perfused over collagen/TF. Phe-Pro-Arg-chloromethylketone (PPACK) is a potent thrombin inhibitor [37]. As expected, no significant fibrin formation occurred in the +PPACK channels, while fibrin formed in the control (no PPACK) channels (Fig. 2-1A and B, upper panels; Supp. Fig. S2-6). Platelet images in both  $\pm$ PPACK channels were similar in morphology (Fig. 2-1A and B, upper panels) and FI (Supp. Fig. S2-6). Annexin V distribution at early time points in both  $\pm$ PPACK channels was similar (Fig. 2-1A lower panel). However, at 15 minutes, the annexin V distribution changed morphologically, with enhanced PS sorting in the +PPACK channels compared to the control channels (Fig. 2-1B lower panel). Annexin V FI was similar between both conditions throughout the experiment (Fig. 2-1C). Contraction was significantly more pronounced ( $p < 0.0001$ ) in the +PPACK condition than in the control (Fig. 2-1D), showing fibrin limits clot contraction.

We evaluated both the temporal changes of PS distribution within clots, as well as differences in final PS spatial distribution between  $\pm$ PPACK conditions. We used an

autocorrelation metric to evaluate the extent of PS spatial sorting at the final time point in both conditions. Greater autocorrelation values correspond to greater PS spatial sorting, while smaller values correspond to less PS spatial sorting (Supp. Fig. S2-4). We found that +PPACK channels had a significantly greater autocorrelation metric than -PPACK channels ( $p = 0.0008$ ; Fig. 2-1E). We measured PS temporal sorting using the Pearson correlation coefficient between annexin V images at 9 minutes and 15 minutes (Supp. Fig. S2-5). Higher Pearson correlation coefficients indicate more similar images, which correspond to less PS temporal sorting. Conversely, lower Pearson correlation coefficients indicate less similar distributions, which correspond to more PS temporal sorting. We found that +PPACK had a significantly lower Pearson correlation coefficient than the control (0.31 and 0.79, respectively; Fig. 2-1F), indicating more PS temporal sorting in the absence of fibrin.

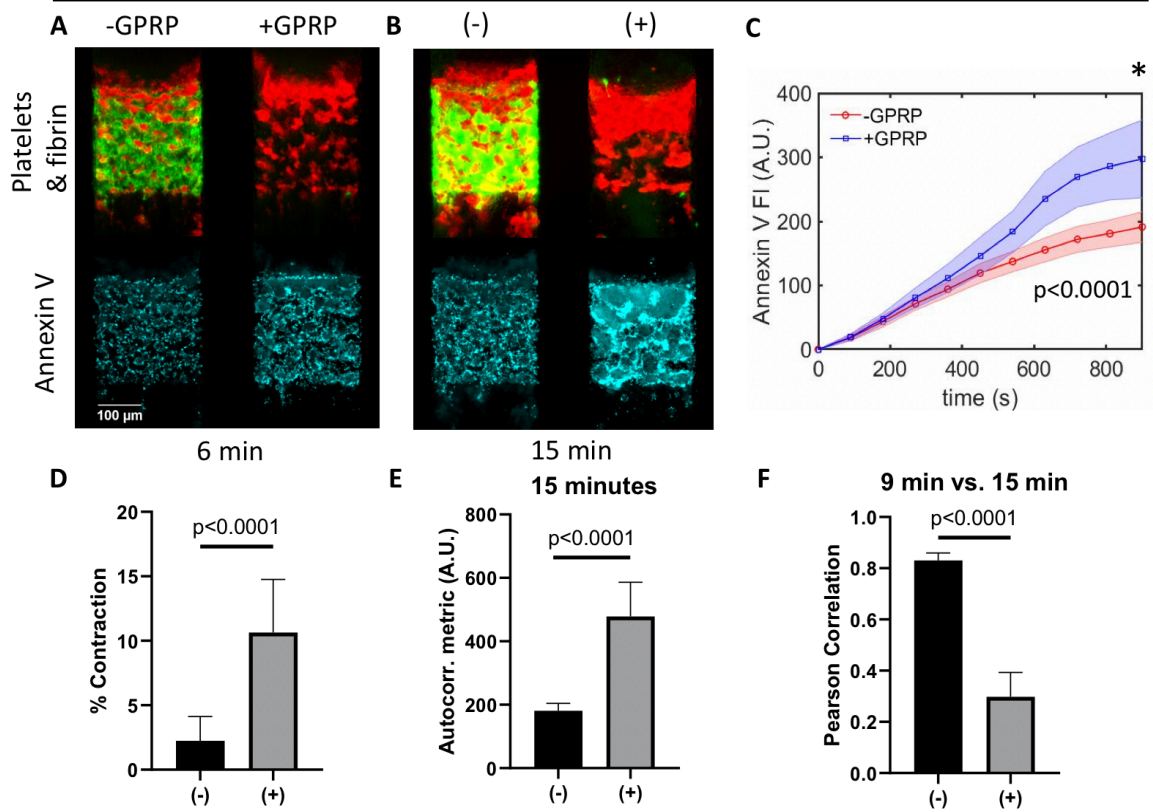


**Figure 2-2. Inhibition of fibrin polymerization enhances PS exposure and sorting.**

High CTI WB was perfused with and without GPRP over collagen/TF at an initial shear rate of  $100 \text{ s}^{-1}$ . CD61, fluorescent fibrinogen, and annexin V were added to stain for platelets, fibrin, and PS, respectively. Images of clots were taken in 90-second intervals for 15 minutes; example images are illustrated at 6 minutes (A) and 15 minutes (B) of CD61 (red), fluorescent fibrinogen (green), and annexin V (cyan). Annexin V FI was measured during the course of the experiment as average FI  $\pm$  standard deviation (C). Contraction was measured as % contraction between 9 and 15 minutes in clots (D). An autocorrelation metric was calculated for the final (15-minute) annexin V image for each clot as a measure of PS spatial sorting (E). The Pearson correlation coefficient was calculated between 9- and 15-minute annexin V images for each clot as a measure of PS temporal sorting (F). Data are from 3 different donors (N=3) and 21 individual clots (n=21). A.U. = arbitrary units

### Inhibition of fibrin polymerization enhances PS exposure and sorting

Since PPACK inhibits thrombin and subsequently prevents fibrin formation, we next sought to determine how thrombin would affect PS sorting. We tested CTI-treated WB  $\pm$  GPRP perfused over collagen/TF. Gly-Pro-Arg-Pro (GPRP) inhibits fibrin

polymerization [38]. Unlike in the presence of PPACK, thrombin was not inhibited in the presence of GPRP. As expected, no significant fibrin formation occurred in the +GPRP channels, while fibrin formed in the control (no GPRP) channels (Fig. 2-2A and B, upper panels; Supp. Fig. S2-7). Platelet FI was similar in both  $\pm$ GPRP channels (Fig. 2-2A and B, upper panels; Supp. Fig. S2-7). PS distribution in  $\pm$ GPRP conditions at early time points was similar (Fig. 2-2A lower panel), but enhanced PS sorting occurred in +GPRP channels at later time points (Fig. 2-2B lower panel). Annexin V FI was initially similar in both conditions until around 450s, when the +GPRP condition had a noticeable increase in annexin V FI (Fig. 2-2C), with the final annexin V FI for +GPRP significantly greater ( $p < 0.0001$ ) than -GPRP. This indicated that fibrin in the control condition may be inhibiting thrombin (via antithrombin I activity) from contributing to PS exposure, while thrombin in the +GPRP condition, where fibrin had not formed, was able to contribute to increased PS exposure.

Similar to +PPACK results, contraction was significantly greater in the +GPRP condition than in the control (Fig. 2-2D), further showing that fibrin limits contraction. In terms of PS spatial sorting, +GPRP had a significantly ( $p < 0.0001$ ) greater autocorrelation metric than the control, indicating much more PS spatial sorting in +GPRP (Fig. 2-2E). Lastly, we found that the Pearson correlation coefficient for PS temporal sorting was significantly lower in the +GPRP condition than in the control (0.30 and 0.83, respectively; Fig. 2-2F), indicating greater PS temporal sorting for +GPRP channels.

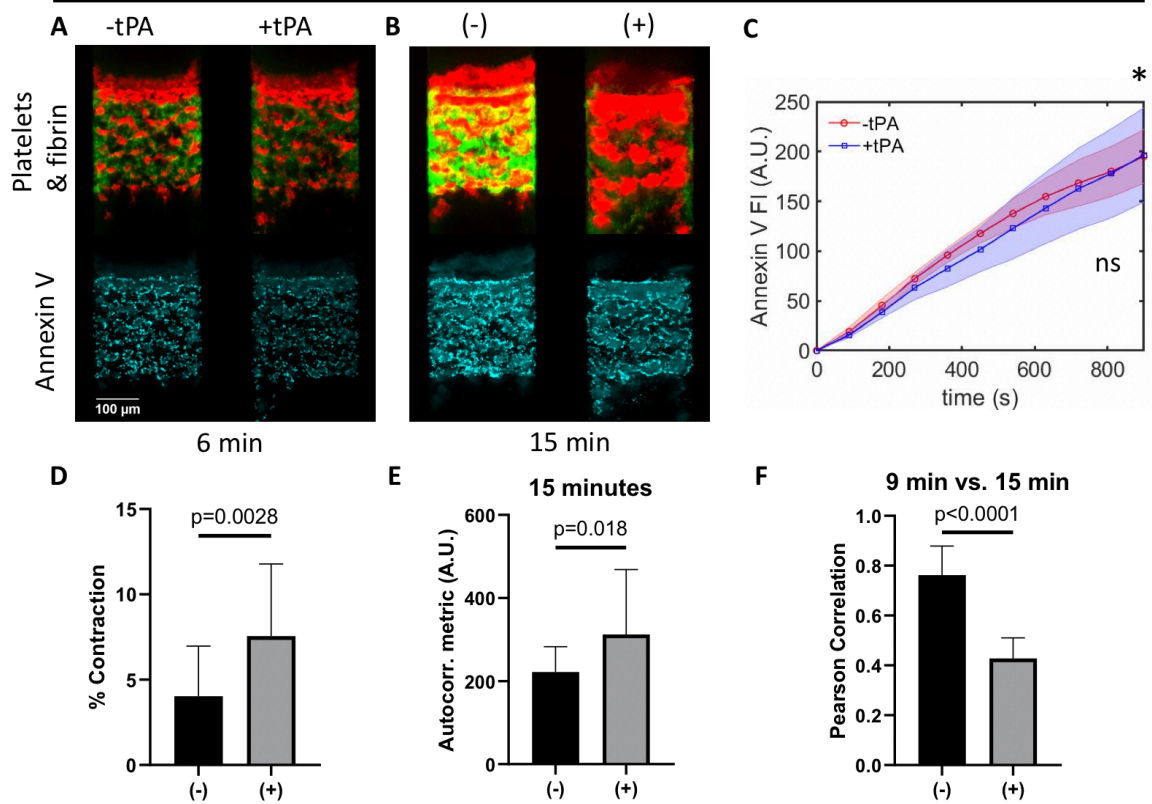


**Figure 2-3. Fibrinolysis enhances PS sorting.**

High CTI WB was perfused with and without tPA over collagen/TF at an initial shear rate of  $100\text{ s}^{-1}$ . CD61, fluorescent fibrinogen, and annexin V were added to stain for platelets, fibrin, and PS, respectively. Images of clots were taken in 90-second intervals for 15 minutes; example images are illustrated at 6 minutes (A) and 15 minutes (B) of CD61 (red), fluorescent fibrinogen (green), and annexin V (cyan). Annexin V FI was measured during the course of the experiment as average FI  $\pm$  standard deviation (C). Contraction was measured as % contraction between 9 and 15 minutes in clots (D). An autocorrelation metric was calculated for the final (15-minute) annexin V image for each clot as a measure of PS spatial sorting (E). The Pearson correlation coefficient was calculated between 9- and 15-minute annexin V images for each clot as a measure of PS temporal sorting (F). Data are from 3 different donors (N=3) and 22 individual clots (n=22). A.U. = arbitrary units

### Fibrinolysis enhances PS sorting

We then evaluated the effect of fibrinolysis on PS distribution by testing CTI-treated WB  $\pm$  tissue plasminogen activator (tPA) perfused over collagen/TF. Plasminogen can localize on the ballooned “cap” of PS-exposing platelets [39]. The role of fibrinolysis

in PS sorting at the whole thrombus level is more complex since fibrin is present, then subsequently dissolves. At early time points, fibrin formed in both the presence and absence of tPA (Fig. 2-3A upper panel). However, as fibrin continued to form, tPA-generated plasmin dissolved the fibrin until most of the fibrin had been solubilized (Fig. 2-3B upper panel). Fibrin FI for both conditions was similar until around 300s, where the fibrin FI for the +tPA condition soon plateaued and then decreased, while the control (no tPA) fibrin FI continued to increase throughout the experiment (Supp. Fig. S2-8). Platelet FI for  $\pm$ tPA conditions was nearly the same throughout the course of the experiment (Supp. Fig. S2-8). Annexin V distribution for both conditions was fairly similar at early time points (Fig. 2-3A lower panel), but annexin V in +tPA condition began to sort more than in control at later time points (Fig. 3B lower panel), similar to annexin V distribution in +PPACK and +GPRP conditions. Annexin V FI was similar for both conditions throughout the experiment (Fig. 2-3C) with no significant difference in final annexin V FI.

Contraction was significantly greater ( $p = 0.0028$ ) in +tPA channels than in control (Fig. 2-3D). The autocorrelation metric suggested greater PS spatial sorting in +tPA than in -tPA, as +tPA had a statistically greater autocorrelation metric than -tPA condition ( $p=0.018$ ; Fig. 2-3E). The Pearson correlation coefficient was significantly lower in the +tPA condition than in control (Fig. 2-3F), indicating greater PS temporal sorting in +tPA, similar to +PPACK and +GPRP conditions.

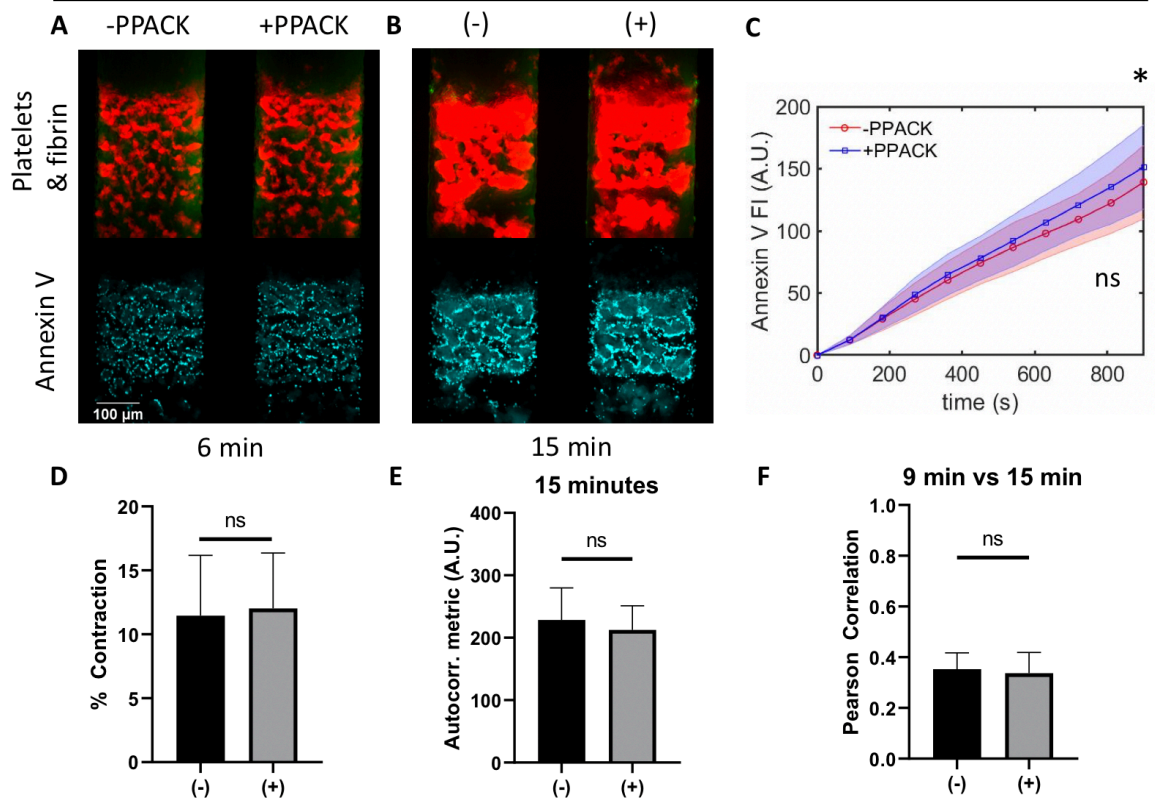


**Figure 2-4. PS sorting is enhanced in the absence of procoagulant conditions (no TF).**

High CTI WB was perfused with and without PPACK over collagen (no TF) at an initial shear rate of  $100 \text{ s}^{-1}$ . CD61, fluorescent fibrinogen, and annexin V were added to stain for platelets, fibrin, and PS, respectively. Images of clots were taken in 90-second intervals for 15 minutes; example images are illustrated at 6 minutes (A) and 15 minutes (B) of CD61 (red), fluorescent fibrinogen (green), and annexin V (cyan). Annexin V FI was measured during the course of the experiment as average FI  $\pm$  standard deviation (C). Contraction was measured as % contraction between 9 and 15 minutes in clots (D). An autocorrelation metric was calculated for the final (15-minute) annexin V image for each clot as a measure of PS spatial sorting (E). The Pearson correlation coefficient was calculated between 9- and 15-minute annexin V images for each clot as a measure of PS temporal sorting (F). Data are from 3 different donors (N=3) and 20 individual clots (n=20). A.U. = arbitrary units

### PS sorting is enhanced in the absence of procoagulant conditions (no TF)

We tested CTI-treated WB  $\pm$  PPACK perfused over collagen (no TF). With no extrinsic pathway available to trigger fibrin formation, we expected both conditions



( $\pm$ PPACK) to have little to no fibrin formation, and therefore significant PS sorting. Platelet deposition and FI were nearly identical between both conditions and as expected, little to no fibrin formed in either condition (Figure 2-4A and B, upper panels; Supp. Fig. S2-9). Annexin V distribution was more evenly distributed at early time points for both  $\pm$ PPACK (Fig. 2-4A lower panel), but by 15 minutes, PS had sorted in both conditions (Fig. 2-4B lower panel). Annexin V FI was similar in both  $\pm$ PPACK conditions throughout the experiment (Fig. 2-4C), with no statistical difference between final annexin V FIs.

There was no significant difference in contraction between  $\pm$ PPACK, as expected because neither condition had fibrin formation (Fig. 2-4D). Contraction was pronounced in both conditions, similar to the magnitude of contraction in +PPACK in Figure 2-1 and +GPRP in Figure 2-2. There was no statistical difference in the autocorrelation metric between  $\pm$ PPACK conditions, suggesting the same degree of PS spatial sorting occurred in both conditions (Fig. 2-4E). PS temporal sorting was prevalent in both conditions, indicated by the relatively low Pearson correlation coefficients, with no significant difference between  $\pm$ PPACK (Fig. 2-4F).

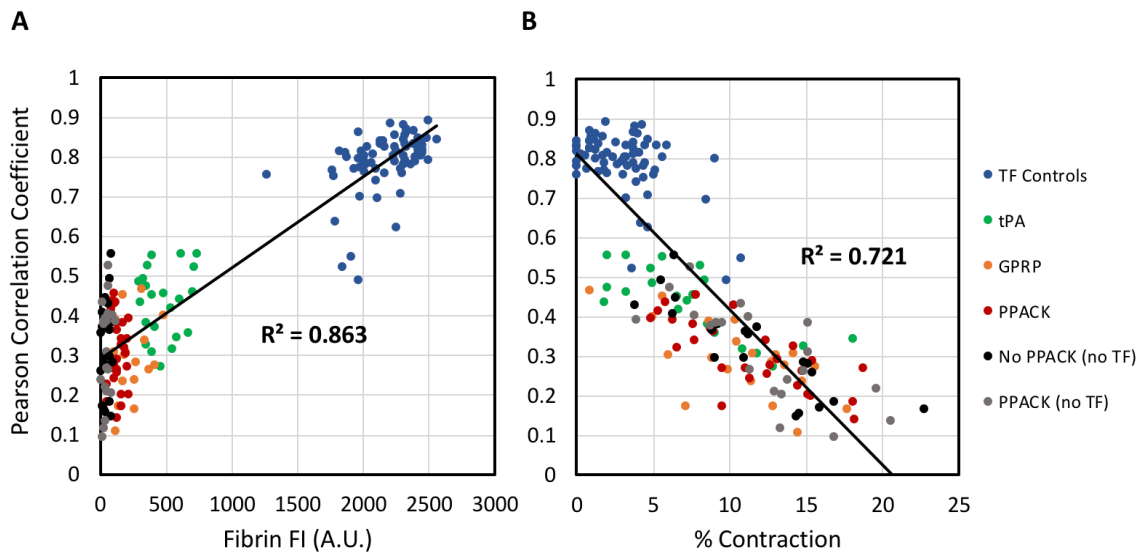


**Figure 2-5. PS sorting correlates with contraction, and correlates inversely with fibrin FI.**

The Pearson correlation coefficient between 9- and 15-minute images of annexin V fluorescence was calculated as a measure of PS temporal sorting for each clot. The final fibrin FI (at 15 minutes) was measured for each clot. The % contraction between 9- and 15-minute annexin V images was also measured for each clot. (A) The graph compares the final fibrin FI to the Pearson correlation coefficient for PS temporal sorting for each clot tested. (B) The graph compares the % contraction to the Pearson correlation coefficient for PS temporal sorting for each clot tested. All conditions tested are included (TF controls refer to -PPACK, -GPRP, and -tPA controls). Data points include all data from Figures 2-1 through 2-4.

### Contraction correlates with PS sorting, but fibrin attenuates contraction and PS sorting

During experiments, we observed differences in thrombus contraction between clots that did and did not have fibrin. This was in agreement with recent research that fibrin limits clot contraction in vivo [30]. We investigated if PS sorting correlated with fibrin. Our results for fibrin FI and PS temporal sorting showed a strong correlation ( $R^2 = 0.863$ ; Fig. 2-5A). Clots with greater fibrin FI had greater Pearson correlation coefficients and thus less PS temporal sorting. We also investigated the relation between PS sorting

and contraction. The results showed that the Pearson correlation coefficient correlated inversely with % contraction ( $R^2 = 0.721$ ; Fig. 2-5B). Clots with greater % contraction had smaller Pearson correlation coefficients, and thus greater PS temporal sorting.

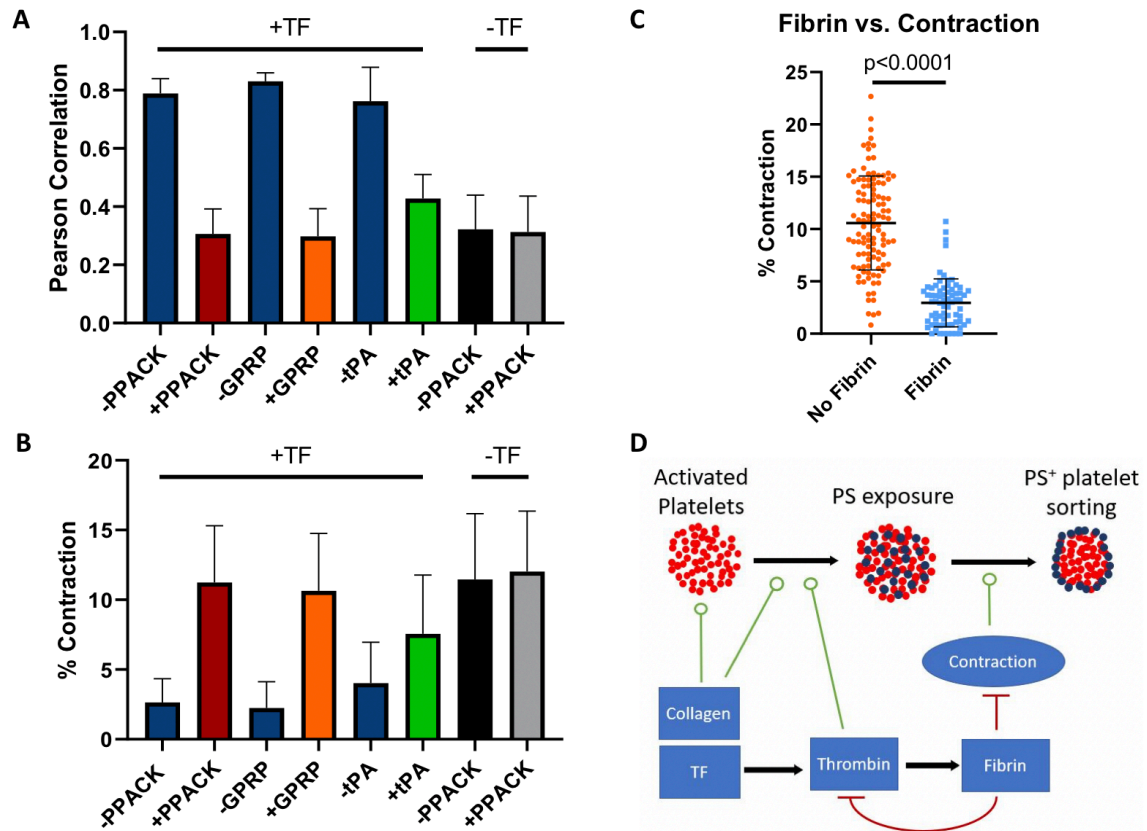


**Figure 2-6. Extent of PS sorting and % contraction is consistent across similar fibrin conditions.**

We compared the % contraction in clots where fibrin was inhibited or dissolved (+PPACK, +GPRP, +tPA, ±PPACK no TF) and clots where fibrin formed (-PPACK, -GPRP, -tPA) (A). The Pearson correlation coefficients for PS temporal sorting for all conditions tested were compared to each other (B). The % contraction for all conditions tested were compared to each other (C). Schematic of PS exposure and PS<sup>+</sup> platelet sorting (D). Green lines with circles indicate contributing driving factors for an action (e.g. contraction contributes to PS<sup>+</sup> platelet sorting). Red lines with bars indicate inhibiting or limiting factors for an action (e.g. fibrin limits contraction).

We noted that the 3 control conditions that had normal fibrin formation (-PPACK, -GPRP, and -tPA) all had similarly high Pearson correlation coefficients (0.79, 0.83, and 0.76, respectively), indicating much less PS temporal sorting (Fig. 2-6A). All other

conditions (+PPACK, +GPRP, +tPA, ±PPACK no TF) that resulted in little to no final fibrin FI had similarly low Pearson correlation coefficients (0.31, 0.30, 0.43, 0.32, and 0.31, respectively), indicating much greater PS temporal sorting. The Pearson correlation coefficient for +tPA was slightly greater (0.43) than the other conditions without fibrin, likely because initial fibrin formation in +tPA resulted in a small, residual amount of fibrin present by 15 minutes.

We also wanted to compare the % contraction across all conditions (Fig. 2-6B). The conditions with normal fibrin formation had similar magnitudes of contraction, at around 2-4% on average. Conditions where fibrin formation was inhibited (+PPACK, +GPRP, ±PPACK no TF) all had similarly high % contraction, at around 10-12% on average. Although +tPA had significantly greater contraction than conditions with fibrin, contraction was slightly less (average = 7.6%) than conditions where fibrin formation was inhibited. This may be due from some residual or transient low levels of fibrin that were not fully lysed by 15 minutes. This slightly decreased contraction in +tPA is in agreement with the Pearson correlation for +tPA being slightly higher (0.43) than in conditions where fibrin is inhibited (0.31, 0.30, 0.32, and 0.31), further supporting the inverse relationship between Pearson correlation coefficient and % contraction. To evaluate the relation between fibrin and contraction, we compared the final fibrin FI to % contraction for each clot. Clots with no fibrin formation (+PPACK, +GPRP, ±PPACK no TF) or significant fibrinolysis (+tPA) had a 3.6X greater clot contraction than clots where fibrin formed normally (-PPACK, -GPRP, and -tPA), which was significantly greater (Fig. 2-6C). Lastly, we illustrated how PS exposure and PS sorting relate to the

coagulation cascade (Fig. 2-6D), noting that fibrin attenuates contraction and subsequent PS sorting.

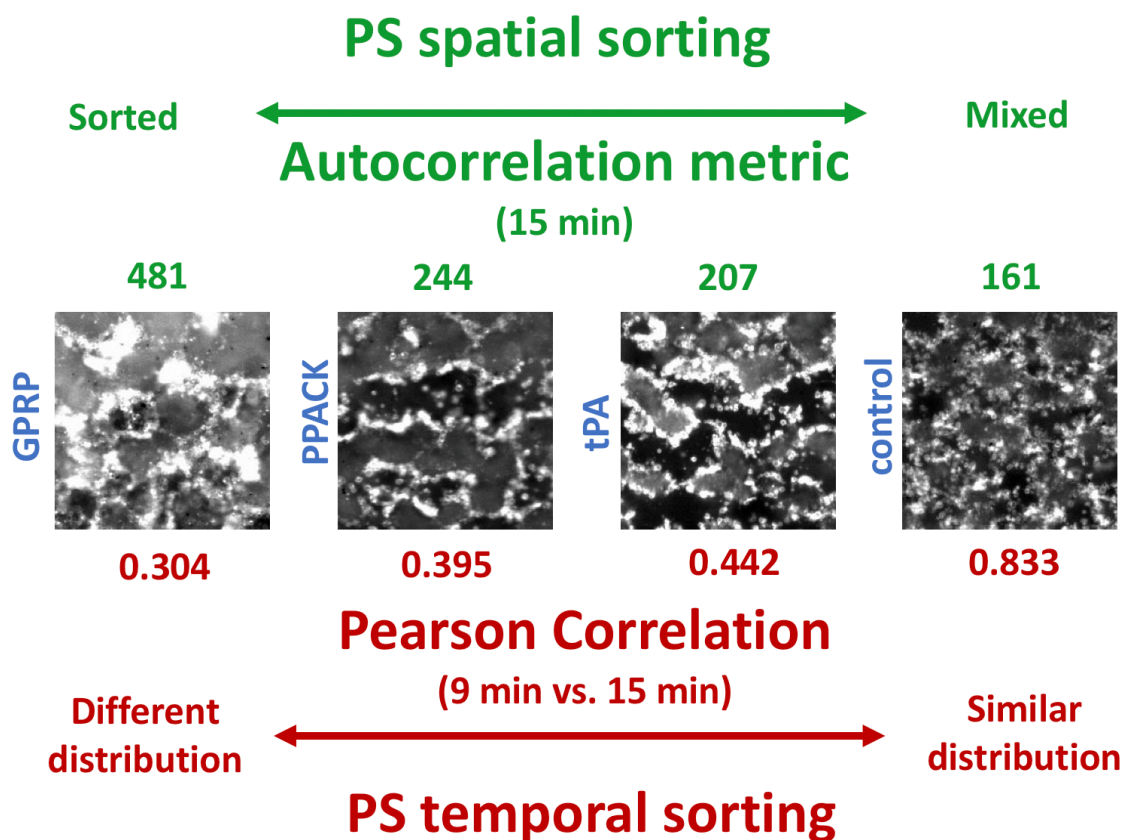


**Figure 2-7. Pearson correlation coefficient measures PS temporal sorting and autocorrelation metric measures PS spatial sorting.**

Example images of PS distribution of clots from GPRP, PPACK, tPA, and control experiments at 15 minutes. Higher Pearson correlation coefficients indicate more similar distributions between 9 minute and 15 minute images; lower Pearson correlation coefficients indicate different distributions between 9 and 15 minutes images. Higher autocorrelation metric values indicate a more sorted distribution of PS at 15 minutes; lower autocorrelation metric values indicate a more mixed distribution of PS at 15 minutes.

The consistency in Pearson correlation coefficient values for conditions where fibrin was inhibited (Fig. 2-6A) demonstrates the robustness of using a Pearson correlation coefficient to measure PS temporal sorting. Similarly, the autocorrelation

metric used to evaluate the extent of PS spatial sorting consistently showed significant differences between  $\pm$ fibrin conditions. The autocorrelation metric values for GPRP were notably higher than for PPACK and tPA, suggesting free thrombin availability may have contributed to PS sorting. Figure 2-7 illustrates how Pearson correlation coefficients decreased from similar to different distributions (between 9 and 15 minutes), and how the autocorrelation metric decreased from sorted to mixed distributions (at 15 minutes).

**PS sorting occurs in the presence of fibrin, but PS sorting is greater when fibrin is inhibited or lysed**

We also evaluated the differences in autocorrelation metric values between images at 6 minutes and 15 minutes in clots (Supp. Fig. S2-10). We found that for all conditions, the average autocorrelation metric increased significantly from 6 to 15 minutes, supporting the previous finding by Nechipurenko, et al. that some degree of PS sorting occurs in the presence of fibrin [28]. We note here that at 6 minutes, there were no statistical differences in autocorrelation metric values between +PPACK, +GPRP, and +tPA and their respective controls (Supp. Fig. S2-10), but there were statistical differences at 15 minutes, with +PPACK, +GPRP, and +tPA all statistically greater (more sorted) than their controls (Fig. 2-1E, Fig. 2-2E, Fig. 2-3E). While our results support the finding that PS sorting can occur to some extent with fibrin present, fibrin plays an attenuating role limiting the extent of PS sorting.

## 2.4 Discussion

We performed an in vitro study with physiological human blood flow conditions using microfluidics to evaluate the spatial distribution of PS and the role of fibrin and fibrinolysis. In new results, we demonstrate that clots without fibrin exhibit enhanced PS sorting and clot contraction compared to clots with fibrin. We first showed that in PPACK-treated WB, annexin V spatially and temporally sorted into areas of locally high and low FI, confirming a heterogeneous localization around the periphery of the platelet mass previously reported by others [27,28]. By comparison, non-PPACK-treated WB had a more homogeneous annexin V distribution throughout the platelet masses. We showed that with thrombin present, PS still sorted in the absence of fibrin polymerization. In the case of fibrinolysis, our results showed that as fibrin breaks down, PS spatial and temporal sorting subsequently occurred. In preventing extrinsic pathway coagulation by removing TF, PS sorting occurred regardless of whether PPACK is present. As fibrin limits contraction, PS sorting correlated with clot contraction and correlated inversely with fibrin FI. Using both spatial and temporal image correlation metrics for PS sorting under diverse pharmacological conditions, we quantitatively demonstrated that fibrin limited the extent of contraction and subsequent PS sorting.

Recent studies have explored the spatial distribution of annexin V on platelets and the role of clot contraction in driving PS<sup>+</sup> platelets to the clot periphery [27,28]. Additionally, fibrin stiffens clots and limits contraction [29,30,40,41]. While Nechipurenko, et al. [28] observed ~6 PS<sup>+</sup> platelets at the periphery of a platelet mass when fibrin was present (Ref. [28] Supp. Fig. 9), there was no quantification of PS<sup>+</sup>

platelet sorting as a function of fibrin level. Munnix, et al. [27] noted that PS at the periphery seemed to appear from initial stages of clot growth, while Nechipurenko, et al. [28] observed that PS<sup>+</sup> platelets translocate to the periphery via contraction. We sought to determine if blocking fibrin enhances clot contraction and PS<sup>+</sup> platelet sorting. We show fibrin limited contraction (Fig. 2-6C) and PS<sup>+</sup> platelet sorting was attenuated as fibrin levels increased (Fig. 2-5A). It is worth noting a limitation in this study is the use of microfluidics. While in vitro studies can help elucidate important phenomena, future in vivo studies should be considered to further validate findings in this study.

Nechipurenko, et al. [28] observed no noticeable difference in PS sorting between clots with and without fibrin. However, this conclusion was drawn from a single observation of ~6 individual PS<sup>+</sup> platelets at the periphery of a platelet mass with fibrin present. While our results are in agreement that there is a detectable degree of PS sorting in the presence of fibrin (Supp. Fig. S2-10), we clearly observed much greater PS sorting when fibrin is inhibited. In our assay, at lower shear rates, thousands of platelets for analysis cover the full 250  $\mu\text{m}$  x 250  $\mu\text{m}$  collagen patch. At higher shear rates, platelet deposition and embolism is much more variable and heterogeneous. Thus, we explored a lower shear rate to allow highly consistent platelet deposition across different donors and different experiments.

We developed two independent imaging algorithms to quantify localization processes: cross correlation and autocorrelation. Cross correlation analysis compared 2 images at different time points (9 minutes and 15 minutes) to give a Pearson correlation coefficient as an indication of PS temporal sorting. Autocorrelation analysis compared an



image with itself (image at 15 minutes) to give an autocorrelation metric as an indication of PS spatial sorting. There was a difference in sensitivity to detect PS changes between the Pearson correlation (measuring temporal changes) and the autocorrelation metric (measuring spatial heterogeneity). When fibrin is inhibited or lysed, the temporal changes in PS distributions were more pronounced than the spatial differences in PS distributions. Pearson correlation addressed the question “does the PS distribution change?” while the autocorrelation metric then goes further, addressing “how does the distribution change (i.e. more or less spatially sorted)?”

Our observation that fibrin limits contraction, confirming what previous studies have found, was the primary reason for the difference in PS sorting between clots with and without fibrin. Samson, et al. [30] observed reduced clot contraction when endogenous fibrinolysis was blocked, suggesting fibrin contributes to clot rigidity. Red blood cells (RBCs) may also play a role in clot contraction. Fibrin cross-linking due from FXIIIa has been shown to be important for RBC retention in clots [42,43]. Tutwiler, et al. [40,41] showed that the presence of RBCs in clots decreases the extent of clot contraction. Thus, these studies suggest clots with cross-linked fibrin may be more rigid and contain RBCs, which would limit clot contraction compared with clots without fibrin, as we have seen in our results.

In the case of tPA experiments, +tPA showed statistically greater contraction, greater autocorrelation metric values, and greater PS temporal sorting than -tPA (Fig. 2-3); however, these differences were not as pronounced as they were with +PPACK or +GPRP and their respective controls. This was likely because of two processes. First, the

initial fibrin formation and some residual fibrin present by the end of experiments may have caused +tPA contraction to be slightly less and the Pearson correlation coefficient to be slightly more than in +PPACK or +GPRP. Second, the transience of fibrinolysis tends to result in greater variability in when and to what extent fibrin is lysed compared to GPRP or PPACK, which may have caused statistical differences to be less pronounced in +tPA than in +PPACK or +GPRP.

Interestingly, GPRP significantly increased PS exposure compared to control conditions, while PPACK and tPA showed no significant differences in annexin V FI compared to control. PS exposure occurs as a result of increased  $\text{Ca}^{2+}$  flux, which can be achieved by stimulating GPVI (in this case, via collagen) or PAR1 or PAR4 (via thrombin) [15,44]. We have previously shown that fibrin captures >85% of locally generated thrombin [45]. In the presence of GPRP, thrombin flux increased steadily until ~500s, and then saw an accelerated increase most likely due from FXIa-dependent thrombin amplification [45]. Interestingly, this correlates with our finding here that the annexin V FI increased steadily for both  $\pm$ GPRP conditions until ~450s, where annexin V FI in the +GPRP condition then increased much more quickly than in the control (Fig. 2-2C). This suggests that increased thrombin available in the +GPRP condition contributed significantly to increased PS exposure.

In the +GPRP condition, the  $\text{PS}^+$  platelet masses were notably larger than other conditions, which ultimately caused the PS distribution at 15 minutes to be more heterogeneous (or sorted) and thus, the autocorrelation values for this condition were greater. With GPRP present, the lack of fibrin may be related to (1) increased local

thrombin (loss of antithrombin I activity) and (2) more locations available to fill with platelets that would have contained fibrin.

These microfluidic results with human blood support a role of fibrin in consolidating the clot, both mechanically and biologically. Restriction by fibrin of PS distribution may limit continued thrombin generation, an outcome that is also fortified by the antithrombin I activity of fibrin. The mitigating role of fibrin on contraction may set the later stage for fibrinolytic resolution of a clot. This consolidating role of fibrin is also consistent with our previous observation that fibrin also limits NETosis in sterile occlusive human thrombi [46]. Intrathrombus fibrin limits a number of processes during thrombosis under flow. For example, fibrin binds thrombin [45,47], reduces the formation of shear-induced NETosis [46], and, as seen in this study, attenuates clot contraction and the degree of PS<sup>+</sup> platelet sorting.

## **CHAPTER 3: THE ROLE OF ADP AND TXA<sub>2</sub> IN LIMITING CONTRACTION**

### **3.1 Introduction**

Clot contraction is an important process that occurs in hemostasis to ensure clot resolution and return of unobstructed blood flow. Contraction involves a number of elements, including fibrin, fibrinogen, platelets, RBCs, von Willebrand factor (VWF), and collagen, among others. The process of clot contraction actually consists of a number of distinct processes that occur, including, but not limited to, reduction of clot size [2,3,40,48], stiffening of the clot matrix [3,4,49], deformation of RBCs [50,51], extrusion of procoagulant platelets [28,52], and redistribution of fibrin [3,48]. The significance of contraction as a process can be seen in diseases where there are defects in non-muscle myosin, resulting in increased bleeding [6]. Additionally, reduced contraction can lead to increased risk of venous thromboembolism [53,54], which could ultimately lead to acute ischemic stroke [55].

Platelet contraction via cytoskeletal actin and myosin plays a key role in strengthening and stabilizing clots [6,56,57]. Non-muscle myosin is a driving force of platelets' contractile ability; when blebbistatin is present to inhibit non-muscle myosin, clot contraction is significantly reduced [6,30,57]. Although platelets contribute significantly to clot contraction, many viscoelastic measurement techniques to evaluate contraction require the presence of thrombin and/or fibrin, which does not allow for the independent evaluation of the contractile ability of platelets [3,58–60]. Additionally, many of these contraction measurement techniques are not performed under physiologic,

or near-physiologic, conditions. Our in vitro microfluidic system allows us the ability to observe clot development, including contraction, on a macro scale, evaluating multiple platelet aggregates in a fully formed clot, in a physiologically relevant environment.

Upon binding of collagen and VWF, platelets release ADP and thromboxane A<sub>2</sub> (TXA<sub>2</sub>), which propagate further activation of nearby platelets to contribute to the stability of a growing platelet mass [49,61,62]. As shown in the core/shell model, Stalker, et al. suggest that ADP and TXA<sub>2</sub> moderate the growth of the P-selectin(-) shell region of the clot, while ADP and TXA<sub>2</sub> inhibitors have a limited effect on the stable core region, making these inhibitors ideal for limiting platelet accumulation while also preventing bleeding [16]. As such, TXA<sub>2</sub> inhibitors like aspirin and ADP inhibitors like clopidogrel are commonly used in a number of patient conditions, but the effects of these types of drugs on clot contraction is not fully elucidated. Ting, et al. [49] evaluated ADP and TXA<sub>2</sub> inhibitors on platelet contractile forces using a microfluidic device with a block and post. They observed that acetylsalicylic acid (ASA, aspirin), a COX-1 inhibitor that prevents TXA<sub>2</sub> production, and 2-MeSAMP, a P<sub>2</sub>Y<sub>12</sub> inhibitor that prevents ADP signaling, significantly reduce platelet forces and aggregate size. However, these experiments were performed at 8000 s<sup>-1</sup>, which is at the very high end of arterial flow shear rates [63]. Additionally, the block and post device to measure platelet contractile force has limited physiological relevance.

Here, we wanted to evaluate contraction in our microfluidic assay that closely mimics in vivo dynamics of a growing clot. We also evaluated three platelet antagonists: ASA, 2-MeSAMP, and MRS-2179, which is a P<sub>2</sub>Y<sub>1</sub> inhibitor that prevents ADP

signaling. We added these platelet antagonists to PPACK-treated whole blood (WB), to ensure thrombin and fibrin inhibition. This allowed us to focus primarily on platelet-platelet interactions and not platelet-fibrin interactions. We wanted to differentiate contraction of platelet aggregates in both the core and shell regions, utilizing CD61 and P-selectin antibodies to measure aggregate contraction in different regions of the clot. Additionally, we measured contraction using two different algorithms that we developed, one for global contraction, measuring clot contraction on a macro scale, looking at fully formed clots with multiple platelet aggregates; and one for local contraction, measuring clot contraction on a micro scale, looking at how individual platelet aggregates contract within a larger clot. We found that both ADP and TXA2 inhibitors limited global aggregate contraction, and had an additive effect when used in combination. However, TXA2 inhibition had a significant effect on reducing local aggregate contraction, while ADP inhibition did not. Lastly, P-selectin+ platelets demonstrated limited global and local aggregate contraction, both in the presence and absence of any ADP or TXA2 inhibition. Taken together, the results of this study suggest ADP and TXA2 inhibition may limit aggregate contraction on a macro scale, and TXA2 inhibition in particular may limit aggregate contraction on a micro scale, which have fundamental repercussions in terms of clot development and clot resolution.

## **3.2 Materials and Methods**

### **Reagents and Materials**

Reagents were prepared and kept at appropriate conditions prior to use in experiments: Phe-Pro-Arg-chloromethylketone (PPACK; EMD Millipore, Burlington, MA), acetylsalicylic acid (ASA; Sigma-Aldrich, St. Louis, MO), 2-methylthioadenosine 5'-monophosphate (2-MeSAMP; Sigma-Aldrich, St. Louis, MO), MRS-2179 (Tocris, Minneapolis, MN), AF647 anti-human CD62P (P-Selectin) antibody (BioLegend, San Diego, CA), AF488 mouse anti-human CD61 (Bio-Rad Laboratories, Hercules, CA), Sigmacote (Sigma-Aldrich, St. Louis, MO), type I fibrillar collagen (Chrono-log, Havertown, PA).

### **Preparation of microfluidic device with collagen surface**

Glass slides were rinsed with ethanol and dried with filtered air. Slides were then rinsed with Sigmacote and then DI water to create a hydrophobic surface. A patterning device was vacuum-sealed to the glass slide. Fibrillar collagen (5  $\mu$ L) was perfused through the patterning channel (250  $\mu$ m wide  $\times$  60  $\mu$ m high) of the patterning device to create a 250  $\mu$ m-wide strip of collagen for all experiments, as previously described [13,14,47,64]. Finally, collagen was rinsed with 20  $\mu$ L 0.5% bovine serum albumin (BSA) buffer, and the patterning device was then removed from the glass slide, leaving a strip of collagen.

## **Blood collection and preparation**

Blood donors were self-reported as medication-free for at least 7 days prior to blood collection. All donors provided informed consent under approval of the University of Pennsylvania Institutional Review Board. Blood was obtained via venipuncture into a syringe containing PPACK (1:100 v/v; final concentration of 100  $\mu\text{mol/L}$ ). P-selectin and anti-CD61 fluorophores were then added to whole blood (WB), both in a 1:50 v/v dilution. ADP and TXA2 inhibitors were added where needed, resulting in the following final concentrations: ASA (100  $\mu\text{M}$ ), 2-MeSAMP (100  $\mu\text{M}$ ), MRS-2179 (10  $\mu\text{M}$ ).

## **8-channel microfluidic device contraction assay**

After collagen was patterned, an 8-channel microfluidic device was placed over the collagen strip and vacuum-sealed, with channels perpendicular to the collagen strip. Thus, each channel contained a 250  $\mu\text{m}$  x 250  $\mu\text{m}$  collagen patch. Each channel had a height of 120  $\mu\text{m}$ . Then 35  $\mu\text{L}$  of 0.5% bovine serum albumin (BSA) was added to each of the 8 wells and perfused through each channel. After blood was drawn, fluorophores were added, followed by ADP or TXA2 inhibitors (ASA, 2-MeSAMP, and/or MRS-2179) or their corresponding controls. ASA stock was dissolved in 10% DMSO, with a final concentration of 0.1% DMSO in blood (1:100 ASA dilution). The control for ASA was a 10% DMSO solution (1:100 dilution; 0.1% DMSO final concentration in blood). 2-MeSAMP and MRS-2179 were both dissolved in water; the control for 2-MeSAMP and MRS-2179 was HBS. Once agonists or controls were added to blood, blood of varying conditions was loaded into the corresponding wells. Blood was perfused through



channels by a 1000  $\mu\text{L}$  syringe (Hamilton Co., Reno, Nevada) with a fixed rate to induce blood flow. The syringe pump (Harvard PHD 2000; Harvard Apparatus, Holliston, MA) was set to 24  $\mu\text{L}/\text{min}$ , resulting in an initial venous shear rate of  $100\text{s}^{-1}$  for all experiments. Blood was perfused for 7.5 min, and then flow was paused ( $0\text{ s}^{-1}$ ) at 7.5 min, for the remaining 7.5 min of the experiment, for a total experiment time of 15 minutes. The epifluorescence microscope (Olympus Ix81; Olympus America Inc, Central Valley, PA) captured individual time frames at chosen locations with chosen wavelengths.

## **Image analysis**

### **Fluorescence measurements**

Fluorescence intensity (FI) of fluorophores (CD61 and P-selectin) was measured over time, with images of each clot uploaded and compiled into a time sequence in ImageJ. The initial image ( $t = 0\text{s}$ ) was subtracted from subsequent images to subtract for any background fluorescence. Fluorescence was measured using a rectangular subsection of the central 2/3 of the clot area, to avoid any edge effects. FI values were exported to Matlab, where plots were made of the FI values and experiment time. Values in plots are average  $\pm$  standard deviation of FI values over time.

### **Global contraction measurements**

Images of CD61 and P-selectin fluorescence were uploaded to ImageJ. We wanted to observe the extent of contraction in clots on the collagen surface, which was  $250\text{ }\mu\text{m} \times 250\text{ }\mu\text{m}$ . However, in many instances, platelets aggregated above

and below the collagen surface in the direction of flow. To include this in our contraction measurements, images of individual clots were made to be 250  $\mu\text{m}$  x 300  $\mu\text{m}$ , with the 300  $\mu\text{m}$  dimension in the direction of flow incorporating all platelets in the clot above and below the collagen strip. Images were then uploaded to Matlab and binarized to allow for automated contraction measurements. The threshold for binarizing images was chosen to be half of the average fluorescence of the image (Supp. Fig. 3-1). Binary images had platelets represented in white, and empty space in black.

Once images were binary in Matlab, we measured global contraction by building a Matlab algorithm that automatically drew 5 lines through the central portion of the clot in the same direction as flow. One line was drawn at the middle (of the x direction) pixel of the clot. Four additional lines were drawn at the following locations, relative to the middle line: -50 pixels, -25 pixels, + 25 pixels, and +50 pixels (each in the x direction). Each line was drawn from the top most platelet (white) pixel to the bottom most platelet (white) pixel (in the y direction). This was done for images at 7.5 and 15 min of the same clot. The lengths of the five lines at 7.5 min were averaged, as were the lengths of the five lines at 15 min. The average lengths at 7.5 min and 15 min were then used to calculate the percent global contraction (Supp. Fig. 3-2). This was done for both CD61 and P-selectin images.

### **Local contraction measurements**

In addition to global contraction, we used binary images in Matlab to calculate local contraction for CD61 and P-selectin images. Binary images at 7.5 min and 15 min for a particular clot were measured in Matlab for their percent platelet coverage, or percent of the image containing white space (representing platelets). The percent coverage between 7.5 min and 15 min images were each used to calculate local contraction (Supp. Fig. 3-3). This was done for both CD61 and P-selectin images.

### **Statistical Analyses**

Statistical differences between conditions were calculated using unpaired Welch's t-tests in GraphPad (ns signifies  $p > 0.05$ ).

### 3.3 Results

PPACK WB ( $\pm$  ASA, 2-MeSAMP, MRS-2179)  $\rightarrow$  collagen ( $100 \text{ s}^{-1} \rightarrow 0 \text{ s}^{-1}$ ): Qualitative images

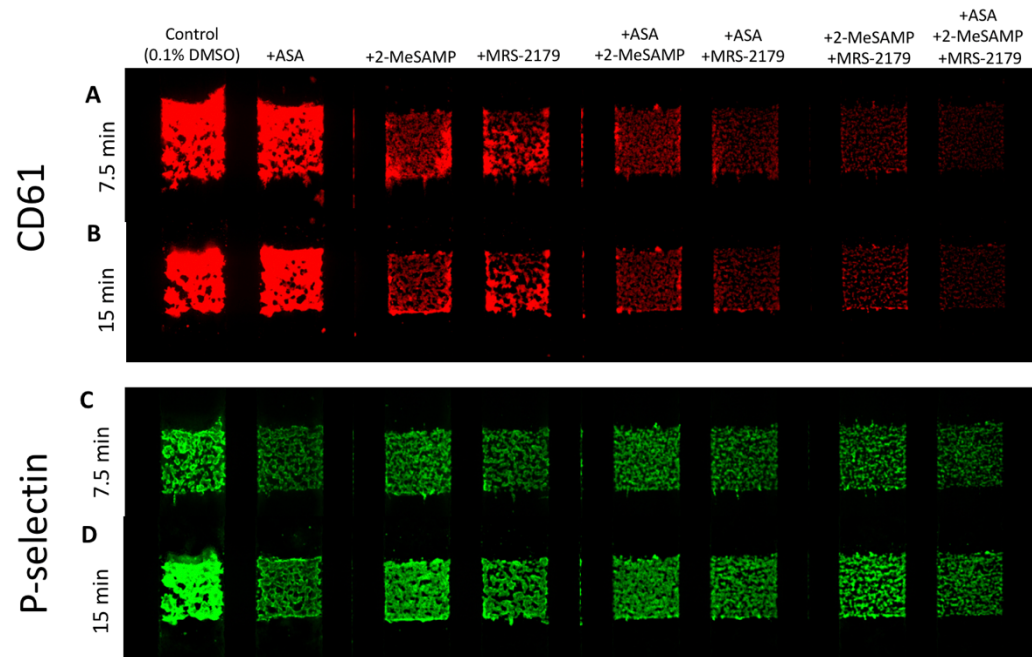


**Figure 3-1. ASA, 2-MeSAMP, and MRS-2179 have an additive effect on limiting platelet deposition, but do not have an additive effect on limiting P-selectin display.**

PPACK WB with and without ASA, 2-MeSAMP, and MRS-21279 was perfused over collagen at  $100 \text{ s}^{-1}$  for 7.5 min, then flow was stopped for 7.5 min. CD61 fluorophore was added to label platelets, with images taken at 7.5 min (A) and 15 min (B). P-selectin fluorophore was added to label platelet activation via alpha-granule release, with images taken at 7.5 min (C) and 15 min (D).

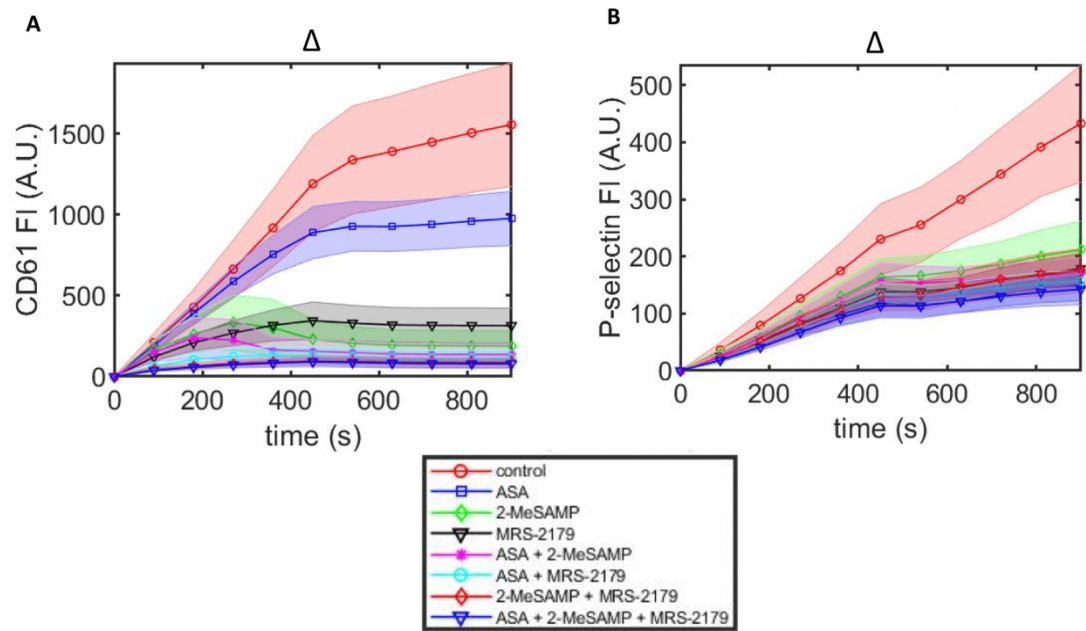


**Figure 3-2. Quantitative fluorescence data from Figure 3-1.**

PPACK WB with and without ASA, 2-MeSAMP, and MRS-2179 was perfused over collagen at  $100 \text{ s}^{-1}$  for 7.5 min, then flow was stopped for 7.5 min. Platelet (A) and P-selectin (B) fluorescence intensities were measured throughout the course of the experiment amongst the different conditions. Delta signifies change from  $100 \text{ s}^{-1}$  to  $0 \text{ s}^{-1}$  flow rate at 7.5 min. (N = 3 donors, n = 6 clots for each panel; A.U. = arbitrary units)

### ASA, 2-MeSAMP, and MRS-2179 have an additive effect on limiting platelet deposition.

To measure how ADP and TXA2 inhibition affect clot contraction, we perfused PPACK whole blood (WB) with and without ASA, 2-MeSAMP, and MRS-2179 over collagen at  $100 \text{ s}^{-1}$  for 7.5 min, followed by stopping flow for 7.5 min. ASA, 2-MeSAMP, and MRS-2179 were each added individually, and in combination with each other. We added CD61 fluorophore to WB to label for platelets. By 7.5 min, platelets had deposited normally in control conditions, while there appeared to be slightly reduced platelet deposition in +ASA conditions, and considerably reduced platelet deposition in +2-

MeSAMP, +MRS-2179, and all combinatorial conditions (Fig. 3-1A, 3-2A). From 7.5 min to 15 min, with flow stopped, platelet fluorescence intensity (FI) in control continued to increase slightly, but at a slower rate than from 0 min to 7.5 min. This increase in platelet FI while flow had stopped was likely due from contraction. All other conditions remained nearly constant from 7.5 min to 15 min (Fig. 3-1B, 3-2A). Notably, the combinatorial conditions (with 2 or 3 ADP and/or TXA2 inhibitors present) had lower final FI than either of the conditions with only one inhibitor present, suggesting an additive effect of ASA, 2-MeSAMP, and MRS-2179 on reducing platelet deposition.

**ASA, 2-MeSAMP, and MRS-2179 did not have an additive effect on limiting P-selectin display.**

In addition to CD61, we also added P-selectin fluorophore to WB to label for alpha-granule release. By 7.5 min, P-selectin display was prominent in each condition, with the control showing slightly greater fluorescence than the conditions with ADP/TXA2 inhibitors present (Fig. 3-1C and 3-2B). From 7.5 min to 15 min, with flow stopped, P-selectin fluorescence continued to increase steadily in the control condition (Fig. 3-1D and 3-2B). This continued increase was greater than the increase in platelet deposition from 7.5 min to 15 min, indicating that the increase in P-selectin from 7.5 min to 15 min was likely not solely due from contraction. Additionally, P-selectin display in conditions with ADP and/or TXA2 inhibitors continued to slightly increase from 7.5 min to 15 min, which was not the case for platelet deposition. Like platelet deposition, P-selectin display appeared to be markedly reduced by the presence of any ADP or TXA2 inhibitors. However, unlike with platelet deposition, ADP and/or TXA2 inhibition did not

appear to have a strong additive effect on reducing P-selectin fluorescence, as differences in final fluorescence among different conditions with ADP and/or TXA2 inhibitors showed fairly similar FI values, with a few, minimal statistical differences between different conditions (Fig. 3-2B).

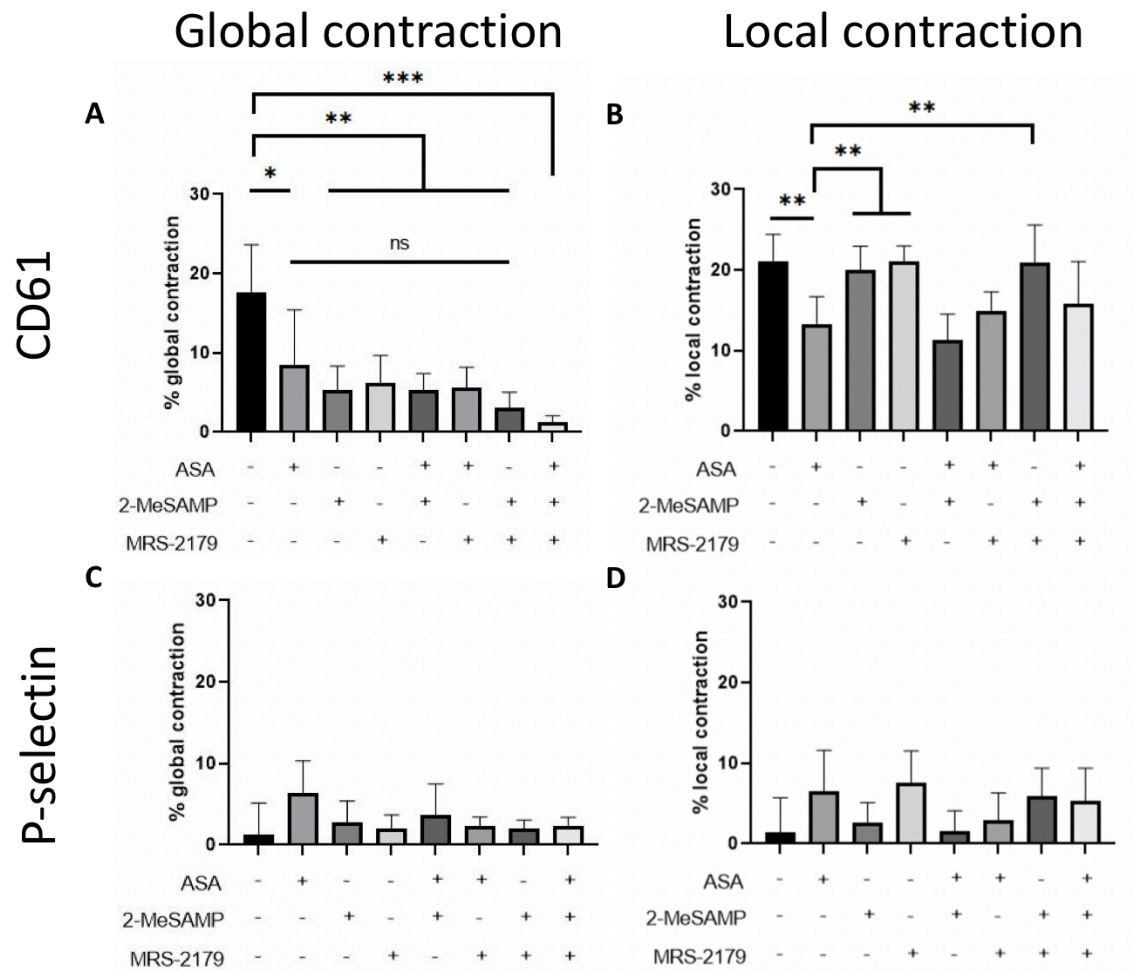


**Figure 3-3. P-selectin+ platelets have limited global and local contraction; ASA, 2-MeSAMP, and MRS-2179 have a limiting effect on global platelet contraction, while only ASA limits local platelet contraction.**

Images from Figure 3-1 were measured for global and local contraction. Global contraction measured the change in distance in clot length between 7.5 min and 15 min images of a clot. Local contraction measured the change in percent area coverage of a clot between 7.5 min and 15 min. Global contraction for platelets (A), local contraction for platelets (B), global contraction for P-selectin (C), and local contraction for P-selectin (D) were compared among the various conditions. (N = 3 donors, n = 6 clots for each panel;

\*p<0.05, \*\*p<0.01, \*\*\*p<0.001)

### **ASA, 2-MeSAMP, and MRS-2179 have a limiting effect on global aggregate contraction**

Global and local contraction measurements were made based on images taken from experiments in Figure 3-1. Global contraction for platelet aggregates was measured as the % change in distance from the top edge of the clot to the bottom edge, between 7.5 min and 15 min images (Fig. 3-3A). Measurements for the control condition showed pronounced contraction. With individual ADP or TXA2 inhibitors added (ASA alone, 2-MeSAMP alone, or MRS-2179 alone), contraction was significantly reduced. Contraction was reduced even further when inhibitors were added in combination (ASA + 2-MeSAMP, ASA + MRS-2179, and 2-MeSAMP + MRS-2179), and decreased the most when all three inhibitors were present. This demonstrated an additive effect of ADP and/or TXA2 inhibitors on reducing global aggregate contraction.

Like global contraction, local contraction for platelet aggregates was pronounced under control conditions (Fig. 3-3B). However, unlike global contraction, local contraction for platelet aggregates was affected differently by ADP and/or TXA2 inhibition. Conditions with 2-MeSAMP and MRS-2179 showed no consistent pattern in altering local aggregate contraction relative to control, suggesting ADP inhibition did not have much of an effect on local aggregate contraction. However, conditions with ASA consistently showed reduced local contraction, with significant differences. This suggested that TXA2 inhibition may play a role in limiting local platelet aggregate contraction.



### **P-selectin+ platelets have limited global and local contraction**

In addition to CD61+ platelets, we also measured global (Fig. 3C) and local (Fig. 3D) contraction in P-selectin images. Global and local contraction for P-selectin in control was minimal relative to global and local aggregate (CD61+) contraction. This suggests that the P-selectin+ core of the clot was less contractile relative to the P-selectin(-) shell region of the clot under control conditions. Additionally, ADP or TXA2 inhibition alone, or in combination, showed limited global and local contraction. Some ADP and/or TXA2 conditions showed marginally higher % contraction than control, but there did not appear to be a noticeably significant trend. Thus, the P-selectin+ core of the clot was generally less contractile, and was not significantly affected by ADP or TXA2 inhibition.

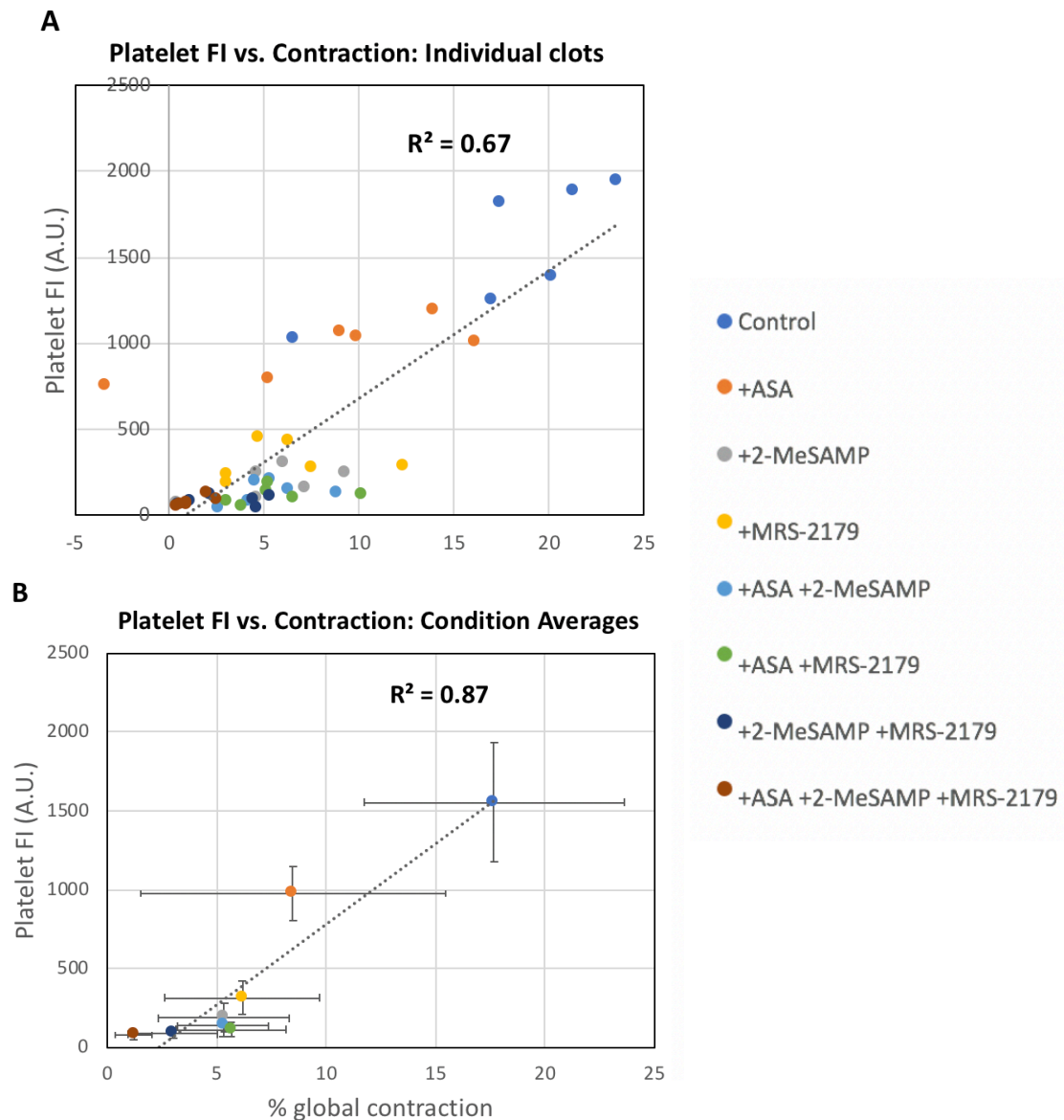


**Figure 3-4. Platelet fluorescence correlates with global contraction.**

Final platelet fluorescence and % global contraction were graphed for individual clots (A). Average fluorescence and contraction values for each condition were also graphed (B). (N = 3 donors, n = 6 clots for B; A.U. = arbitrary units)

### Platelet fluorescence correlates with global contraction

As observed in Figure 3-2A, platelet FI was greatest for control, while TXA2 inhibition with ASA noticeably reduced platelet FI. ADP inhibition (via either 2-

MeSAMP or MRS-2179) significantly reduced platelet FI relative to control, and combinations of ADP and TXA2 inhibitors reduced platelet FI even further, suggesting ADP and TXA2 inhibition had an additive effect on reducing platelet deposition. In Figure 3-3A, we saw contraction was greatest in control, and then significantly reduced when ADP and TXA2 inhibitors were present. ADP and TXA2 inhibition together showed the greatest reduction in global aggregate contraction, again suggesting ADP and TXA2 may have had an additive effect on reducing global aggregate contraction. Because of the potential additive effects of ADP and TXA2 inhibition on platelet deposition and global aggregate contraction, we wanted to see how platelet deposition and aggregate contraction correlated for each clot and for each condition. To do this, we compared the % global aggregate (CD61+) contraction and platelet FI for each clot (Fig. 3-4A) and for the average of all clots in a given condition (Fig. 4-4B). With each clot graphed, there was a noticeable correlation ( $R^2 = 0.67$ ) between platelet FI and global aggregate contraction (Fig. 4-4A). However, there was some deviation in individual clots; when the average of each condition was taken, the correlation improved considerably ( $R^2 = 0.87$ ; Fig. 4-4B). This demonstrated an observable correlation between platelet FI and global aggregate (CD61+) contraction.

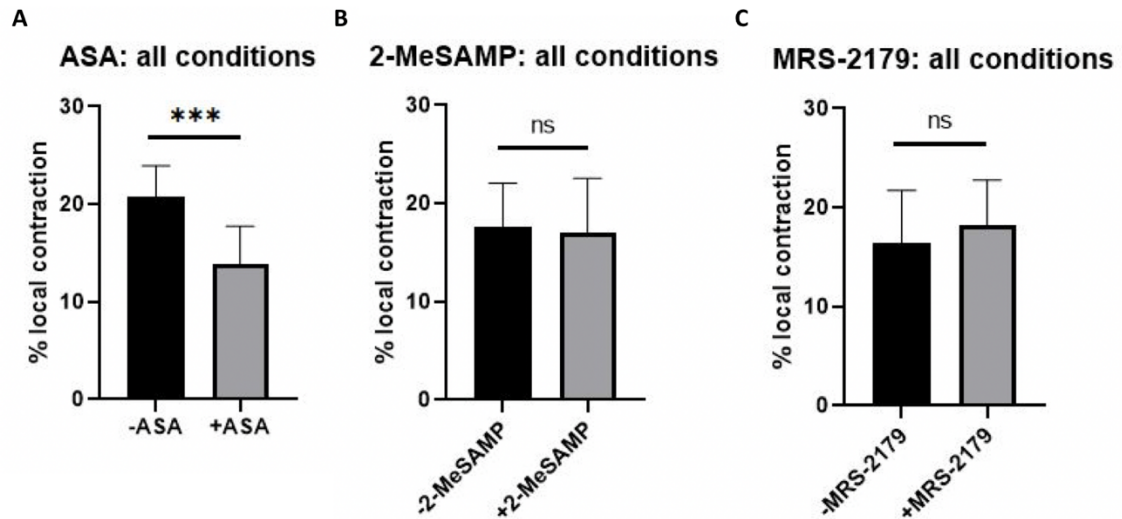


**Figure 3-5. ASA limits local platelet contraction, while 2-MeSAMP and MRS-2179 have no effect.** We performed a meta-analysis of data from Figure 3-3B by segregating data into different component conditions. Each of the 4 conditions with ASA and each of the 4 conditions without ASA were averaged and compared (A); the same was done for 2-MeSAMP (B) and MRS-2179 (C). (N = 3 donors, n = 24 clots for each panel; \*p<0.05, \*\*p<0.01, \*\*\*p<0.001)

### **ASA limits local aggregate contraction, while 2-MeSAMP and MRS-2179 have no effect**

In Figure 3-3B, conditions that had ASA present tended to have reduced local aggregate contraction. To determine the significance ASA had on limiting local aggregate contraction, we grouped all conditions that either had or did not have ASA (Fig. 3-5A), 2-MeSAMP (Fig. 3-5B), or MRS-2179 (Fig. 3-5C). When conditions were separated based on the presence or absence of 2-MeSAMP, there was no significant difference in local aggregate contraction (Fig. 3-5B). The same was true for MRS-2179 (Fig. 3-5C), suggesting ADP inhibition had no significant effect on local aggregate contraction. However, when conditions were separated based on the presence or absence of ASA, there was a significant difference ( $p<0.0001$ ) in local aggregate contraction, with ASA

conditions showing reduced contraction relative to conditions without ASA (Fig. 3-5A). This suggests that TXA2 inhibition may have had a limiting effect on local aggregate (CD61+) contraction.

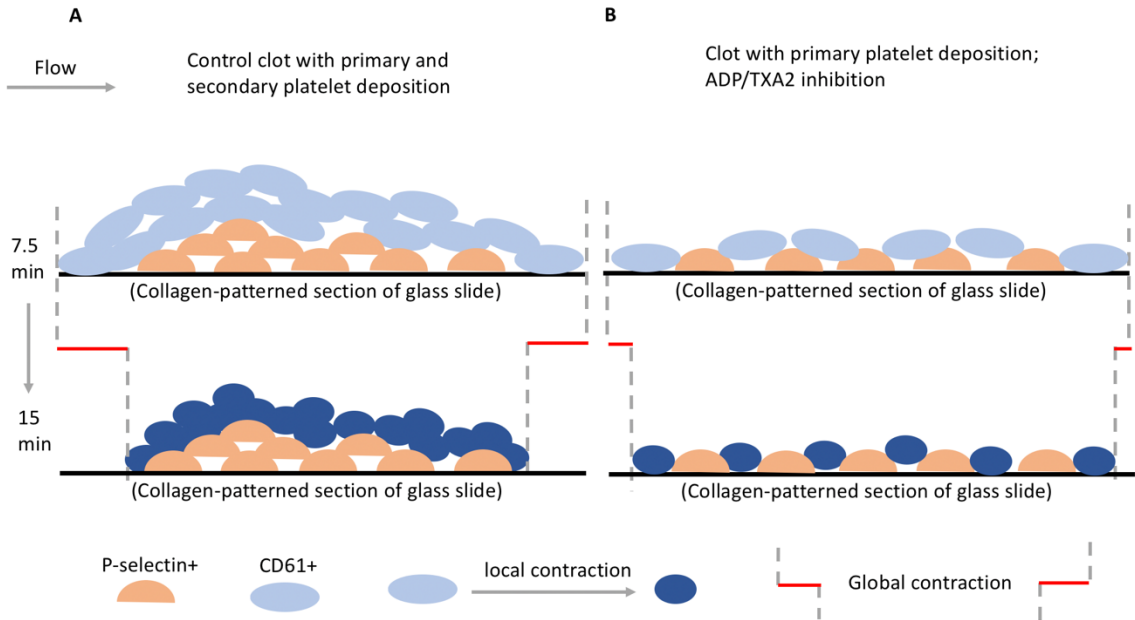


**Figure 3-6. Schematic of clot development and contractile processes under control conditions (A) and with ADP/TXA2 inhibitors present (B).**

### 3.4 Discussion

Clot contraction is a key element of clot resolution, and platelet contractility plays a significant role in contributing to contraction. Using our microfluidic device, we were able to evaluate clot contraction due from platelet contractility on a global and local basis in the presence of ADP and TXA2 inhibitors. To our knowledge, this is the first report evaluating platelet contractility in the presence of ADP and TXA2 inhibitors using microfluidics at a venous shear rate. We found that ASA, 2-MeSAMP, and MRS-2179 had an additive effect in limiting CD61+ platelet deposition, but not with P-selectin+

platelets. P-selectin+ platelet aggregates had limited global and local contraction regardless of ADP or TXA2 inhibition. On the other hand, ADP and TXA2 inhibition seemed to have an additive effect on limiting global contraction of CD61+ platelet aggregates, while TXA2 inhibition, not ADP inhibition, limited local CD61+ aggregate contraction. Lastly, we found that platelet FI correlates with global CD61+ aggregate contraction.

We have summarized these findings in Figure 3-6, which illustrates our understanding of clot contraction in the presence or absence of ADP and TXA2 inhibition. When there was no ADP or TXA2 inhibition, we saw significant CD61+ platelet deposition and P-selectin display at 7.5 min, and then after 7.5 min of flow cessation, CD61+ platelets contracted locally, which contributed to global contraction of CD61+ platelet aggregates. For P-selectin, there was limited local and global contraction. When ADP and TXA2 inhibitors were present, we saw reduced CD61+ platelet deposition and reduced P-selectin+ platelet deposition. We still saw local CD61+ aggregate contraction (which was reduced by TXA2 inhibition), but because there was significantly less CD61+ platelets when ADP and TXA2 inhibitors were present, they were not able to affect global CD61+ aggregate contraction as much.

Our finding that P-selectin+ platelets had limited contractility is in agreement with previous findings [2,16,65]. In the core/shell model of clot heterogeneity, P-selectin+ platelets in the core are more closely packed, while P-selectin(-) platelets in the shell are loosely packed [2,16,65]. It would follow then that P-selectin+ platelets would not be able to contract as much if they are closely packed, compared to CD61+ platelets

in the shell region that are loosely connected and have greater ability to physically contract. We also observed that ADP inhibition and TXA2 inhibition each reduced CD61+ platelet deposition and P-selectin+ platelets in clots. However, we found that the combination of ADP and TXA2 inhibition further reduced CD61+ platelet deposition, while it did not further reduce P-selectin display. This may demonstrate that ADP and TXA2 inhibition had a greater effect on P-selectin(-) shell platelets than on P-selectin+ core platelets. Additionally, P-selectin+ platelets are closer to collagen than shell platelets; ADP and TXA2 inhibition may no longer be effective at reducing P-selectin after a certain point, possibly due from collagen-induced P-selectin display.

We found that ASA limits local CD61+ platelet contraction, while 2-MeSAMP and MRS-2179 did not. While the pharmacological mechanism for this difference should be studied further, it was likely not due from differences in clot morphology, since clots of varying degrees of platelet deposition were included in both +ASA and -ASA conditions (Figure 3-1A and B), and there was a consistent decrease in % local platelet contraction in conditions with ASA compared to conditions without ASA (Figure 3-3B). In terms of global CD61+ platelet contraction, we found that ADP and TXA2 inhibition reduced platelet contraction, which is in agreement with previous findings [49]. We observed a trend where greater platelet deposition generally resulted in greater global platelet contraction, which we confirmed in our data ( $R^2 = 0.87$ ; Fig. 3-4B). While a greater number of platelets can physically limit the ability of a clot to contract, the more platelet-platelet interactions there are, the greater contractile connectivity in the clot. In clots where ADP and TXA2 severely limited CD61+ platelet deposition, there were

reduced platelet-platelet interactions, and as we saw in our results, ultimately less global contraction.

It is important to note this study was limited to evaluating platelet-driven contraction; in addition to platelets, leukocytes and red blood cells (RBCs) can also be found in blood clots. It has been shown that monocytes can aid platelet-driven contraction [66]. In the case of ischemic stroke patients, thrombi with greater leukocyte composition were associated with increased fatality [67]. In contrast to leukocytes, RBCs impair clot contraction [40]. RBCs contracting within a clot have a polyhedron shape, forming a compact array of polyhedral structures [51,68]. In patients with sickle cell disease, impaired clot contraction is due from decreased RBC deformability [69]. Future studies should focus further on evaluating the roles of leukocytes and RBCs on global and local aggregate contraction.

Fibrinogen plays an important role in platelet aggregation. Fibrinogen binds platelets via integrin  $\alpha_{IIb}\beta_3$ , which allows for platelet-platelet interactions. However, fibrinogen has been shown to limit clot contraction [40]. It has also been shown that ischemic stroke patients had higher fibrinogen levels compared to healthy subjects [55]. While fibrinogen was not extensively investigated in this study, it should be studied further for its limiting effect on clot contraction at higher concentrations [40].

Impaired clot contraction has been implicated as a complicating factor in a number of conditions. Clinical correlations based on patient data suggest that impaired clot contraction may be a risk factor for ischemic stroke [55]. Reduced clot contraction



has also been seen in patients with venous thromboembolism [53,54].

Hyperhomocysteinemia, or increased homocysteine levels, causes excessive platelet activation and impairs contraction, making clots larger and more obstructive [70].

Reduced clot contraction in blood of systemic lupus erythematosus patients impairs blood flow and could be a risk factor for increased thrombosis [71]. In sickle cell patients, clots have impaired contraction due to pathological stiffening of RBCs in blood clots [69].

Reduced clot contraction is a pathological risk factor for and is correlated with a number of pro-thrombotic conditions. This study and future studies focused on better understanding clot contraction will help in our ability to better mitigate and resolve these types of pro-thrombotic conditions.

These results demonstrate a necessary balance in platelet deposition and aggregate contraction. For hemostasis to be properly maintained, hyper-activation of platelets must be limited to prevent thrombosis or embolization, but there also must be sufficient platelet deposition to allow for a clot to form and subsequently contract. ADP and TXA2 inhibitors seek to alter this balance by preventing thrombosis, but too much inhibition can result in bleeding. Part of the reason for this potential bleeding, from our results here, could be due from ADP and TXA2 inhibitors' ability to limit clot contraction and clot resolution. Understanding the fundamental mechanisms behind how these inhibitors affect clot contraction has potentially significant clinical benefits in deciding how to treat patients who may require anti-platelet agents.

## **CHAPTER 4: THE EFFECT OF ANTI-GPVI FAB E12 ON PLATELET DEPOSITION AND PHOSPHATIDYLSERINE EXPOSURE**

### **4.1 Introduction**

Glycoprotein VI (GPVI) is a known platelet-specific receptor that binds collagen and subsequently activates platelets [72,73]. Upon initial vessel injury, collagen becomes exposed, allowing for GPVI binding and strong signaling in platelets. This interaction between collagen and platelets is crucial for primary activation and aggregation [74,75], with GPVI as a mediator for this process [76,77]. However, recent reports demonstrate that GPVI may bind with other ligands as well, such as fibrin [72,78]. Thus, GPVI may have a secondary role in clot formation after collagen is covered by platelets, such as mediating platelet recruitment during secondary deposition [79] or contributing to clot contraction caused by fibrin [80].

There are a number of different previous studies that have evaluated GPVI-deficiency in a number of different contexts: using different anti-GPVI antibodies [80–85], indirect inhibition of GPVI on human platelets [86,87], in vivo GPVI-deficient mouse models [88,89], in vitro models with GPVI-deficient mouse blood [72,81–83], models with GPVI-deficient human blood [83,90], testing different surface activating materials [80,90], human atherosclerotic plaque material [80,85], microfluidic venous valve model [84], among others. Dubois, et al. showed a significant decrease in platelet accumulation for GPVI-deficient mouse platelets compared to WT when thrombin was inhibited [88]. However, Mangin, et al. showed that when thrombin is present, this

decrease in platelet accumulation is abolished, leading to the conclusion that thrombin is able to overcome GPVI-deficiency and allow thrombus formation to occur normally [89].

Recent research has been focused on developing a specific inhibitor to GPVI [76]. In previous studies, inhibition of GPVI was mostly achieved through blocking of kinases in subsequent activation pathways, such as inhibition of Src Family Kinases (SFK), spleen tyrosine kinase (Syk) and Bruton's tyrosine kinase (BTK) [86,91–93]. Some of these inhibitors are irreversible, which serves as a “knockout” condition for GPVI. However, this method has its own limitations. These kinases serve more than one role and function downstream of different platelet receptors [94,95]. The recent development of direct inhibition of GPVI, mostly led by Watson [91] and Nieswandt [75,77], alleviates these concerns. Additionally, evaluation of the effects of GPVI inhibition under flow more accurately mimics in vivo dynamics compared to static in vitro assays [76]. To differentiate the role of GPVI at different stages of clot formation under flow, the inhibition of GPVI can be controlled in a microfluidic assay, which is difficult to achieve in vivo and in aggregometry assays [74,86].

Therefore, we aimed to investigate the role of a novel anti-GPVI Fab (the Fab fragment of human GPVI blocking antibody (clone E12)) developed by the Nieswandt research group under hemodynamic conditions using our microfluidic assay. GPVI interaction with fibrin(ogen) has previously been reported to play a role in arterial conditions [80,83]. Lehmann, et al. developed a venous thrombosis model with dimensional similarity to venous valves, showing that GPVI is essential for platelet activation and subsequent thrombus propagation [84]. Thus, GPVI has been shown to

play significant roles in both arterial and venous thrombus formation [96]. However, we limited this study to evaluating E12 under venous conditions rather than arterial, as arterial shear rates can cause clot heterogeneity and increased risk of embolization in our microfluidic model. Studies conducted in this in vitro microfluidic assay have demonstrated that a perfusion-switch experimental design can be used to rapidly change conditions [87], fluids, or shear [97] during experiments, and to study the characteristics of clots at different stages of coagulation. We also utilized confocal microscopy to validate our in vitro microfluidic assay results.

We found that GPVI played a role in primary and secondary platelet deposition, as well as fibrin polymerization, but this role was modulated by the presence of thrombin generation. With thrombin present, anti-GPVI Fab did not limit platelet deposition, as thrombin was the most likely cause of normal platelet deposition. With our perfusion-switch experimental design, we showed that the initial layer of platelets was crucial for clot development, as switching from control to anti-GPVI WB had little to no effect on the clot, while switching from anti-GPVI WB to control WB restored normal clot development. Together, our results demonstrate a deeper understanding of the role GPVI plays in primary and secondary deposition, fibrin polymerization, and PS exposure.

## **4.2 Materials and Methods**

### **Materials**

Reagents were obtained as follows: anti-human CD61 antibody (BD Biosciences, San Jose, CA. Cat#: 555754), Alexa Fluor anti-human CD62P (P-Selectin) Antibody (BioLegend, San Diego, CA. Cat#: 304918), Alexa Fluor 546–conjugated human fibrinogen, Alexa Fluor 488-conjugated annexin V (ThermoFisher Scientific, Waltham, MA. Cat#: A13201), Dade Innovin prothrombin time (PT) reagent (Siemens, Malvern, PA. Cat#: B4212-40), collagen (type I; Chrono-Log, Havertown, PA. Cat#: 385), Sigmacote® (Millipore Sigma, Burlington, MA. Cat#: SL2-100ML), H-Gly-Pro-Arg-Pro-OH (GPRP; Millipore Sigma, Burlington, MA. Cat#: 03-34-0001), GR-144053 (Tocris Biosciences, Bristol, UK. Cat#: 1263), Phe-Pro-Arg-chloromethylketone (PPACK, Haematologic Technologies, Essex Junction, VT. Cat#: FPRCK-01) and corn trypsin inhibitor (CTI, Haematologic Technologies, Essex Junction, VT. Cat#: CTI-01). The Fab fragment of human GPVI blocking antibody (clone E12) was a generous gift from N. Stefano and Dr. B. Nieswandt from University of Würzburg.

### **Preparation and characterization of collagen/TF surface**

Glass slides were rinsed with ethanol, then deionized water, and dried with filtered air. Sigmacote® was used to create a hydrophobic surface on the glass. A volume of 5  $\mu$ L of fibrillar collagen was perfused through a patterning channel (250  $\mu$ m wide  $\times$  60  $\mu$ m high) of a microfluidic device to create a single 250  $\mu$ m-wide strip of fibrillar collagen for all experiments, as previously described [47,64]. For experiments without

thrombin interaction, collagen was rinsed and blocked with 20  $\mu$ L 0.5% bovine serum albumin (BSA) buffer. For experiments that study the effect of thrombin, lipidated TF was absorbed to the collagen surface by perfusing 5  $\mu$ L of Dade Innovin PT reagent (20 nM stock concentration), rinsed and blocked with 20  $\mu$ L 0.5% BSA, then incubated for 30 min without flow, as previously described [47,64].

### **Blood collection and preparation**

Blood was obtained via venipuncture into a syringe containing high concentration of CTI (40  $\mu$ g/mL) from healthy donors who self-reported as free of alcohol use for at least 72 hours and medication for at least a week prior to blood collection. All donors provided informed consent under approval of the University of Pennsylvania Institutional Review Board. Blood was treated with anti-human CD61 antibody (1:50 v/v in whole blood) and Alexa Fluor-conjugated human fibrinogen (1.5 mg/mL stock solution, 1:80 v/v in whole blood) immediately after blood collection for platelet labeling and fibrin labeling, respectively. Annexin V (1:80 v/v in whole blood) was added for PS labeling. Anti-GPVI Fab was added to collected whole blood at a final concentration of 10  $\mu$ g/mL (stock solution 1 mg/mL, dissolved in biology grade water). GPRP (5 mM final concentration in blood) and GR-144053 (1  $\mu$ M final concentration in blood) were both dissolved in Millipore water. All experiments were initiated within 5 min after phlebotomy.

### **Microfluidic clotting assay on collagen surfaces with or without TF**

An 8-channel polydimethylsiloxane (PDMS) flow device was vacuum-sealed perpendicularly to collagen/TF surfaces forming 8 parallel-spaced prothrombotic patches ( $250 \times 250 \mu\text{m}$ ), as previously described [47,64]. The microfluidic device channel height used was  $120 \mu\text{m}$  to prevent occlusion, with an initial wall shear rate of  $100 \text{ s}^{-1}$ . CTI-treated blood was perfused across the 8 channels by withdrawal through a single outlet. Drug-treated blood was added to the inlet reservoir without stopping flow, thus providing a rapid change in perfusion pharmacology within  $< 15 \text{ sec}$  without hemodynamic crosstalk between channels during the perfusion switch. All clotting events were initiated simultaneously in the microfluidic device on the collagen strip. Initial wall shear rate was controlled by a syringe pump (Harvard PHD ULTRA / Harvard PHD 2000; Harvard Apparatus, Holliston, MA) connected to the outlet on the flow device. Platelet, fibrin, and/or PS activities were monitored simultaneously by epifluorescence microscopy (IX81; Olympus America Inc., Center Valley, PA) at 10X magnification. For each set of experiments, blood samples from  $N \geq 3$  donors were taken, unless otherwise specified. Additionally, each clot was extremely well localized on the  $250 \mu\text{m} \times 250 \mu\text{m}$  collagen patch and contained tens of thousands of platelets, ideal for obtaining whole clot fluorescence intensities (i.e. total clot mass) with time. Images were captured with a charged coupled device camera (Hamamatsu, Bridgewater, NJ) and were analyzed with ImageJ software (National Institutes of Health). To avoid side-wall effects, fluorescence values were taken only from the central 75% of the channel.

## **Confocal Microscopy**

To determine the 3-dimensional orientation of platelets, fibrin, and PS exposure, we utilized confocal microscopy to develop images of the clots in the microfluidic device. For confocal images, all clots imaged were formed under high CTI WB perfused over collagen/TF ( $100\text{s}^{-1}$ ) for 7.5 min. After 7.5 minutes of WB perfusion, WB was switched with BSA (+ 5mM  $\text{CaCl}_2$ ) and perfused for about 2 minutes to clear out any remaining blood in the channels. After BSA perfusion, any remaining BSA (+ 5mM  $\text{CaCl}_2$ ) in the wells was replaced with 4% paraformaldehyde (+ 5mM  $\text{CaCl}_2$ ) and perfused for about 2 minutes to fix clots and prevent contraction. After 2 minutes of perfusion with 4% paraformaldehyde (+ 5mM  $\text{CaCl}_2$ ), perfusion was stopped and devices were transferred to the confocal microscope, with clots still maintained in the 8-channel microfluidic device. Z-stack images were taken of fixed clots using the Leica TCS SP8 laser scanning confocal microscope at the CDB Microscopy Core at the University of Pennsylvania. Images were compiled to form a 3D rendering of a clot endpoint in ImageJ.



### 4.3 Results

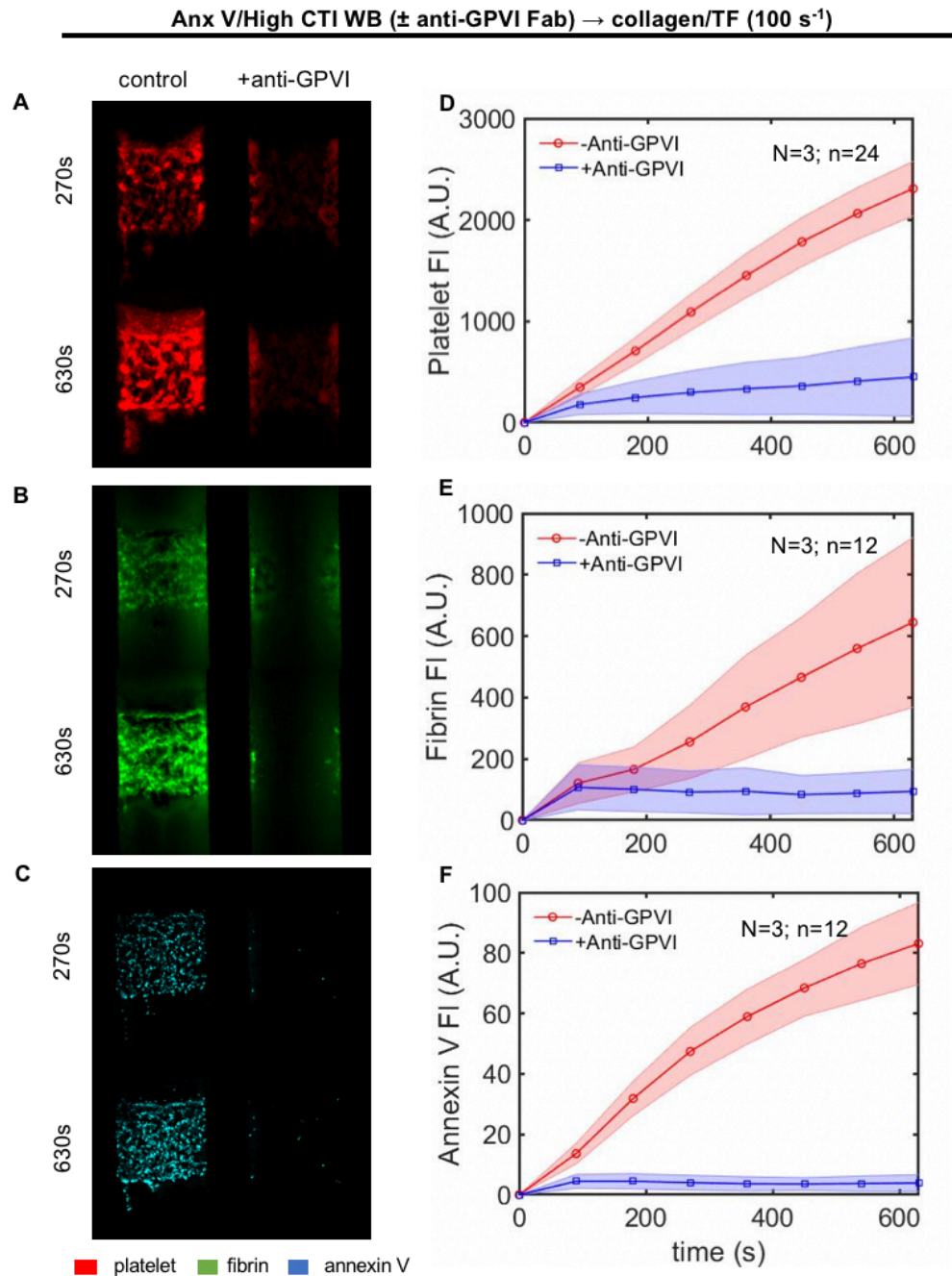


**Figure 4-1. Inhibition of GPVI shows significant decrease in PS exposure.**

High CTI WB with and without anti-GPVI Fab was perfused over collagen/TF at  $100 \text{ s}^{-1}$  for 10.5 minutes. CD61, fluorescent fibrinogen, and annexin V fluorophores were added to label platelets (A), fibrin (B), and PS exposure (C), respectively, with images taken at 270s and 630s. Fluorescence intensities for platelets (D), fibrin (E), and annexin V (F) were measured throughout the course of the experiments. (A.U. = arbitrary units)

**Anti-GPVI Fab inhibits fibrin polymerization and PS exposure in clot development when added at t=0**

To investigate the role of anti-GPVI in PS exposure, we perfused CTI-treated WB  $\pm$  anti-GPVI Fab over collagen/TF ( $100\text{s}^{-1}$ ) looking at platelet, fibrin, and phosphatidylserine (PS) fluorescence. We observed normal platelet deposition in control and limited platelet deposition from the initial stages of clot development with anti-GPVI Fab present (Fig. 4-1A, 4-1D), and normal fibrin polymerization in control and limited fibrin polymerization with anti-GPVI Fab (Fig. 4-1B, 4-1E). Compared to control, we saw essentially no PS exposure when anti-GPVI Fab is present (Fig. 4-1C, 4-1F).

Anx V/High CTI WB ( $\pm$  GR-144053, GPRP, or anti-GPVI Fab)  $\rightarrow$  collagen/TF ( $100 \text{ s}^{-1}$ )

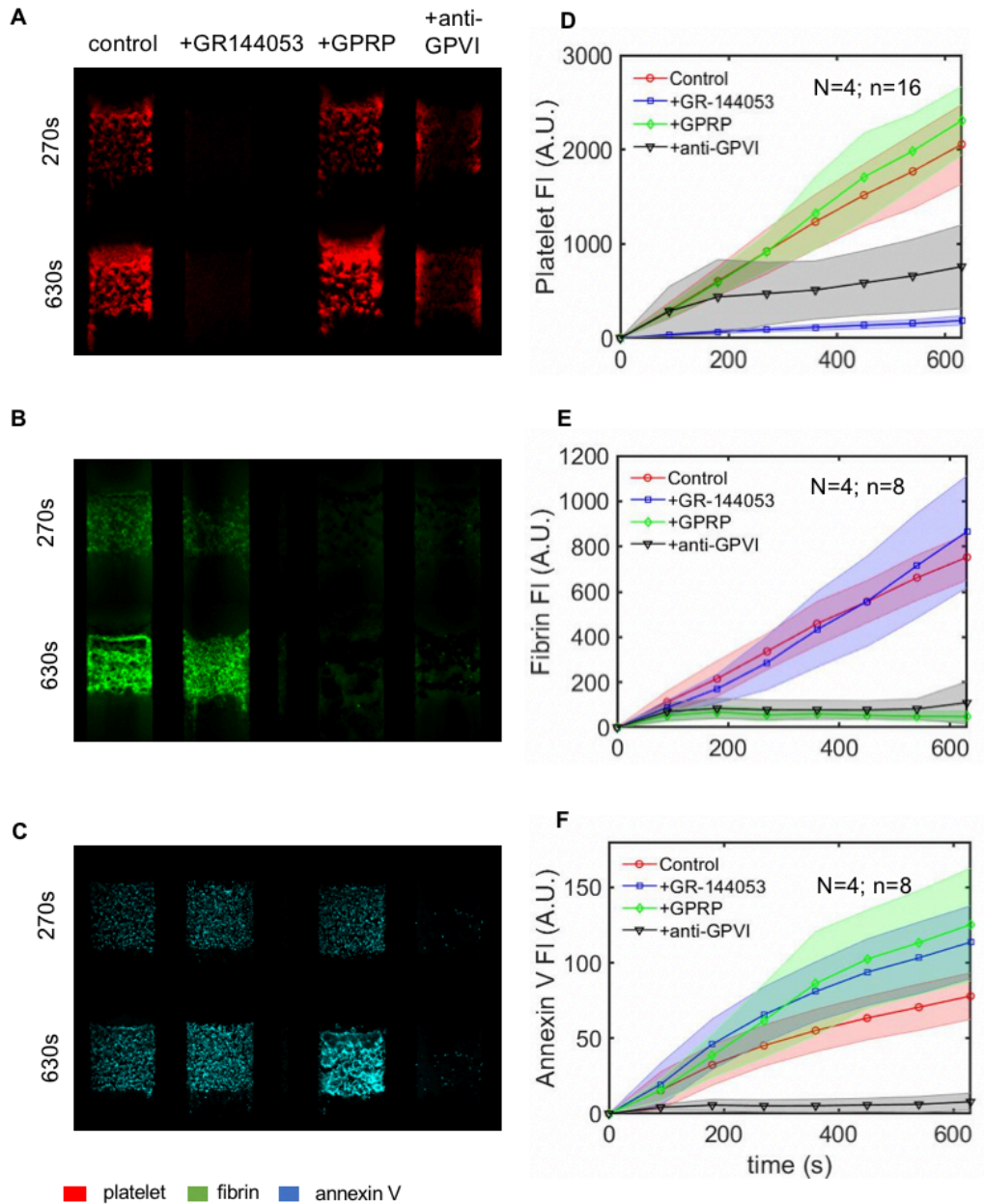


**Figure 4-2. Decrease in annexin V in the presence of anti-GPVI is due from anti-GPVI, not limited platelet deposition or fibrin polymerization.**

High CTI WB with control (HBS), GR-144053, GPRP, or anti-GPVI Fab, was perfused over collagen/TF at  $100 \text{ s}^{-1}$  for 10.5 minutes. CD61, fluorescent fibrinogen, and annexin V fluorophores were added to label platelets (A), fibrin (B), and PS exposure (C), respectively, with images taken at 270s and 630s.

Fluorescence intensities for platelets (D), fibrin (E), and annexin V (F) were measured throughout the course of the experiments. (A.U. = arbitrary units)

We then wanted to validate that the limited PS exposure in anti-GPVI channels was indeed due from anti-GPVI Fab rather than limited platelet deposition or fibrin polymerization. To do this, we compared annexin V FI in the presence of anti-GPVI Fab, GR-144053, or GPRP. GR-144053 inhibits integrin  $\alpha_{IIb}\beta_3$ , thereby preventing platelet-platelet interactions and results in a platelet monolayer [98]. We perfused CTI-treated WB  $\pm$  GR-144053, GPRP, or anti-GPVI Fab over collagen/TF at an initial wall shear rate of  $100\text{s}^{-1}$ . Platelet deposition was normal in control and GPRP, while there was reduced platelet deposition in anti-GPVI, and only a platelet monolayer in GR-144053 (Fig. 4-2A, 4-2D). Fibrin levels were normal in control and GR-144053, while there was little to no fibrin in GPRP or anti-GPVI (Fig. 4-2B, 4-2E). We observed slightly increased PS exposure with GR-144053 or GPRP compared to control, while anti-GPVI Fab once again had essentially no PS exposure (Fig. 4-2C, 4-2F).

Anx V/High CTI WB ( $\pm$  anti-GPVI Fab @ 0s, 30s, or 90s)  $\rightarrow$  collagen/TF ( $100 \text{ s}^{-1}$ )

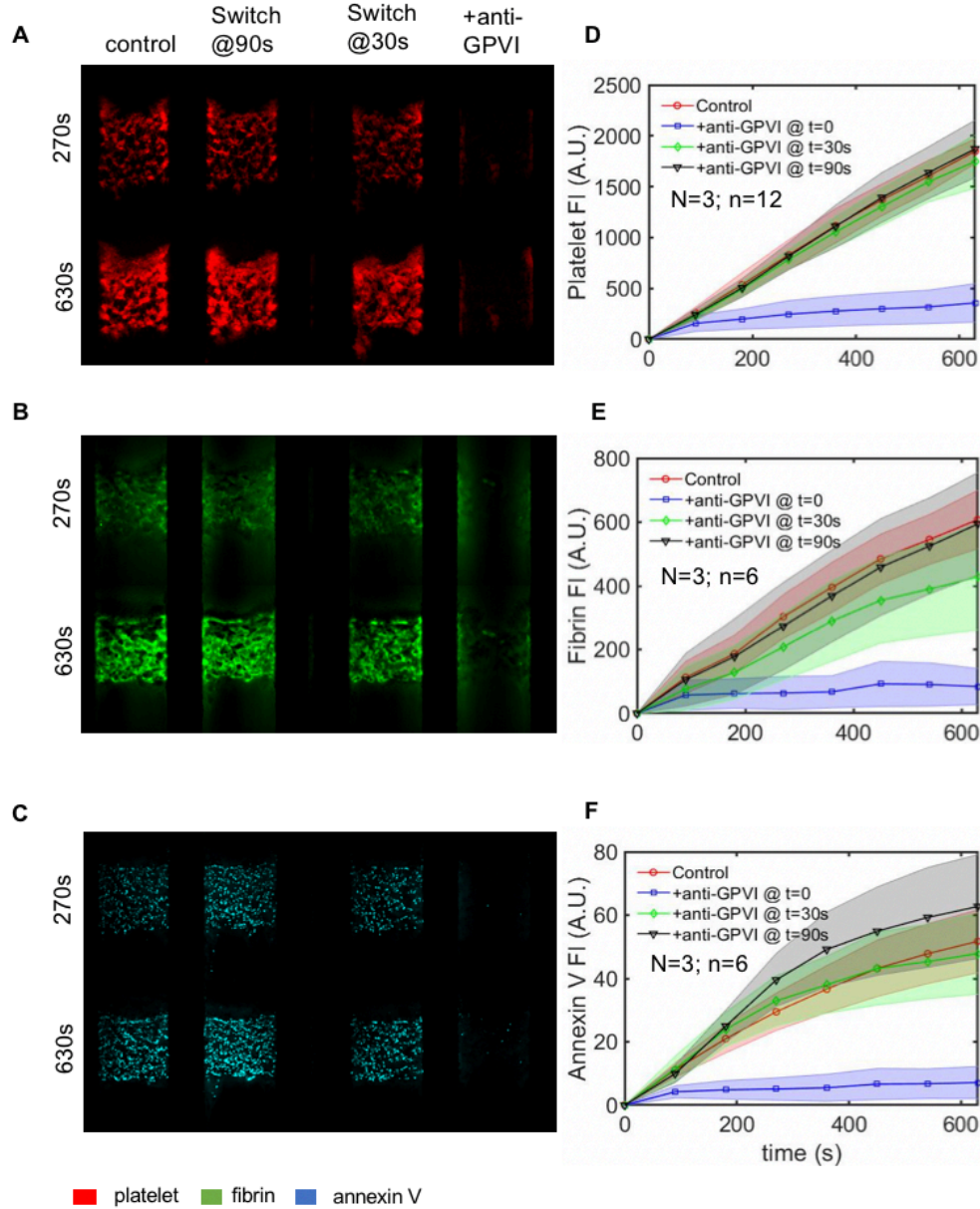


**Figure 4-3. Effects of anti-GPVI Fab require its presence from the initiation of clot development in the presence of thrombin.**

High CTI WB with or without anti-GPVI Fab was perfused over collagen/TF at  $100 \text{ s}^{-1}$  for 10.5 minutes. The two middle channels started with control WB perfusion, with a switch to anti-GPVI WB at either 30s or 90s. CD61, fluorescent fibrinogen, and annexin V fluorophores were added to label platelets (A), fibrin (B), and PS exposure (C), respectively, with images taken at 270s and 630s. Fluorescence intensities for platelets (D), fibrin (E), and annexin V (F) were measured throughout the course of the experiments. (A.U. = arbitrary units)

**Anti-GPVI Fab has little to no effect on platelet deposition, fibrin polymerization, or PS exposure when added after  $t=0s$**

We next investigated the effect of anti-GPVI Fab addition at different time points to determine if early or later inhibition of GPVI affected PS exposure. We perfused CTI-treated WB under 4 different conditions: (1) control WB with no switch, (2) control WB at 0s, followed by a switch to anti-GPVI WB at 30s, (3) control WB at 0s, followed by a switch to anti-GPVI WB at 90s, and (4) anti-GPVI WB with no switch. We found that platelet deposition was similar in conditions (1), (2), and (3) throughout the experiment (Fig. 4-3A, 4-3D), illustrating that anti-GPVI Fab had little to no effect on platelet deposition when control blood was present from the start. Fibrin polymerization was also similar among conditions (1), (2), and (3) throughout the experiment (Fig. 4-3B, 4-3E), also illustrating that anti-GPVI Fab had little to no effect on fibrin polymerization when control blood was present initially. In terms of PS exposure, annexin V binding was fairly similar between conditions (1), (2), and (3), while there was essentially no PS exposure in anti-GPVI Fab at  $t = 0s$  condition (4) (Fig. 4-3C, 4-3F). These results demonstrate that when control WB was initially present to all platelet interactions with collagen, GPVI signaling, and thrombin generation, the addition of anti-GPVI Fab at later time points had little to no effect on platelet deposition, fibrin polymerization, and PS exposure.



Anx V/High CTI WB + anti-GPVI ( $\pm$  control @ 0s, 90s, or 270s)  $\rightarrow$  collagen/TF ( $100 \text{ s}^{-1}$ )

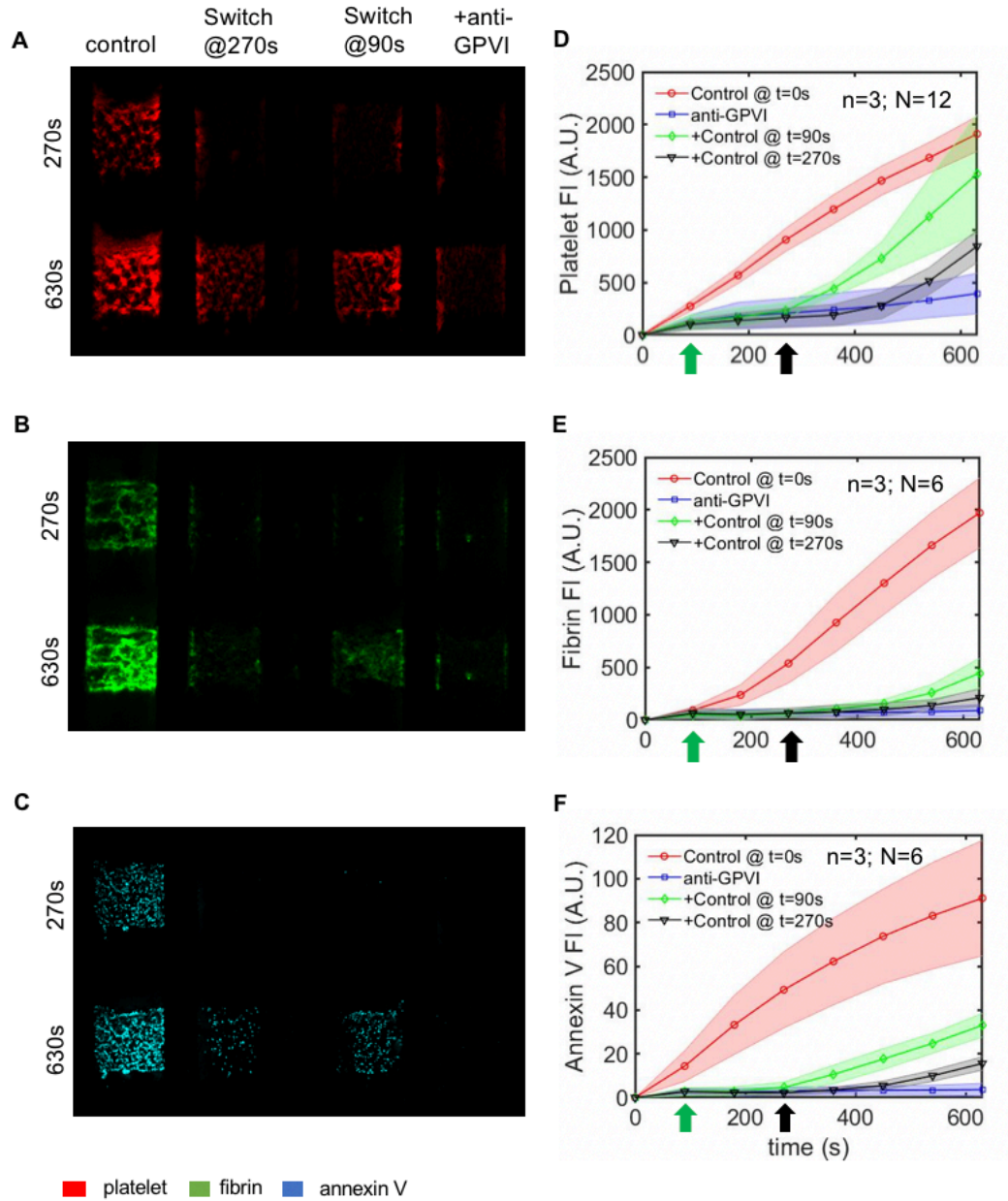


**Figure 4-4. Effects of anti-GPVI Fab on clot development are reversible.**

High CTI WB with or without anti-GPVI Fab was perfused over collagen/TF at  $100 \text{ s}^{-1}$  for 10.5 minutes. The two middle channels started with anti-GPVI WB perfusion, with a switch to control WB at either 90s or 270s. CD61, fluorescent fibrinogen, and annexin V fluorophores were added to label platelets (A), fibrin (B), and PS exposure (C), respectively, with images taken at 270s and 630s. Fluorescence intensities for platelets (D), fibrin (E), and annexin V (F) were measured throughout the course of the experiments. The green arrows in FI plots indicate when 90s switches occur and black arrows indicate when 270s switches occur (A.U. = arbitrary units)

**The effects of anti-GPVI Fab are reversible for platelet deposition, fibrin polymerization, and PS exposure when switched to control blood**

Lastly, we wanted to evaluate the effect of switching from anti-GPVI Fab-treated WB back to control WB lacking Fab. We perfused CTI-treated WB again under 4 conditions: (1) control WB with no switch, (2) anti-GPVI WB at  $t=0s$ , followed by a switch to control WB at 90s, (3) anti-GPVI WB at  $t=0s$ , followed by a switch to control WB at 270s, and (4) anti-GPVI WB with no switch. Platelet deposition in condition (1) formed normally, while there was limited platelet deposition in anti-GPVI condition (4) (Fig. 4-4A, 4-4D). In the switch conditions, both conditions initially had limited platelet deposition, but after about 180s post-switch, there was a significant increase in platelet levels in both conditions relative to condition (4). There were statistical differences in final fluorescence values between conditions (2) and (4) ( $p = 0.0032$ ) and between conditions (3) and (4) ( $p=0.0014$ ). After platelets levels began increasing in the switch channels, the platelet clot morphology was restored back to control conditions. In terms of fibrin fluorescence, we again observed normal fibrin formation in condition (1) and essentially no fibrin formation in condition (4), as expected and as previously shown. In the switch channels, there was essentially no fibrin polymerization throughout nearly the entirety of the experiment, except at the very end where there was a slight increase in fibrin (Fig. 4-4B, 4-4E). Even still, these slight increases were found to be statistically significant compared to anti-GPVI; there were statistical differences in final fibrin fluorescence between conditions (2) and (4) ( $p=0.0009$ ) and between conditions (3) and



(4) ( $p=0.017$ ). Lastly, annexin V levels were normal in condition (1) and essentially negligible in condition (4), again in agreement with previous results. In the switch conditions, annexin V was negligible initially, as expected, and then eventually increased after the switch to control WB (Fig. 4-4C, 4-4F). Again, there were statistical differences in final annexin V fluorescence between conditions (2) and (4) and between conditions (3) and (4) (both  $p<0.0001$ ). There was again an approximate 180s time lag between the switch and when annexin V levels began increasing in both conditions. This is in line with the platelet restoration time lag.

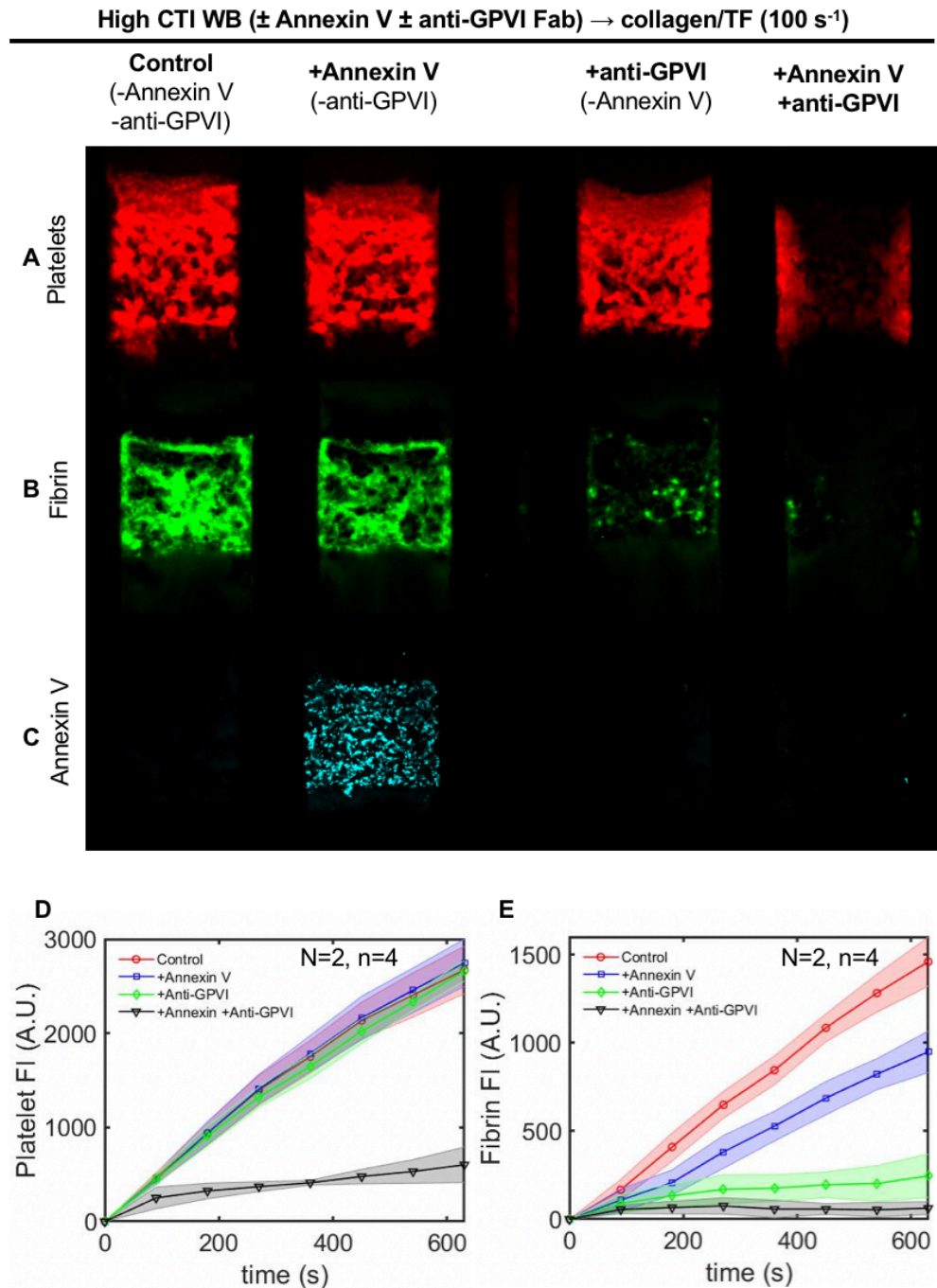


**Figure 4-5. Annexin V and anti-GPVI Fab have additive effect on limiting platelet deposition.** High CTI WB, with and without annexin V and anti-GPVI, was perfused over collagen/TF at  $100 \text{ s}^{-1}$  for 10.5 min. CD61, fluorescent fibrinogen, and annexin V fluorophores were added for platelets (A), fibrin (B), and PS exposure (C). Annexin V was not added in channels with (-annexin V). Representative images were taken at the end of the experiment (10.5 min). Fluorophores were measured throughout the course of the experiment for platelet fluorescence (D) and fibrin fluorescence (E). Representative data are from 2 individual donors ( $N = 2$ ) and 4 individual clots ( $n = 4$ ). (A.U. = arbitrary units).

### **The combination of annexin V and anti-GPVI Fab significantly impedes platelet deposition in CTI-treated WB perfused over collagen/TF**

We wanted to further evaluate the effect of anti-GPVI Fab and annexin V on PS exposure in clot development. Annexin V binds to exposed PS on the surface of platelets; as a result, this annexin V binding may prevent PS on the platelet surface from fully contributing to platelet procoagulant activity, and ultimately delaying and/or lowering fibrin generation [99]. We have previously shown this to be the case in our assay, where annexin V contributed to a delay in fibrin formation compared to when annexin V was absent [52]. To investigate the effect of annexin V in the presence of anti-GPVI Fab on clot development, we perfused CTI-treated WB with anti-GPVI alone, with annexin V alone, or with both anti-GPVI Fab and annexin V, over collagen/TF ( $100 \text{ s}^{-1}$ ) (Fig. 4-5A-C). Results showed that anti-GPVI or annexin V alone had almost no effect on platelet deposition (Fig. 4-5A, 4-5D). Annexin V channels had a slight delay and decrease in fibrin polymerization (in agreement with ref. [52]), while anti-GPVI Fab channels showed inhibition of fibrin polymerization (Fig. 4-5B, 4-5E). However, when both anti-GPVI Fab and annexin V were present, there was a striking decrease in platelet deposition (Fig. 4-5A, 4-5D). Fibrin deposition was also reduced in the presence of both anti-GPVI Fab and annexin V, resulting in levels slightly lower than anti-GPVI Fab alone (Fig. 4-5D), all consistent with strong collagen signaling via GPVI along with thrombin enhancing the procoagulant activity of platelets.

(A) Bottom view (on coverslip). (B) Top view. (C) Side view. (D) Outlet view. (E) Slice of clot view with orthogonal slices pointed out. (F) Vertical orthogonal slice. (G) Horizontal orthogonal slice.

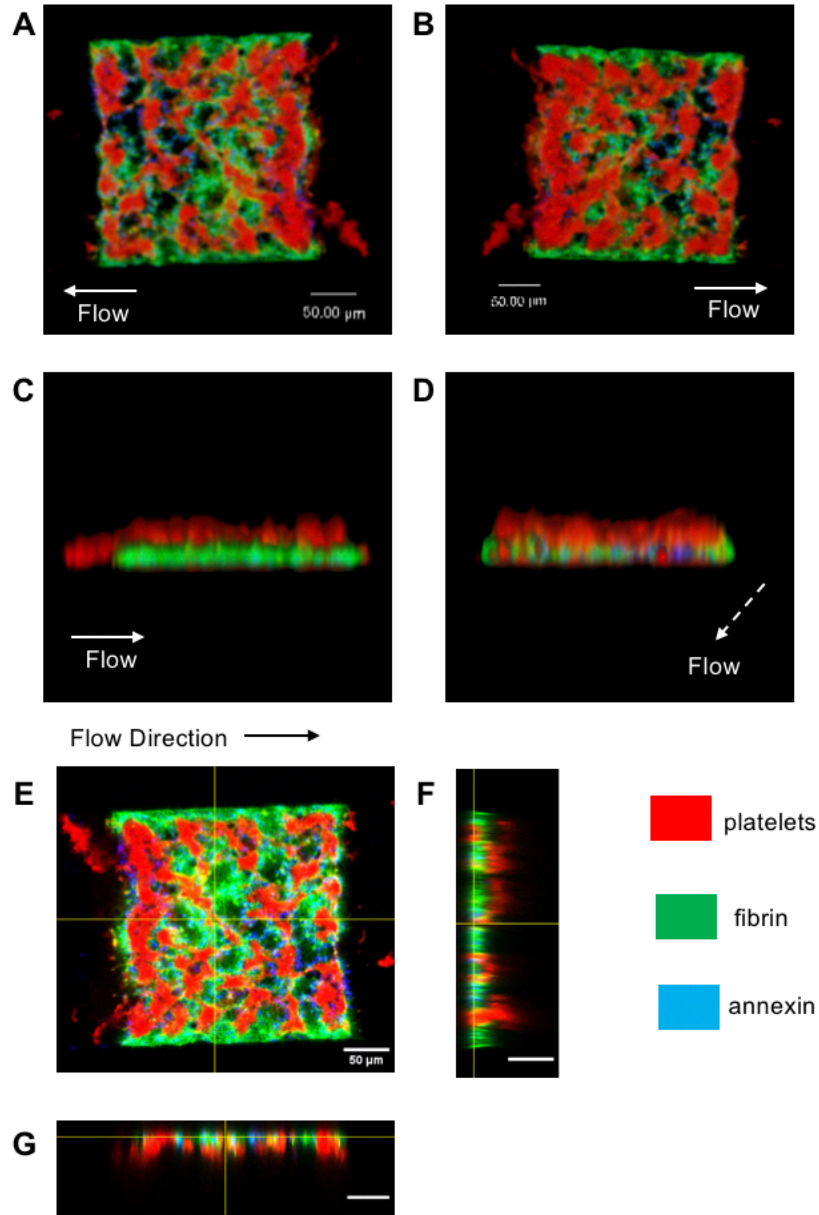


**Figure 4-6. Representative 3D images of clot end point.**

Z-stack images were taken of preserved clots on a confocal microscope to determine the distribution of platelets (red), fibrin (green) and annexin V (blue). (A) Bottom view of clot (on coverslip). (B) Top view of clot. (C) Clot side view. (D) Clot outlet view. (E) Single z plane image of clot with orthogonal slices pointed out (yellow lines). (F) Vertical orthogonal slice from wall to wall of microfluidic device channel. (G) Horizontal orthogonal slice from clot inlet to clot outlet.

### **Confocal microscopy confirms fibrin and PS exposure are localized to collagen surface, while platelet deposition occurs throughout the clot thickness**

Confocal images show an example clot from the bottom view (Fig. 4-6A), top view (Fig. 4-6B), side view (Fig. 4-6C), and outlet view (Fig. 4-6D). These images illustrate that fibrin and annexin V were predominantly localized near the collagen surface, while platelets were distributed throughout the clot, most clearly visible at the top layer of the clot. We also took example orthogonal slices of the clot (Fig. 4-6E-G) to further illustrate the localization of fibrin and PS exposure at the collagen surface.

## **4.4 Discussion**

We performed a series of in vitro experiments with human blood using a novel, direct GPVI inhibitor to demonstrate the role GPVI plays in primary and secondary platelet deposition and fibrin polymerization. We observed that anti-GPVI Fab significantly reduced annexin V fluorescence nearly to background levels. To confirm this was due from anti-GPVI Fab rather than reduced platelet aggregation or fibrin inhibition, we compared the annexin V signals of anti-GPVI, GR-144053, and GPRP in the presence of thrombin. We saw that platelet monolayers (via treatment with GR-144053) and fibrin inhibition (via treatment with GPRP) resulted in similar or increased annexin V fluorescence, while annexin V fluorescence in the anti-GPVI condition remained near background levels. This demonstrated the potent effect of anti-GPVI and

annexin V in limiting PS exposure. To better understand this synergistic effect, we performed two experiments to evaluate annexin V fluorescence: (1) switching from control blood to anti-GPVI blood, and (2) switching from anti-GPVI blood to control blood. When control blood was present at the beginning of the experiment, platelet deposition, fibrin polymerization, and PS exposure occurred normally, even when anti-GPVI Fab was present as early as 30s. When anti-GPVI blood was present at the beginning of the experiment, but there was a switch to control blood, platelets, fibrin, and annexin V slowly began to increase after the switch. This demonstrated that the effects of anti-GPVI Fab were reversible, while anti-GPVI Fab was not effective (in the presence of thrombin) when it first became present after control clotting had already been initiated.

There was a synergistic effect of inhibition of GPVI and inhibition of exposed PS on lowering platelet deposition in clot development. Increased PS exposure in GR-144053 compared to control further demonstrated the significance of collagen in stimulating PS exposure, since essentially all platelets in GR-144053 were bound and stimulated via collagen. Increased PS exposure in the presence of GPRP compared to control demonstrated the role of freely available thrombin to contribute to PS exposure, and we have previously shown this before [52]. Therefore, when collagen interactions were inhibited by anti-GPVI Fab and freely available thrombin was reduced by annexin V, it follows that there was very little measurable PS exposure. Our results support the significant role for thrombin generated via PS exposure in stimulating platelet deposition and continued buildup when GPVI is inhibited. Since annexin V binds exposed PS on the platelet surface [100,101], and PS allows for formation of the prothrombinase complex

for conversion of prothrombin to thrombin catalyzed by Factor Xa [102], annexin V binding to PS may have reduced the generation of thrombin at the beginning of the clot growth, thus resulting in limited platelet stimulation via thrombin. Blocking collagen binding and inhibiting thrombin generation are both crucial for attenuating subsequent platelet deposition.

In our perfusion-switch experiments with annexin V present, our results in Figure 4-4 suggest that the time lag between the switch and increase in platelet fluorescence may have consisted of the removal of GPVI-inhibited platelets with control platelets. In addition, the time lag for fibrin formation to be restored took longer than for platelet deposition, which is logical since platelet deposition precedes fibrin polymerization in control conditions, and is in agreement with thrombin kinetics [45,80]. These results suggest switching from anti-GPVI WB to control WB nearly allowed for clot restoration in terms of platelet deposition and morphology, fibrin polymerization, and PS exposure. This was not the case when control WB was switched to anti-GPVI WB, where we saw platelet deposition, fibrin polymerization, and annexin V remained similar to control throughout the experiment (Fig. 4-3).

Many of our findings are consistent with previous studies investigating GPVI deficiency/inhibition. Munnix, et al. studied the effects of an anti-GPVI JAQ1 Fab on platelet deposition and PS exposure in PPACK-treated WB over collagen, and in citrated mouse blood (+CaCl<sub>2</sub> +TF) over collagen at 1000s<sup>-1</sup> [81]. They also observed a significant decrease in annexin V exposure with JAQ1, similar to what was observed with E12 (Fig. 4-1). However, they also observed a decrease in platelet deposition with JAQ1

in the presence of thrombin [81], while we did not see this change in platelet deposition when E12 was added without annexin V present (Fig. 4-5). The reason for this should be studied further to better understand why E12 does not cause a decrease in platelet deposition in the presence of thrombin.

We have shown that with thrombin present, anti-GPVI did not limit platelet deposition, as thrombin was the most likely cause of normal platelet deposition. With our perfusion-switch experimental design, we showed that the initial layer of platelets was crucial for clot development, as switching from control to anti-GPVI WB had little to no effect on the clot, while switching from anti-GPVI WB to control WB restored normal clot development. Together, our results demonstrate a deeper understanding of the role GPVI plays in primary and secondary platelet deposition, fibrin polymerization, and PS exposure.



## CHAPTER 5: FUTURE WORK

### 5.1 Further investigation of PS<sup>+</sup> platelet sorting in clot development

There are a number of further studies that can and should be performed to further our understanding of PS<sup>+</sup> platelet sorting in clots. First, in vivo studies would be particularly useful to see how different anti-coagulant agents may affect this PS<sup>+</sup> platelet sorting phenomenon. Nechipurenko, et al. [28] performed some in vivo studies that observed localization of procoagulant platelets at the clot periphery, but these were limited to mostly images as opposed to quantitative data. Testing anti-coagulants like direct thrombin inhibitors or FXa inhibitors, or accelerating fibrinolysis by exogenous addition of tPA, in an in vivo mouse model would be useful to see if our findings here are robustly observable.

Additionally, studying the effects of blebbistatin in vitro and in vivo would be useful. Blebbistatin is a non-muscle myosin II inhibitor [103,104], which limits internal platelet contraction. Samson, et al. [30] showed that blebbistatin had a potent limiting effect on clot contraction over a 120-minute period. In our microfluidic model, the time frame for clot development is generally from 15-20 minutes, which could make it difficult to observe the effects of blebbistatin in a relatively shorter time frame. However, it could be interesting to see how clots further develop and contract over time once flow has stopped. In future experiments, perfusing CTI-treated WB with and without blebbistatin for 15 minutes, followed by a 2 hour stop flow period to observe contraction, would be useful to determine if blebbistatin prevents PS<sup>+</sup> platelet sorting, which would be

consistent with the observation by Nechipurenko, et al. that non-muscle myosin-deficient mouse blood does not display PS<sup>+</sup> platelet sorting [28].

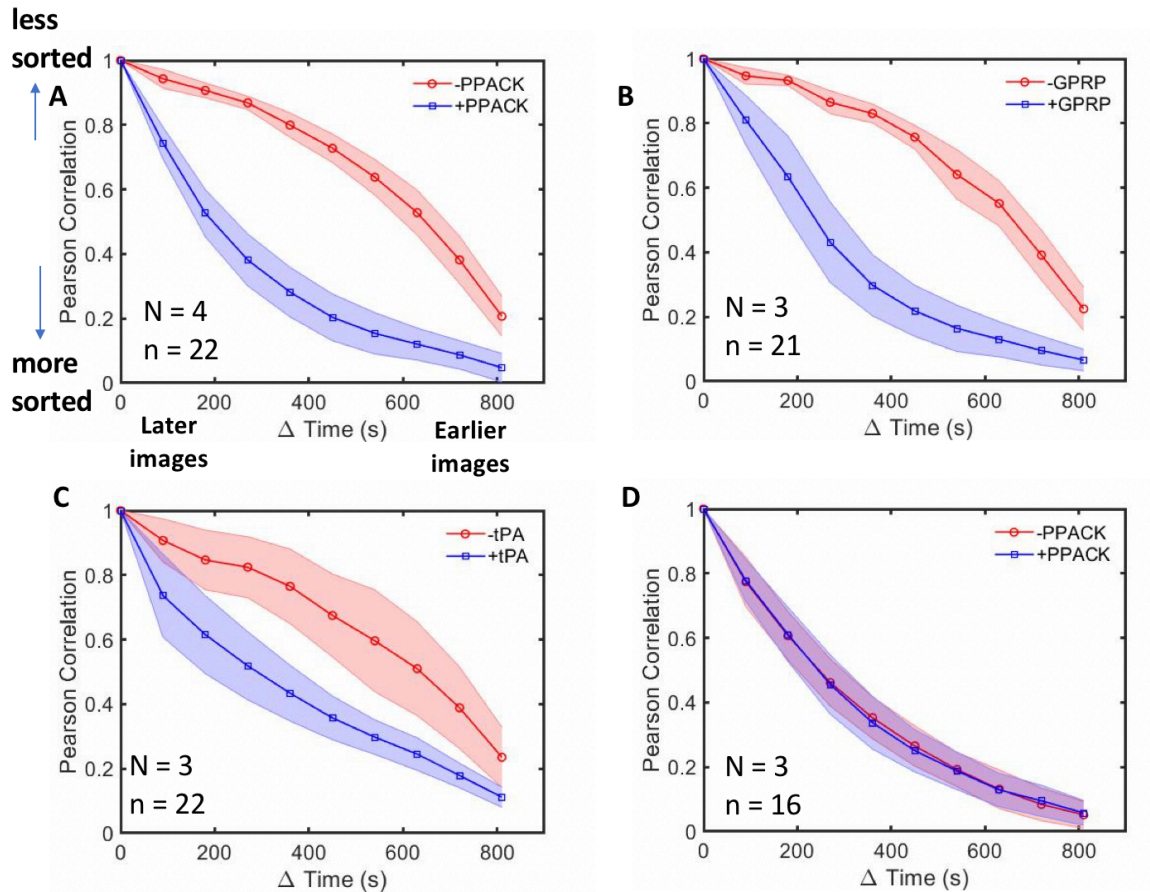


**Figure 5-1. Pearson correlation coefficients of annexin V fluorescence between final clot image (at 15 minutes) and clot image at varying time points among all conditions tested.**

In our experiments, we used Pearson correlation coefficients of annexin V at 9 minutes and 15 minutes. Here, we graphed Pearson correlation coefficient values between the final clot image of annexin V (at 15 minutes) compared to images of annexin V at different time points. Thus, the Pearson correlation coefficient of 9 minutes and 15 minutes would correspond to a time gap of 360s (on the x-axis). However, Pearson correlation coefficients may be chosen between the final image (at 15 minutes) and an image at some other time point (other than 9 minutes). This data here illustrates what those Pearson correlation coefficients would be for PPACK experiments (A), GPRP experiments (B), tPA experiments (C), and PPACK control (no TF) experiments (D).

Lastly, further optimization of the autocorrelation and Pearson correlation metrics could be useful to further distinguish more minute differences in PS sorting that may be observed. For example, Pearson correlation coefficients can be measured at varying time points, as illustrated in Figure 5-1. Here, we measured the Pearson correlation coefficient between 15 minutes and each other image throughout the time course of the experiment. You can see that as the difference in time between images increased, the Pearson correlation decreased, which indicates a change in PS fluorescence distribution. However, we can see for +PPACK, +GPRP, and +tPA conditions, their Pearson correlation coefficient decreased at a much quicker pace compared to control conditions (-PPACK, -GPRP, and -tPA) as the time between images increased. This type of analysis helped us choose a Pearson correlation coefficient of 9 minutes vs. 15 minutes in our analysis, as the differences in Pearson correlation coefficients between  $\pm$ PPACK,  $\pm$ GPRP,  $\pm$ tPA conditions were well pronounced.

We could perform a similar analysis for the autocorrelation metric. Autocorrelation metric values were calculated using a truncated matrix of values (Supp. Fig. S2-3); however, the exact size of this truncated matrix can vary. Further analyses of an optimal truncation size could help to further optimize the autocorrelation metric as a tool to measure heterogeneities in clots. We could also investigate cross correlation values between CD61 fluorescence images and annexin V among different conditions. As PS<sup>+</sup> platelets move to the periphery of platelet masses with fibrin inhibited, conditions with fibrin inhibition may have greater cross correlation between CD61 and annexin V compared to conditions with fibrin present. This would be another useful way to

potentially illustrate the differences between PS sorting in the presence and absence of fibrin.

## **5.2 Evaluating the effects of secondary platelet inhibition on clot contraction**

To expand upon our investigation of ADP and TXA2 inhibition on clot contraction, there are a number of additional studies that could be performed. First, studying a wider variety of ADP and TXA2 inhibitors, or other secondary platelet aggregation inhibitors, would be useful to further analyze different methods of preventing platelet aggregation, and global and local aggregate contraction. Next, studying ADP and TXA2 inhibition in the presence of thrombin and fibrin would be especially important. While our focus here was trying to understand how platelet-platelet interactions affect clot development, under normal conditions, fibrin formation occurs. It is important to understand how inhibition of secondary platelet aggregation affects local and global clot contraction when fibrin is present. To do so, we can perfuse CTI-treated WB  $\pm$ ADP and TXA2 inhibitors over collagen/TF to investigate contraction with thrombin and fibrin present. We can also perfuse CTI-treated WB + GPRP  $\pm$ ADP and TXA2 inhibitors over collagen/TF to investigate contraction with thrombin present, but fibrin still inhibited.

In the future, it would also be insightful to test patient blood to determine how contraction occurs in non-healthy donor blood. Patients who are on anti-platelet or anti-coagulant regimens with a range of dosages would be interesting to analyze. Our observations thus far have been based on data obtained from healthy donors who are medication-free. Ultimately though, patient blood (inhibiting ADP and TXA2

production) would be especially important to see how their blood contracts. It would also be interesting to apply our global and local aggregate contraction measurements to blood of trauma patients. It has been shown that trauma patients exhibit lower than normal platelet contractility, and that severe trauma patients exhibit even lower platelet contractility [49]. In the future, using our global and local aggregate contraction measurements to study blood of trauma patients and its contractile ability may be able to provide further insight into how or in what way blood from trauma patients is less contractile than blood from healthy donors.

Lastly, I would like to further investigate, and potentially further optimize our global and local aggregate measurements. In our experiments, we use 250  $\mu\text{m}$  x 250 $\mu\text{m}$  collagen patches to study clot contraction. However, in vivo, clot formation could vary in size greatly. It would be interesting to see how global and local contraction compares to each other based on clot size. In the future, we could pattern a collagen strip that is thinner or wider, and/or utilize a microfluidic device with a thinner or wider channel width, thereby allowing us to make collagen patches of varying sizes. It would also be useful to further investigate ways of optimizing global and local contraction. For example, the global aggregate contraction algorithm utilizes 5 lines drawn in the middle portion of the clot (Supp. Fig. S3-2). However, we could look to include the middle 10, 20, 50, or 100 lines, for example, to see if this would improve the accuracy of contraction measurements among different clots within the same condition (among the same donor and among different donors).

### 5.3 Further evaluation of anti-GPVI Fab E12 and the role of PS exposure in propagating platelet deposition

High CTI WB  $\pm$ anti-GPVI with switch to PPACK  $\pm$ anti-GPVI @ 90s, 270s, 540s  $\rightarrow$  collagen/TF ( $100 \text{ s}^{-1}$ )

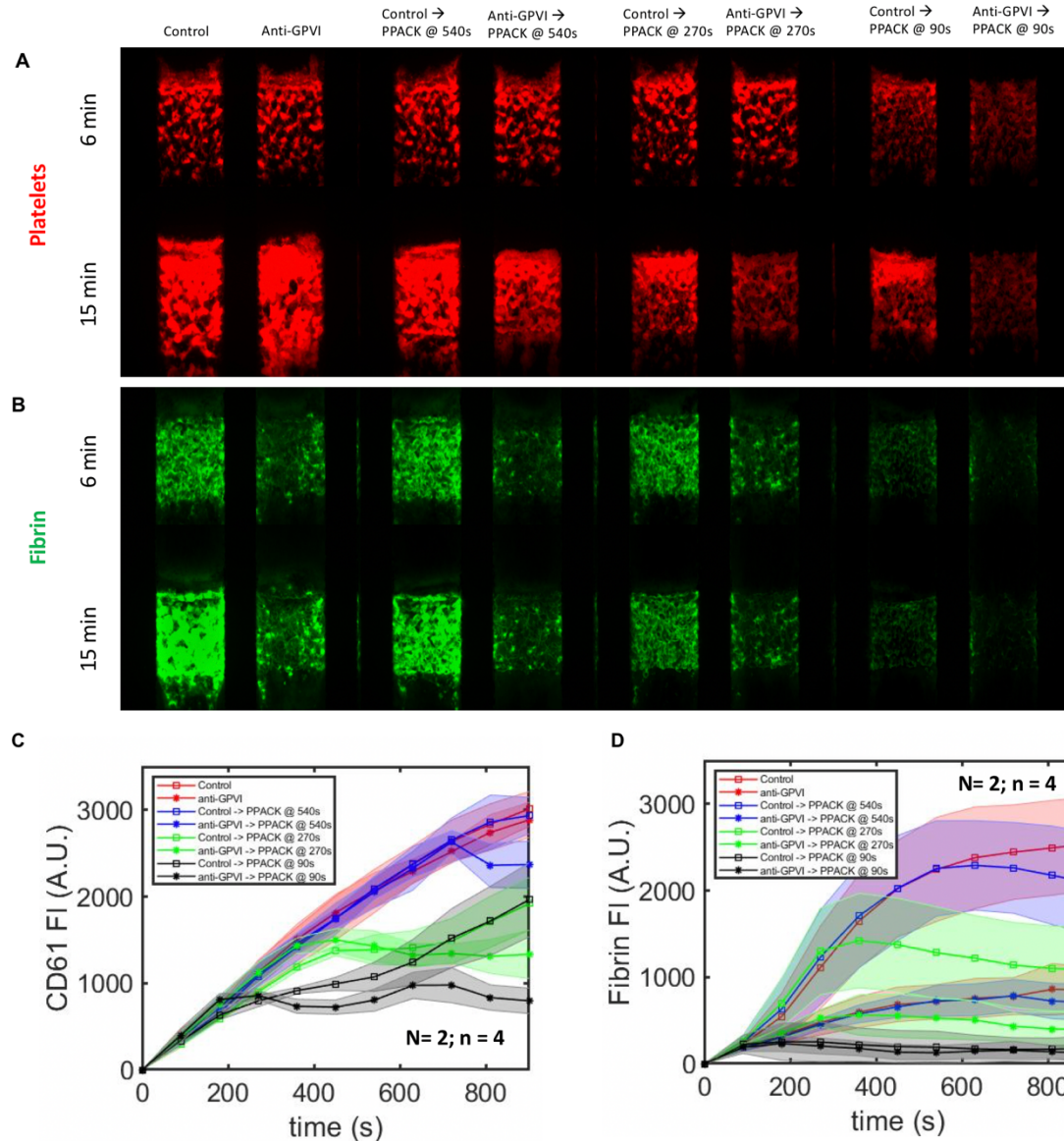


**Figure 5-2. Time-sequential inhibition of thrombin demonstrated varying anti-GPVI potency on platelet deposition and fibrin deposition.**

We perfused CTI-treated WB  $\pm$ anti-GPVI (no annexin V) over collagen/TF for 15 minutes at an initial wall shear rate of  $100 \text{ s}^{-1}$ , with a switch to PPACK-treated WB  $\pm$ anti-GPVI at either 90s, 270s, or 540s. The presence (or absence) of anti-GPVI remained consistent in each channel throughout the experiment, while the switch changed each condition from CTI-treated WB to PPACK-treated WB. We added CD61 fluorophore to label for platelets (A), and fluorescent fibrinogen to label for fibrin (B). We measured fluorescence intensity values for platelets (C) and fibrin (D) over the course of the experiment. (A.U. = arbitrary units)

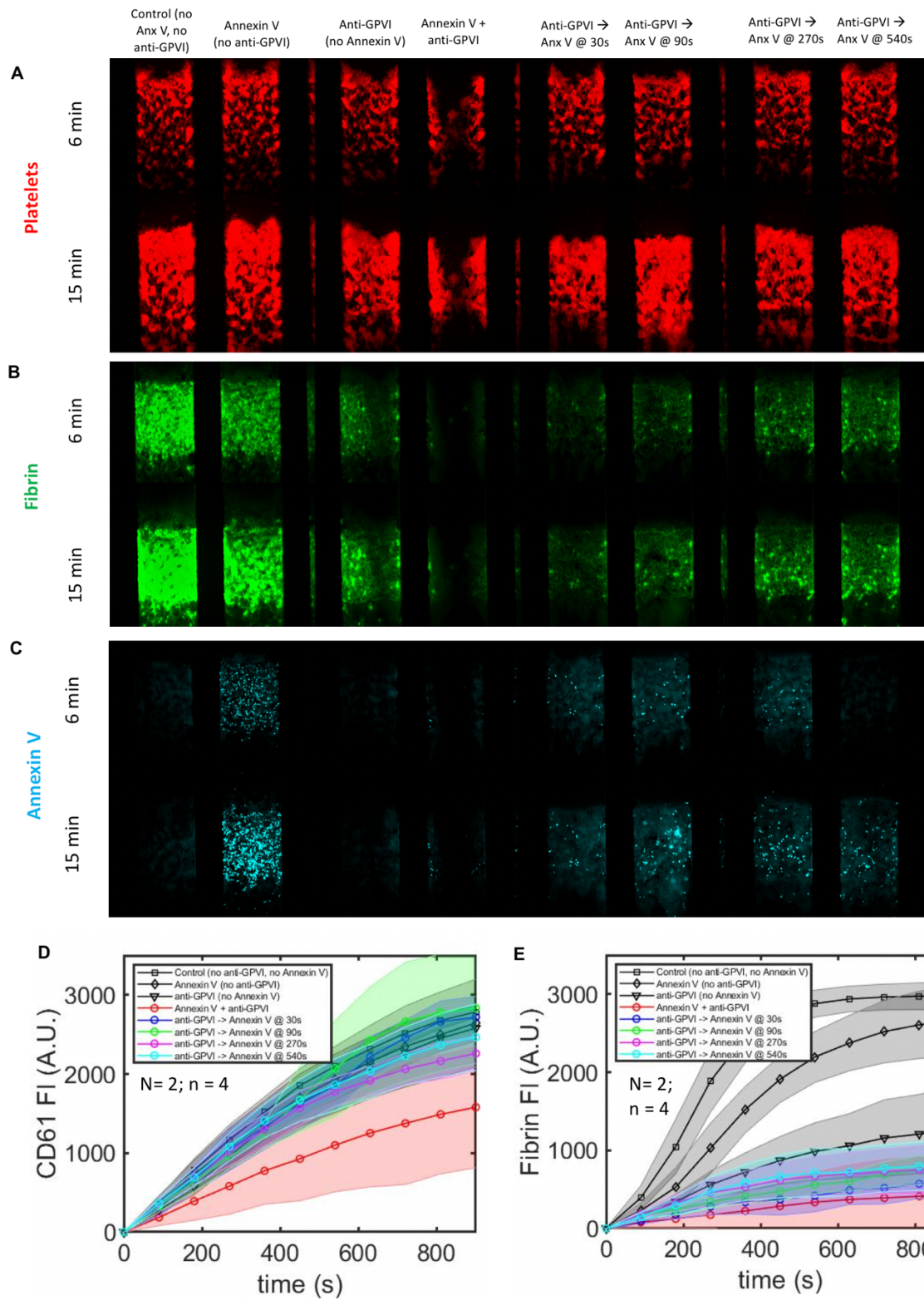
There are a number of further experiments we could perform with anti-GPVI Fab E12 to elucidate its effects on clot development. We showed that when anti-GPVI and annexin V were added in combination from  $t=0s$ , there was significantly reduced platelet deposition (Fig. 4-5); we also showed that when we added anti-GPVI at later times ( $t=30s$  or  $90s$ ), normal platelet deposition still occurred. However, it would be useful to see how inhibiting thrombin at different points in time may affect platelet deposition. We performed a preliminary experiment where we ran CTI-treated WB  $\pm$ anti-GPVI (no annexin V) with a switch to PPACK-treated WB  $\pm$ anti-GPVI at either  $90s$ ,  $270s$ , or  $540s$  (Fig. 5-2). The presence (or absence) of anti-GPVI remained consistent in each channel throughout the experiment, while the switched channels changed each condition from CTI-treated WB to PPACK-treated WB. This allowed us to see how and when thrombin affects the potency of anti-GPVI Fab on platelet deposition. In channels where there was no switch, we observed little difference in platelet deposition between control and anti-GPVI conditions (Fig. 5-2A, C), although there was a significant reduction in fibrin polymerization in anti-GPVI channels (Fig. 5-2B, D), as previously shown in Figure 4-5.

In channels where there was a switch to PPACK-treated WB, the timing of the switch seemed to play a significant role in affecting platelet deposition and fibrin polymerization. Switching at  $90s$  from CTI-treated WB to PPACK-treated WB resulted in a limited and comparable fibrin polymerization for both control and anti-GPVI conditions (Fig. 5-2B, D). However, the  $90s$  switch significantly reduced platelet deposition in anti-GPVI channels compared to control and compared to no switch anti-

GPVI (Fig. 5-2A, C). This showed that, in the presence of anti-GPVI, when thrombin was no longer available to contribute to platelet activation, platelet deposition was reduced. Additionally, in the 90s switch conditions, the control channel had higher platelet FI by the end of the experiment compared to anti-GPVI. This demonstrated the combination of anti-GPVI and thrombin inhibition significantly limited platelet deposition. For switch channels at 270s or 540s, we saw a gradual decrease in fibrin deposition after the switch in both control and anti-GPVI conditions, although fibrin was greater in control compared to anti-GPVI at the switch. In terms of platelet deposition for the 270s and 540s switch conditions, platelet deposition looked similar between control and anti-GPVI up until the switch. After the switch, anti-GPVI channels had a gradual (270s) or slight (540s) reduction in platelet FI compared to control. These results, when considered with Figures 4-3 and 4-4, show the significance of thrombin in allowing for fibrin formation and platelet deposition in the presence of anti-GPVI. Notably, when thrombin was present from  $t=0s$  and anti-GPVI Fab was added at later time points, there was little to no effect on platelet, fibrin, or annexin V FI (Fig. 4-3); when anti-GPVI was present from  $t=0s$  and thrombin inhibitor was added at later times points, there was a significant effect on platelet deposition and fibrin polymerization.



High CTI WB  $\pm$  anti-GPVI  $\pm$  Annexin V with switch to Annexin V @ 90s, 270s, 540s  $\rightarrow$  collagen/TF (100 s<sup>-1</sup>)



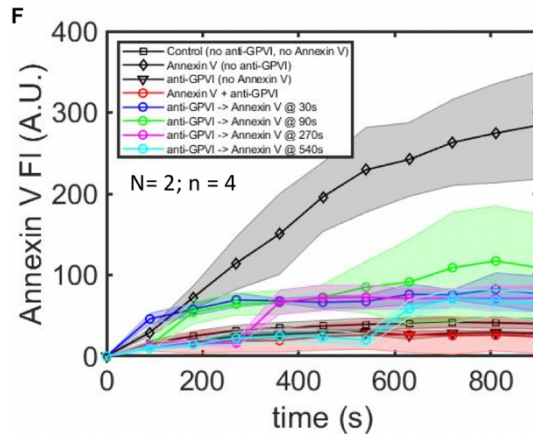


**Figure 5-3. Time-sequential addition of annexin V in the presence of anti-GPVI had little effect on platelet deposition or PS exposure, but a minimal effect on fibrin deposition.**

We perfused CTI-treated WB  $\pm$ anti-GPVI  $\pm$ annexin V over collagen/TF for 15 minutes at an initial wall shear rate of  $100\text{s}^{-1}$ , with a switch to +annexin V at either 30s, 90s, 270s, or 540s. The presence (or absence) of anti-GPVI remained consistent in each channel throughout the experiment, while switch channels went from +anti-GPVI -annexin V to +anti-GPVI +annexin V. We added CD61 fluorophore to label for platelets (A), fluorescent fibrinogen to label for fibrin (B), and annexin V to label for PS exposure (C). We measured fluorescence intensity values for platelets (D), fibrin (E), and annexin V (F) over the course of the experiment. (A.U. = arbitrary units)

We showed in Figure 4-5 that when annexin V or anti-GPVI Fab were added individually, they each had no significant effect on platelet deposition, but when added in combination, they significantly limited platelet deposition. To further understand this effect, it would be helpful to determine if the combination of annexin V and anti-GPVI still has this limiting effect when one is added at a later time point. We investigated adding anti-GPVI Fab at later time points with annexin V present from  $t=0\text{s}$  in Figure 4-3. Here, in preliminary results, we investigated adding annexin V at later time points with anti-GPVI present from  $t=0\text{s}$  (Fig. 5-3). The left four channels mimicked conditions in Fig. 4-5 (Fig. 5-3A, B, C), while the right four channels started with anti-GPVI Fab present at  $t=0\text{s}$ , with annexin V added at either 30s, 90s, 270s, or 540s. We saw that when

annexin V was added at later time points (after  $t=0s$ ), platelet deposition was comparable to control, annexin V alone, or anti-GPVI alone, while anti-GPVI + annexin V ( $t=0s$ ) showed reduced platelet deposition. In terms of fibrin, channels that added annexin V at later times had slightly increased fibrin deposition; however, fibrin FI remained at or below levels in anti-GPVI (no annexin V) channels. Fibrin FI for anti-GPVI + annexin V ( $t=540s$ ) was comparable to fibrin FI for anti-GPVI (no annexin V), while fibrin FI was lower for anti-GPVI + annexin V ( $t=30s$ ) and anti-GPVI + annexin V ( $t=0s$ ), which were similar in value. Annexin V levels for switch channels were much closer to anti-GPVI + annexin V ( $t=0s$ ) channels than to annexin V (no anti-GPVI) channels, regardless of switch time. Annexin V levels were slightly higher for switch channels compared to anti-GPVI + annexin V ( $t=0s$ ), likely because background subtraction of initial,  $t=0s$  images did not have annexin V fluorophore in the switch channels; thus the slight increase in annexin V levels in switch channels (compared to anti-GPVI + annexin V @  $t=0s$ ), while minimal, was likely due from background noise.

High CTI WB  $\pm$  switch to Annexin V @ 90s, 270s, 540s  $\rightarrow$  collagen/TF ( $100 \text{ s}^{-1}$ )

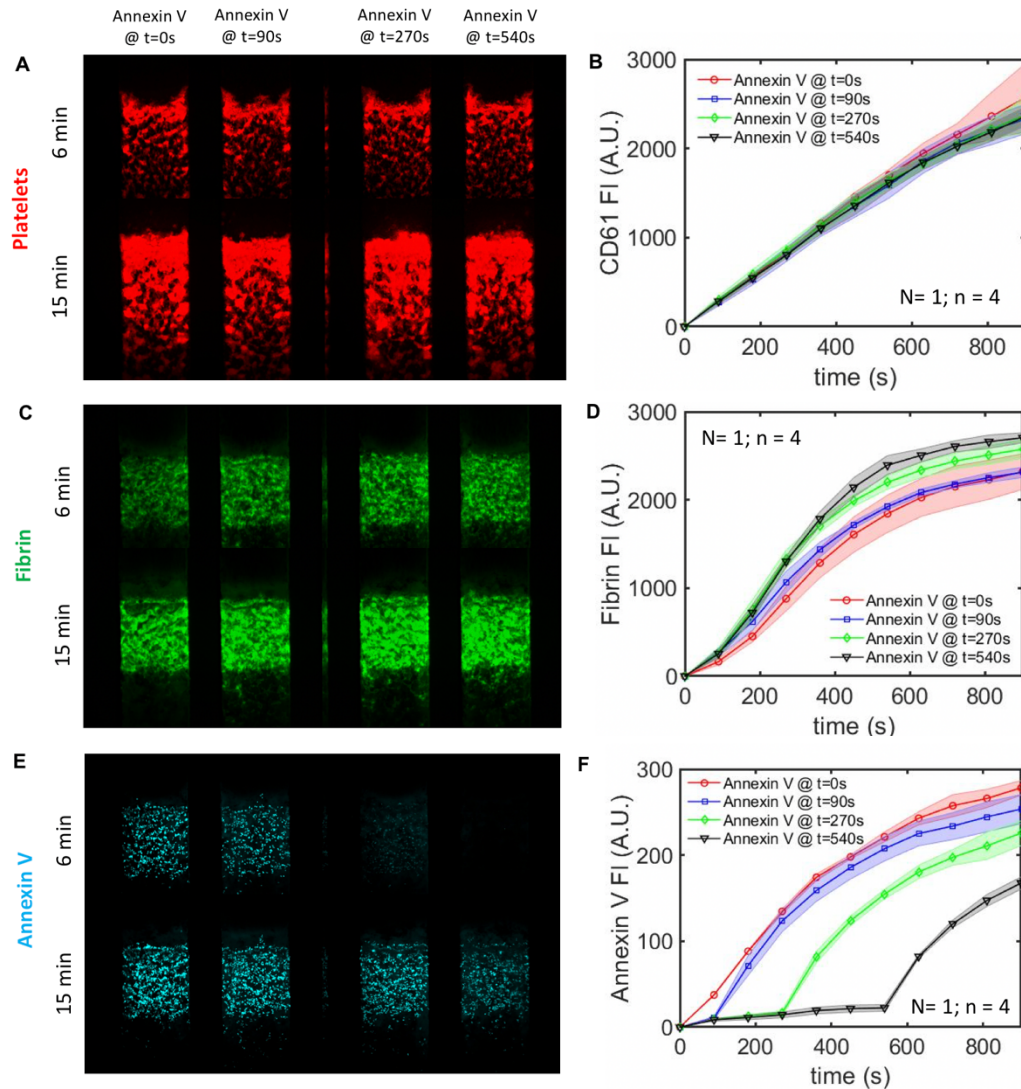


**Figure 5-4. Annexin V has a slight inhibitory effect on fibrin deposition.**

We perfused CTI-treated WB  $\pm$  a switch to annexin V at either 90s, 270s, or 540s over collagen/TF at an initial wall shear rate of  $100 \text{ s}^{-1}$ . We added CD61 fluorophore to label for platelets (A), fluorescent fibrinogen to label for fibrin (C), and annexin V to label for PS exposure (E). We measured fluorescence intensity values for platelets (B), fibrin (D), and annexin V (F) over the course of the experiment. (A.U. = arbitrary units)

Lastly, we demonstrated in Chapter 2 (Supplemental Fig. S2-1) that annexin V has a slight inhibitory effect on fibrin. While we believe this was likely because PS was blocked by annexin V to prevent further propagation of thrombin and subsequent fibrin

polymerization, it would be helpful to further elucidate why and how this occurred. In a preliminary study, we looked at adding annexin V to CTI-treated WB at different time points to see if or how annexin V affects fibrin polymerization throughout the experiment (Fig. 5-4). We perfused CTI-treated WB  $\pm$  switch to annexin V at 90s, 270s, or 540s over collagen/TF at an initial wall shear rate of  $100\text{s}^{-1}$ . We had a control channel with annexin V from  $t=0\text{s}$  (no switch). Across all conditions, we observed no significant differences in platelet deposition (Fig. 5-4A, B). In terms of fibrin polymerization, there were slight deviations between each condition, with annexin V @  $t=0\text{s}$  and annexin V @  $t=90\text{s}$  having the lowest values, followed by annexin V @  $t=270\text{s}$ , and finally annexin V @  $t=540\text{s}$  had the highest fibrin FI. This was in agreement with our earlier results (Supp. Fig. S2-1), but expanded upon the results to show that annexin V can still have slight, albeit observable, effects on fibrin polymerization when added after  $t=0\text{s}$ . Lastly, as expected, annexin V FI values varied greatly between different conditions, since this was entirely dependent on when annexin V was added to different channels.

We have described a handful of experiments here that aim to further clarify the effect of anti-GPVI Fab (especially in combination with annexin V) on platelet deposition, fibrin polymerization, and PS exposure. However, further research, both in our microfluidic device described here, as well as other experimental designs, should be considered to better our understanding of this anti-GPVI Fab E12.

## **APPENDICES**

### **Appendix A: Chapter 2**

#### **Supplemental Methods**

#### **Reagents and Materials**

The following reagents were obtained and kept at the appropriate conditions in accordance with the vendor's instructions: corn trypsin inhibitor (CTI), Phe-Pro-Arg-chloromethylketone (PPACK), H-Gly-Pro-Arg-Pro-OH (GPRP; EMD Millipore, Burlington, MA), recombinant human tissue plasminogen activator (tPA; Abcam, Cambridge, MA), Sigmacote (Sigma, St. Louis, MO), type I fibrillar collagen (Chrono-log, Havertown, PA), tissue factor (TF; Siemens, Malvern, PA). Fluorophores included anti-human CD61 antibody (BD Biosciences, San Jose, CA), AF647 human fibrinogen (Haematologic Technologies, Essex Junction, VT), AF488-conjugated annexin V monoclonal antibody (Thermo Fischer, Waltham, MA).

#### **Blood collection**

Blood donors were self-reported as medication-free for at least 7 days prior to blood collection. All blood draws were done with the use of a high concentration of CTI (40  $\mu\text{g/ml}$ ) to ensure inhibition of contact pathway-induced coagulation. All donors consented in accordance with the University of Pennsylvania Institutional Review Board and the declaration of Helsinki. Fluorophores were added as needed in the following concentrations: anti-CD61 antibody (1:50 v/v dilution), AF647 fibrinogen (1:80 v/v

dilution), AF488 annexin V (1:80 v/v dilution). Additional reagents were added as needed in the following concentrations: PPACK (10 mM stock solution, 1:100 v/v dilution), GPRP (100 mM stock, 1:20 v/v dilution), tPA (1.3 mg/ml stock solution; 30 nM final concentration).

### **Preparation of collagen/TF on glass slide**

Glass slides were first rinsed with ethanol, then dried using filtered air. Sigmacote was then added to glass slides; slides were then rinsed with deionized water and dried. A patterning device was vacuum-sealed to the glass slide. For slides without TF, 5  $\mu$ L of collagen was perfused through the patterning device; 20  $\mu$ L of 0.5% Bovine Serum Albumin (BSA) was then placed on top of both the inlet and outlet ports to incubate for 30 minutes. For slides with TF, 5  $\mu$ L of collagen was perfused through the patterning device, 5  $\mu$ L of TF was then perfused through the patterning device, then 20  $\mu$ L of 0.5% BSA was placed on top of both the inlet and outlet ports to incubate for 30 minutes. After 30 minutes, BSA at the outlet was removed, and the remaining BSA at the inlet port was perfused through the patterning device. Patterning devices were removed, leaving a 250- $\mu$ m wide collagen ( $\pm$ TF) strip.

### **Fluorescence Intensity vs. time**

In order to show fluorescence intensity (FI) of fluorophores (CD61, fluorescent fibrinogen, or annexin V) over time, images of each clot were uploaded and compiled into a time sequence (stack) in ImageJ. The initial image (at  $t = 0$ s) was subtracted from the stack of images to subtract any background fluorescence. A rectangular area

(approximately 2/3 of the central area of the clot) was used to calculate FI in the stack for each fluorophore in each clot. FI values were then exported to Matlab where plots were made with FI values vs. time. Plots were made as average  $\pm$  standard deviation for FI values over time.

### **Autocorrelation metric calculations for PS spatial sorting**

We first input a 150  $\mu\text{m}$  x 150  $\mu\text{m}$  image (corresponding to a 233 x 233 matrix of pixel values) of the final (15-minute) annexin V FI for each condition into Matlab. This matrix of pixel values was then converted to a zero-mean matrix of pixel values by subtracting the matrix average from each matrix element. This was done in order to maximize the values of high fluorescence overlay and low fluorescence overlay between the matrices. This matrix was used to calculate the autocorrelation matrix, which was then truncated and summed to yield an autocorrelation metric.

### **Pearson correlation coefficient calculations for PS temporal sorting**

Images at 9 minutes and 15 minutes for a particular clot were taken at the same size (150  $\mu\text{m}$  x 150  $\mu\text{m}$ ), so both matrices were the same size in Matlab and corresponded to the same location in space in the clot. The 15-minute images were the same images used in the autocorrelation metric calculations.

### **Statistical Analyses**

Statistical differences with p-values between conditions were calculated using unpaired Welch's t-tests in GraphPad (ns signifies  $p > 0.05$ ).



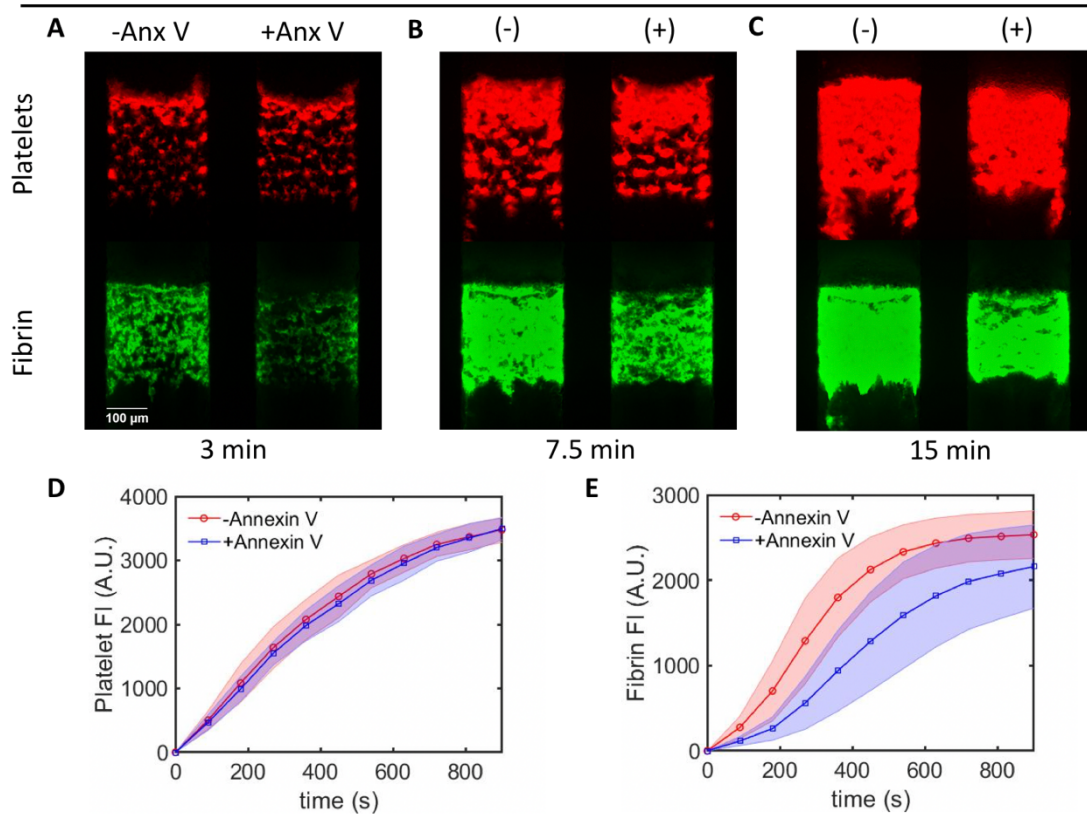
## Supplementary Results

We investigated the role of platelet integrin  $\alpha_{IIb}\beta_3$  on PS sorting. We inhibited  $\alpha_{IIb}\beta_3$  with GR-144053 (GR). We perfused high CTI WB + GR over collagen or collagen/TF. The GR prevented secondary platelet deposition as expected, resulting in a sparse monolayer of platelets bound directly to the collagen. In the presence of TF, we observed fibrin formation in the presence or absence of GR. However, we observed relatively little PS sorting in the +GR condition, regardless of the presence or absence of fibrin. This was expected since the platelets were sparse and unable to make sufficient platelet-platelet contacts and adherent platelets were firmly bound to collagen.

## Supplemental Figures

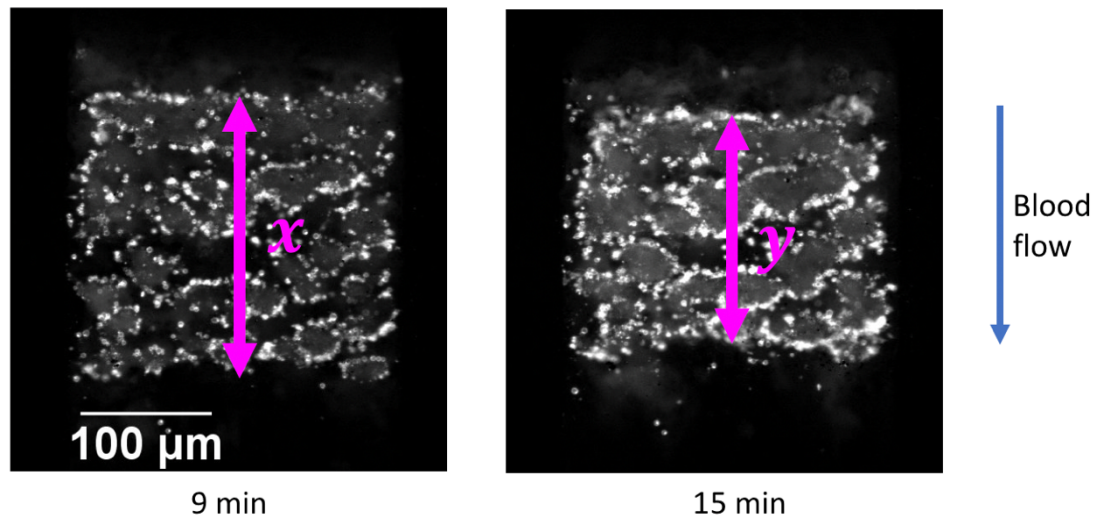
High CTI WB ( $\pm$  annexin V)  $\rightarrow$  collagen/TF ( $100\text{ s}^{-1}$ )

N = 3; n = 21



### Supplemental Figure S2-1. Annexin V has a slight inhibitory effect on fibrin formation.

High CTI WB was perfused with and without annexin V over collagen/TF at an initial shear rate of  $100\text{ s}^{-1}$ . CD61 and fluorescent fibrinogen were both added to label platelets and fibrin, respectively. Images of clots were taken in 90-second intervals for 15 minutes; example images are illustrated at 3 minutes (A), 7.5 minutes (B), and 15 minutes (C). The fluorescence intensities for CD61 (D) and fluorescent fibrinogen (E) were measured over time. Graphs illustrate the average  $\pm$  standard deviation for 3 different donors (N=3) and 21 individual clots (n=21).



$$\% \text{ Contraction} = 100 \left[ \frac{(x-y)}{x} \right]$$

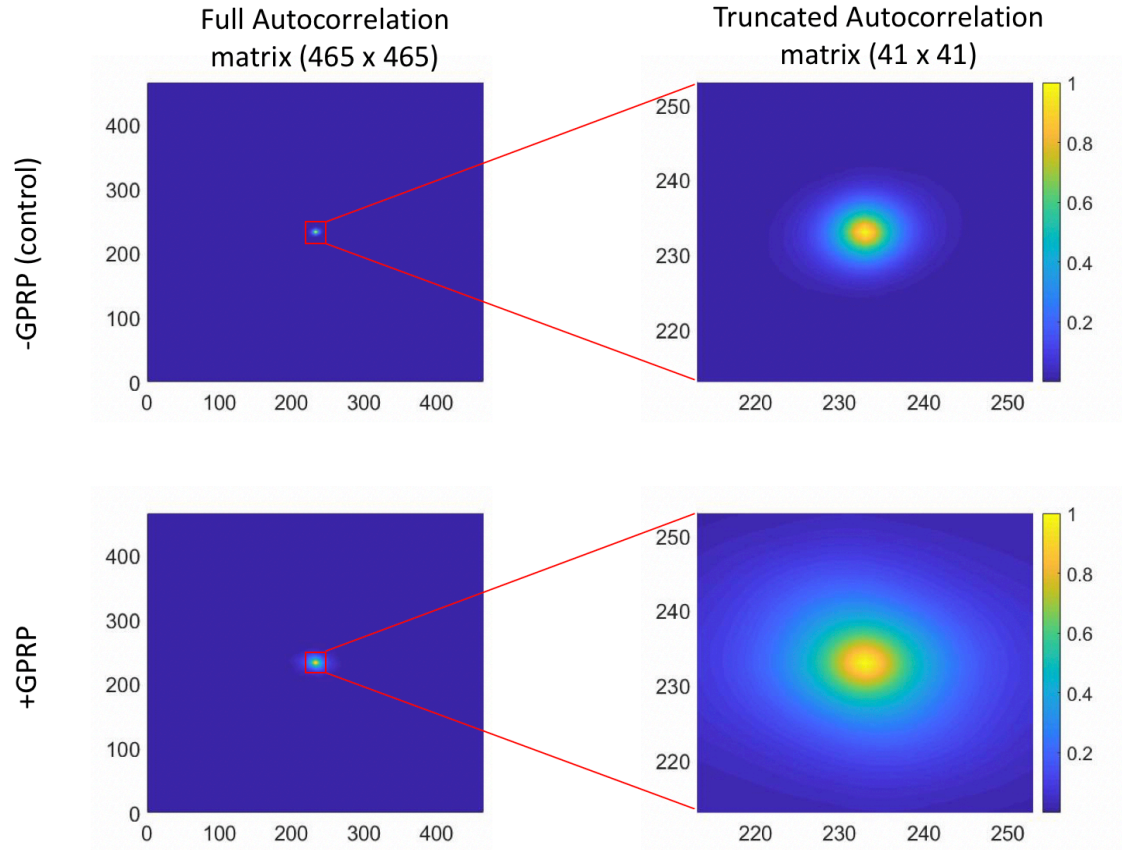
$$x = 211 \text{ } \mu\text{m}$$

$$y = 171 \text{ } \mu\text{m}$$

$$\% \text{ contraction} = 19.0\%$$

**Supplemental Figure S2-2. Illustration of example contraction measurements.**

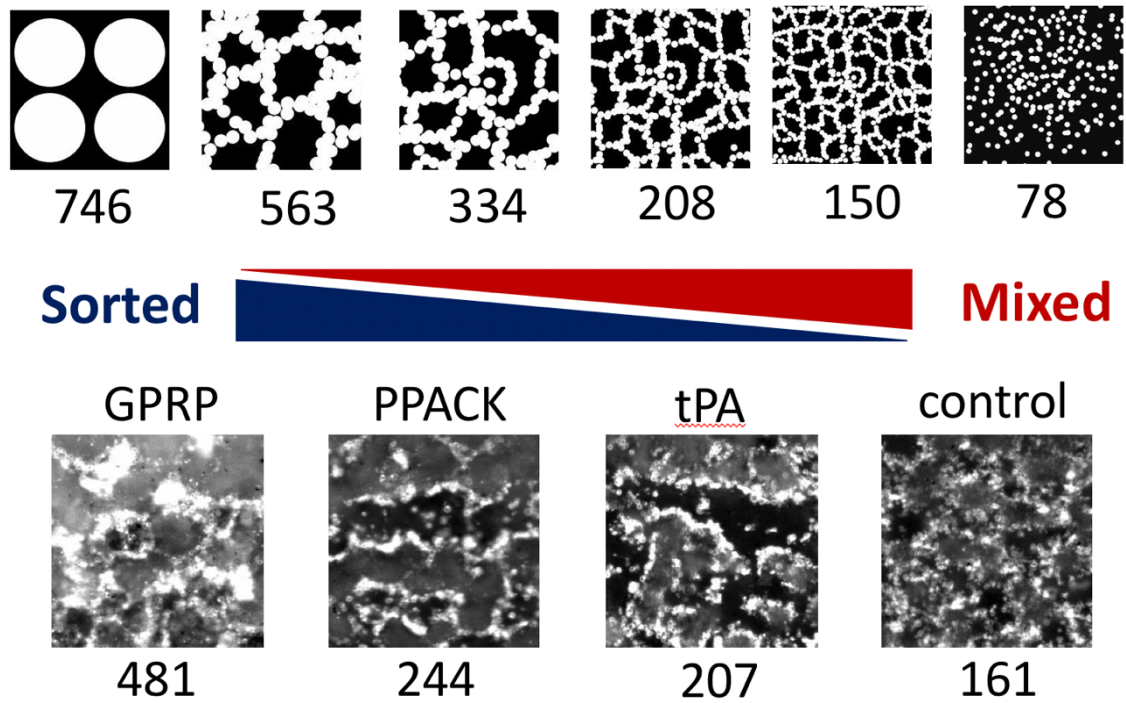
Contraction was measured as % change in clot length between 9- and 15-minute images of annexin V fluorescence.



**Supplemental Figure S2-3. Illustration of example full autocorrelation matrix and truncated autocorrelation matrix.**

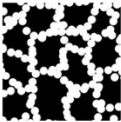
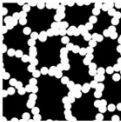
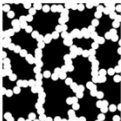
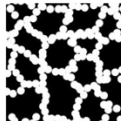
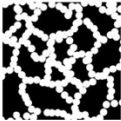
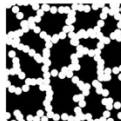


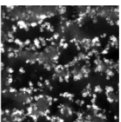
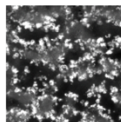
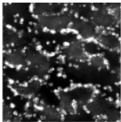
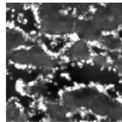
Autocorrelation matrices were calculated using “xcorr2” function in Matlab from 150 x 150  $\mu\text{m}$  clots (233 x 233 pixels). The autocorrelation matrix output was  $(2n-1) \times (2n-1)$  for an  $n \times n$  input image; in the case of a 233 x 233 pixel input image, the autocorrelation matrix dimensions were 465 x 465. The autocorrelation matrix was then truncated by 20 pixels from the center of the autocorrelation matrix (233, 233) in each direction, corresponding to a 41 x 41 truncated matrix. The summation of this matrix was the autocorrelation metric, corresponding to the degree to which an image correlates with itself.

## Autocorrelation Metric for Synthetic and Real clots



### Supplemental Figure S2-4. Illustration of example PS spatial sorting measurements.

PS spatial sorting was measured using an autocorrelation metric to evaluate the final annexin V FI of each clot. Synthetic and real examples illustrate that as images become less sorted and more mixed, the autocorrelation metric decreases. Images of clots used were 150  $\mu\text{m}$  x 150  $\mu\text{m}$  areas of the central portion of a clot.

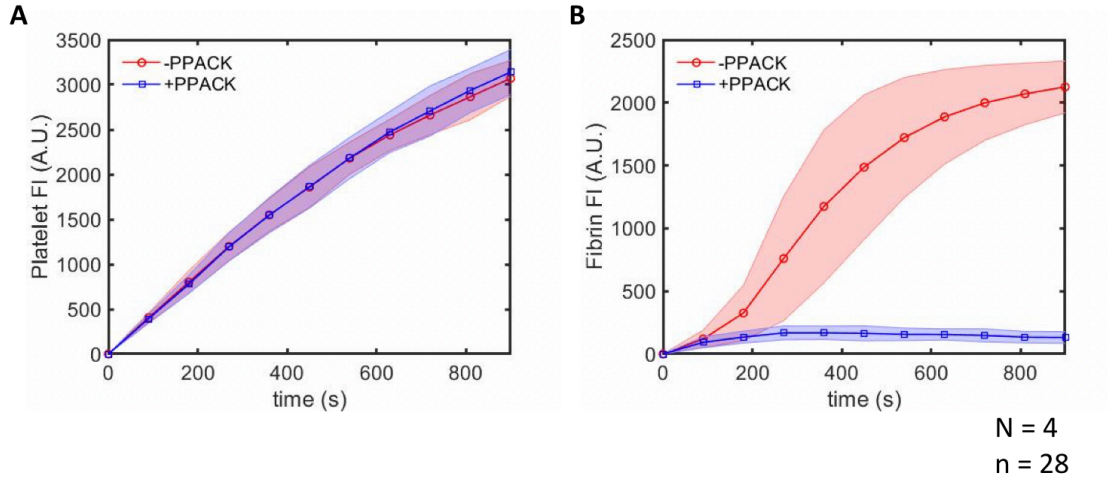
	Image 1	Image 2	Pearson Correlation
Same distribution			1
Very Similar distribution			0.80
Altered distribution			0.36
Random distribution			0.004
Control clot at 9 and 15 min			0.81
PPACK clot at 9 and 15 min			0.34

**Supplemental Figure S2-5. Illustration of example PS temporal sorting measurements.**

PS temporal sorting was measured using a Pearson correlation coefficient between 9- and 15-minute annexin V images within a clot. Synthetic and real examples illustrate that the similarity of distribution between the images correlates with the Pearson correlation coefficient. Images of clots used were 150  $\mu\text{m}$  x 150  $\mu\text{m}$  areas of the central portion of a clot.



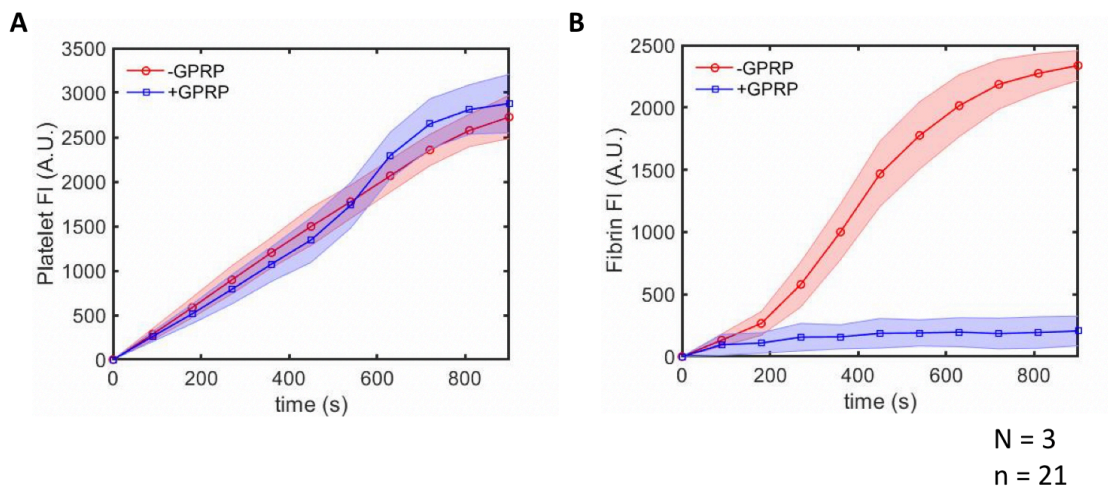
High CTI WB ( $\pm$  PPACK)  $\rightarrow$  collagen/TF ( $100 \text{ s}^{-1}$ ): Average fluorescence intensities



**Supplemental Figure S2-6. Average fluorescence intensities over time for high CTI WB  $\pm$  PPACK perfused over collagen/TF.**

Fluorescence intensities for CD61 (A) and fluorescent fibrinogen (B) over time. Graphs illustrate the average  $\pm$  standard deviation for 4 donors ( $N = 4$ ) and 28 individual clots ( $n = 28$ ).

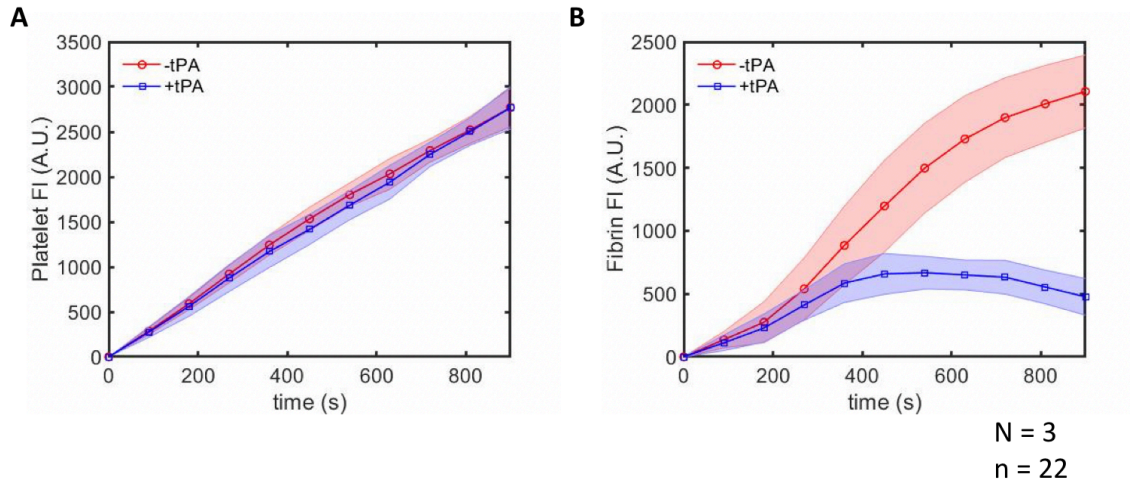
High CTI WB ( $\pm$  GPRP)  $\rightarrow$  collagen/TF ( $100 \text{ s}^{-1}$ ): Average fluorescence intensities



**Supplemental Figure S2-7. Average fluorescence intensities over time for high CTI WB  $\pm$  GPRP perfused over collagen/TF.**

Fluorescence intensities for CD61 (A) and fluorescent fibrinogen (B) over time. Graphs illustrate the average  $\pm$  standard deviation for 3 donors ( $N = 3$ ) and 21 individual clots ( $n = 21$ ).

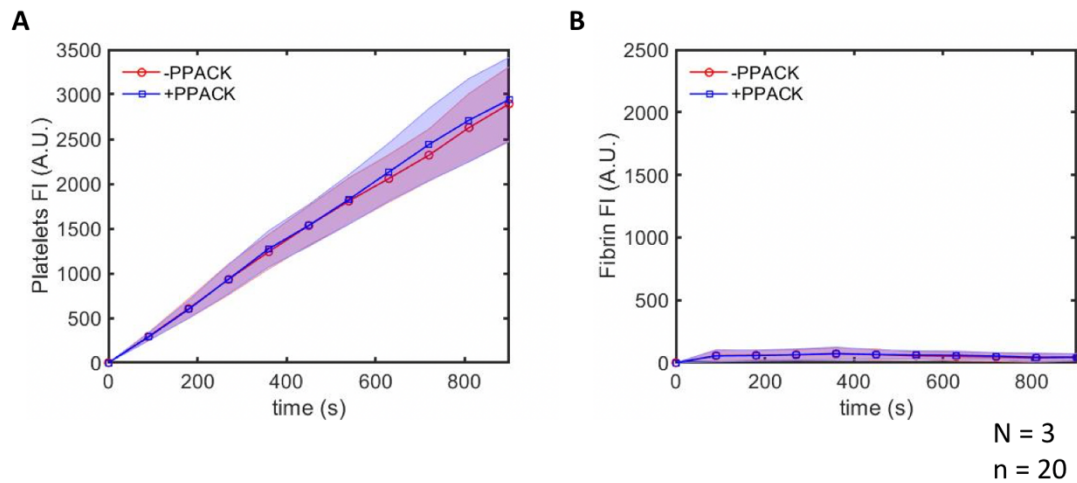
High CTI WB ( $\pm$  tPA)  $\rightarrow$  collagen/TF ( $100 \text{ s}^{-1}$ ): Average fluorescence intensities



**Supplemental Figure S2-8. Average fluorescence intensities over time for high CTI WB  $\pm$  tPA perfused over collagen/TF.**

Fluorescence intensities for CD61 (A) and fluorescent fibrinogen (B) over time. Graphs illustrate the average  $\pm$  standard deviation for 3 donors (N = 3) and 22 individual clots (n = 22).

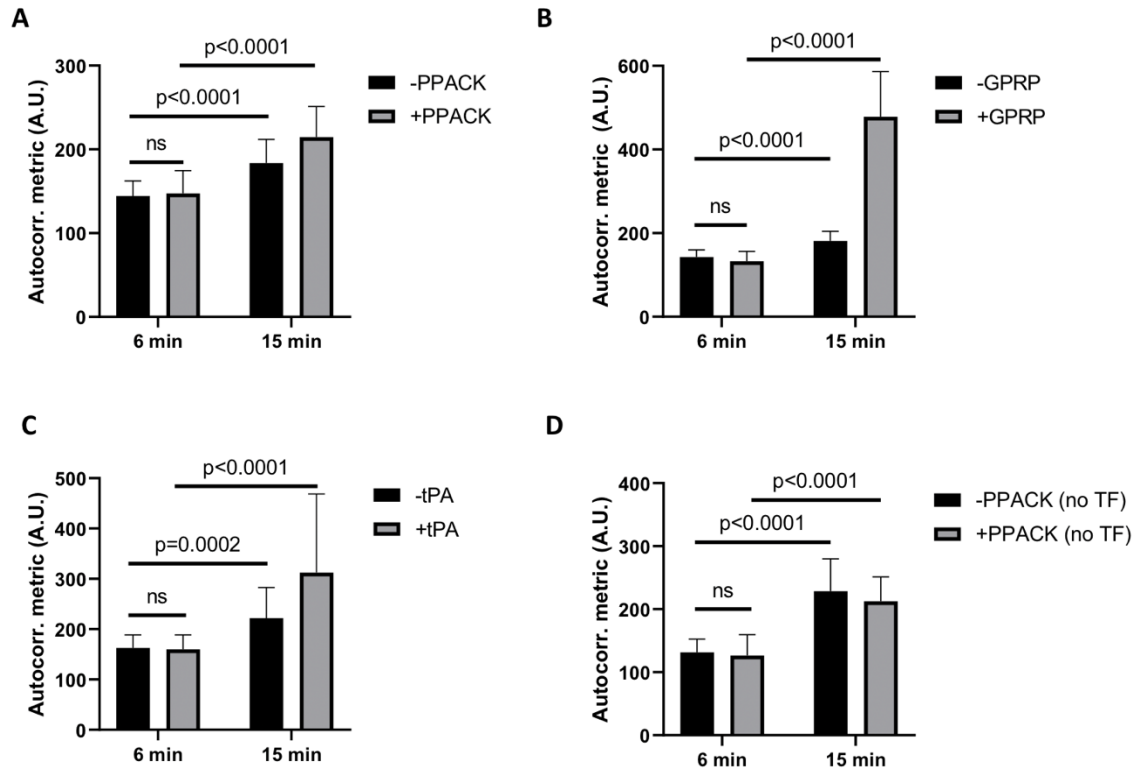
High CTI WB ( $\pm$  PPACK)  $\rightarrow$  collagen ( $100 \text{ s}^{-1}$ ): Average fluorescence intensities



**Supplemental Figure S2-9. Average fluorescence intensities over time for high CTI WB  $\pm$  PPACK perfused over collagen (no TF).**

Fluorescence intensities for CD61 (A) and fluorescent fibrinogen (B) over time. Graphs illustrate the average  $\pm$  standard deviation for 3 donors (N = 3) and 20 individual clots (n = 20).

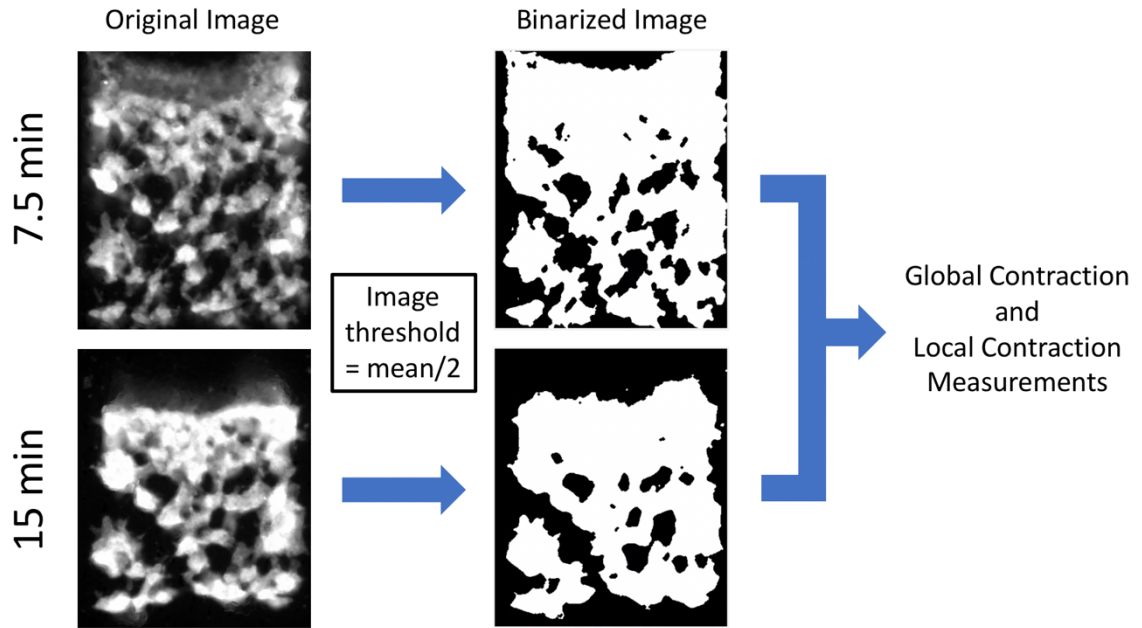




**Supplemental Figure S2-10. Autocorrelation metric at 6 and 15 minutes.**

Autocorrelation metric values were calculated and compared for 6- and 15-minute images for (A)  $\pm$ PPACK over collagen/TF, (B)  $\pm$ GPRP, (C)  $\pm$ tPA, and (D)  $\pm$ PPACK over collagen (no TF).

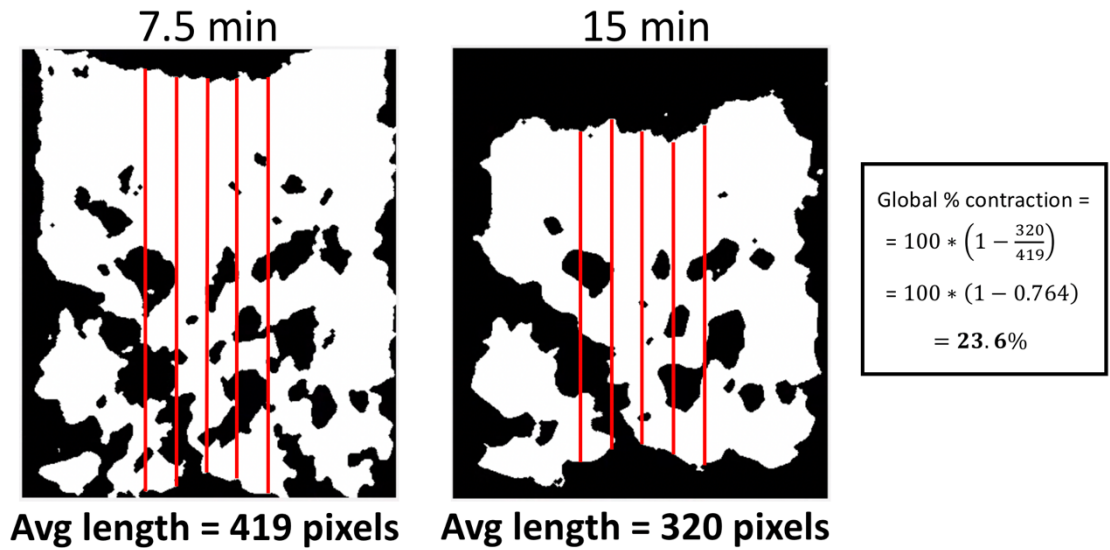
## Appendix B: Chapter 3



### Supplemental Figure S3-1. Explanation of image thresholding process.

Images (for both platelets and P-selectin fluorescence) were made binary in Matlab for contraction analysis. The threshold value for binary images was 1/2 of the mean fluorescence of each image. This threshold value was used consistently across all images. Once binarized, clots were analyzed for global and local contraction.

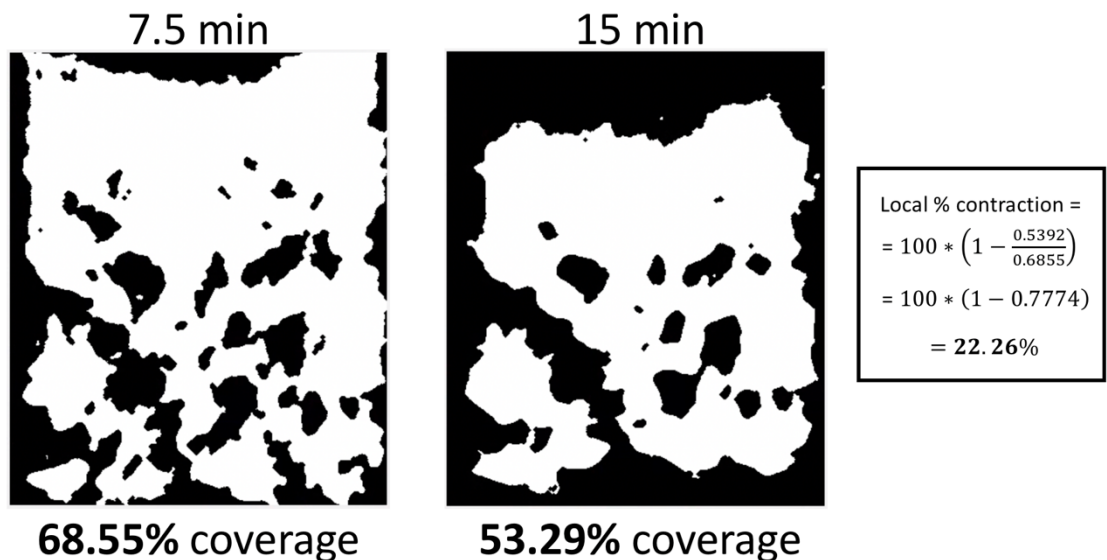
## Global Contraction Measurement



### Supplemental Figure S3-2. Example global contraction measurement.

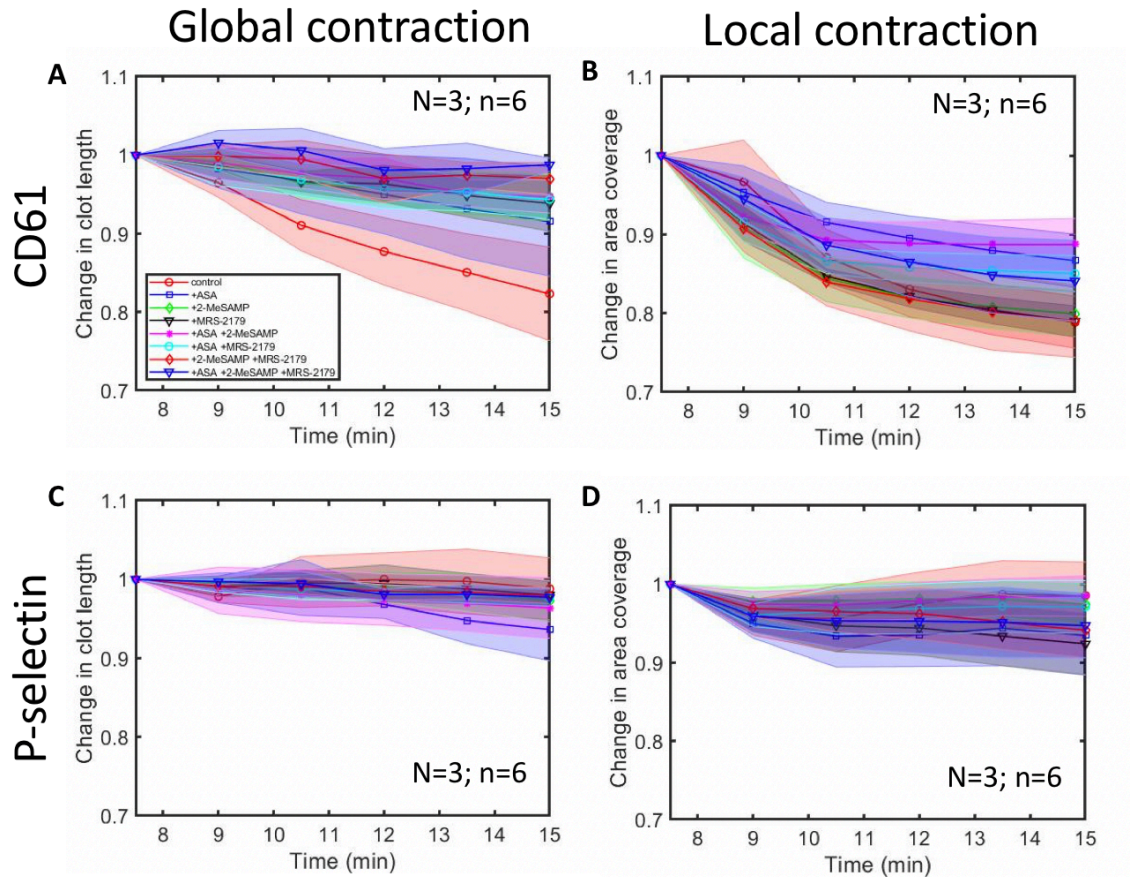
Once images were binary, measurements were made at 5 different points in the x direction of each clot: at the central pixel,  $\pm 25$  pixels, and  $\pm 50$  pixels. These measurements were then averaged and used to calculate the global % contraction for the clot.

## Local Contraction Measurement



### Supplemental Figure S3-3. Example local contraction measurement.

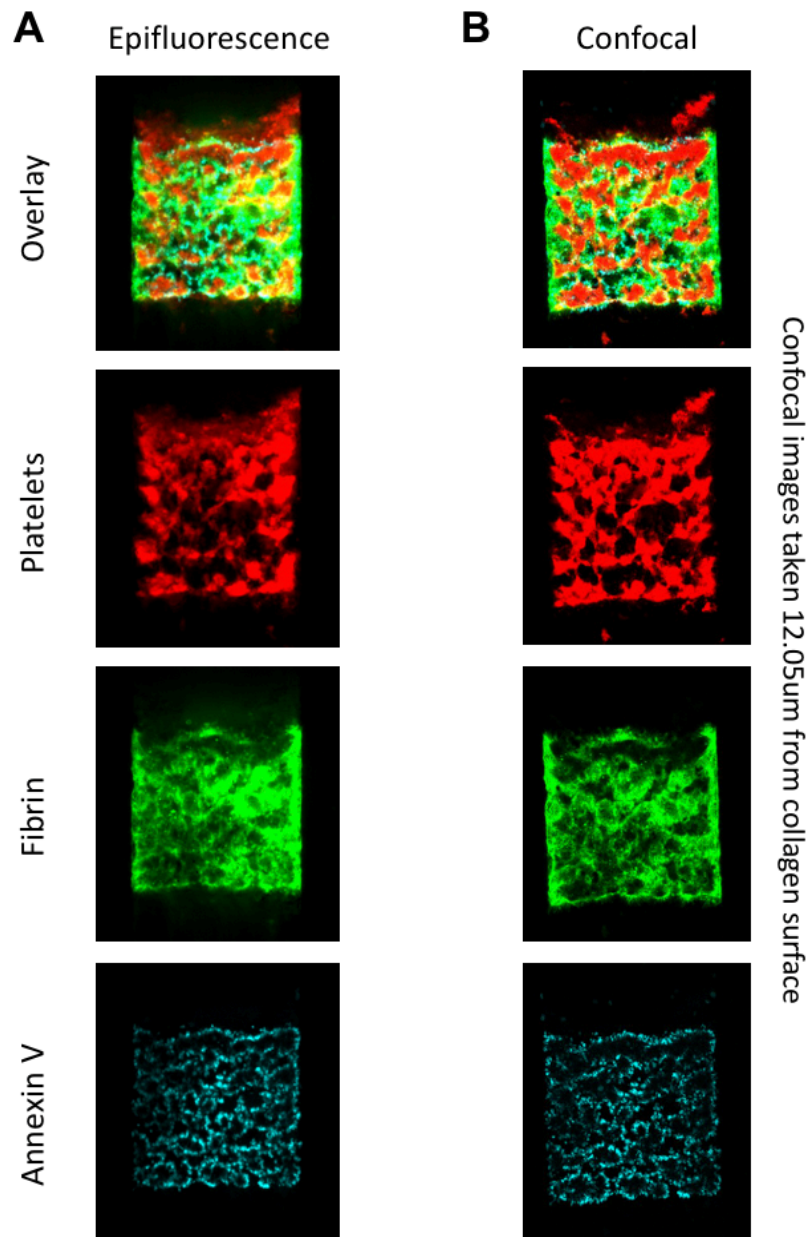
Once images were binary, the % of the clot area covered by platelets (white) was calculated in Matlab for each image of a clot (at 7.5 and 15 min). The % area coverage for each image was used to calculate the local % contraction for the clot.



**Supplemental Figure S3-4. Global and local aggregate contraction changes for CD61 and P-selectin over time.**

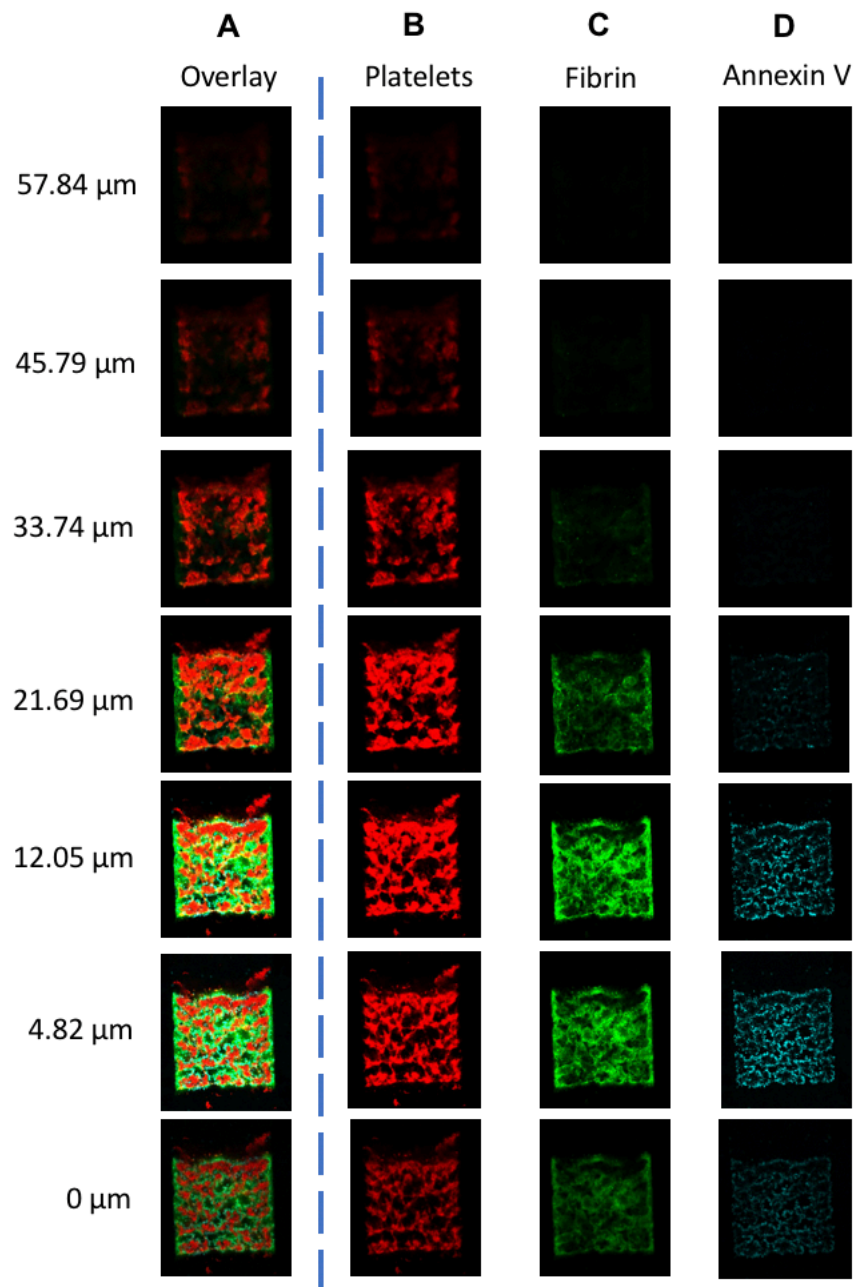
Starting at 7.5 min, global and local contraction was measured every 90s for CD61 and P-selectin images. The graphs correspond to the clot length or area coverage at different time points relative to 7.5 min. This was done for global CD61 contraction (A), local CD61 contraction (B), global P-selectin contraction (C), and local P-selectin contraction (D).

## Appendix C: Chapter 4



### Supplemental Figure S4-1. Comparison of Epifluorescence and Confocal Images.

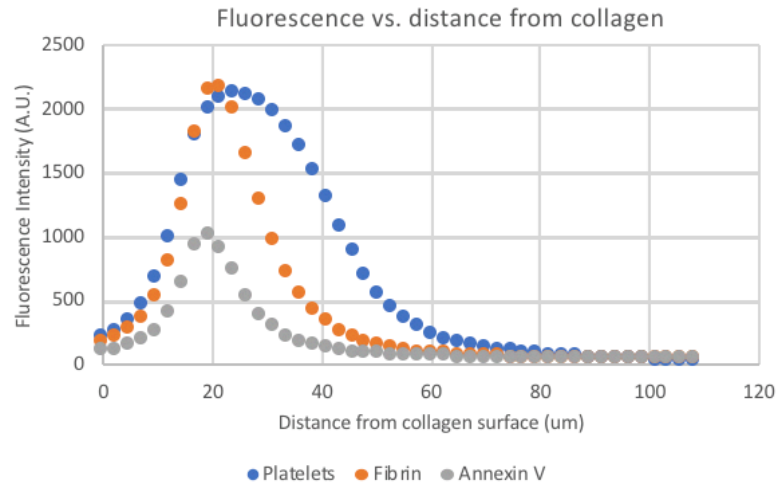
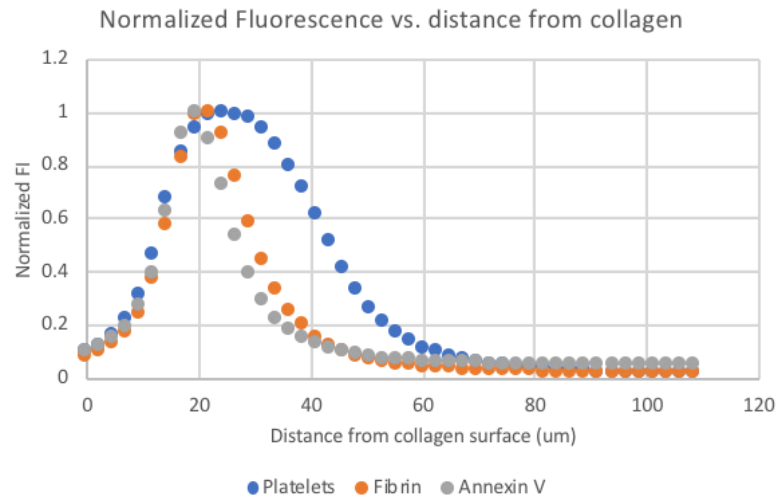
High CTI WB was perfused over collagen/TF for 7.5 min, with images taken using the epifluorescence microscope at 7.5 min (A). Then clots were fixed, as described in Methods, and taken to image using the confocal microscope (B). Representative confocal images are from 12.05  $\mu\text{m}$  above the collagen surface. Images include individual fluorophores for platelets, fibrin, and annexin V, as well as an overlay of all three.



**Supplemental Figure S4-2. Confocal images at different heights in the z-direction.**

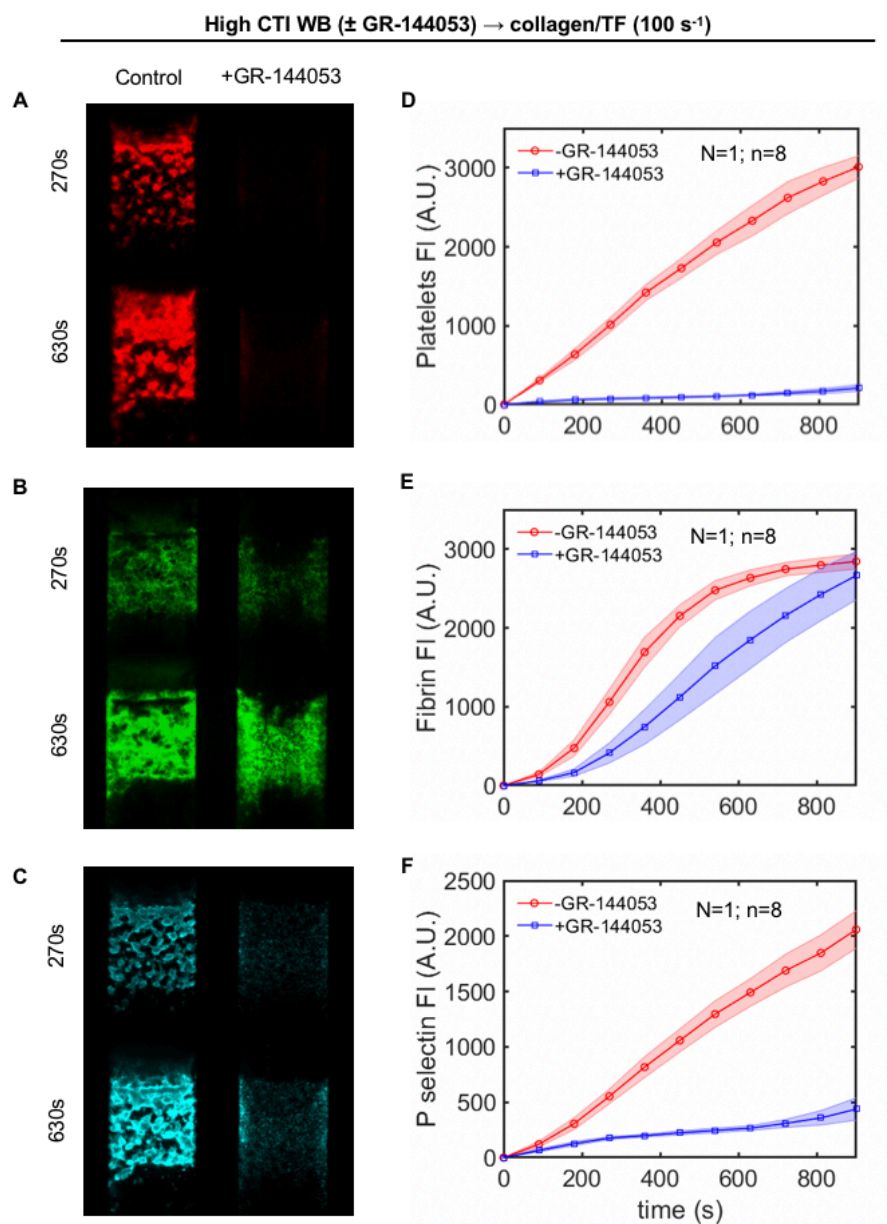
Images from the same clot in Supp. Fig. S4-1 were taken at different heights in the z-direction, starting at the glass surface (0  $\mu\text{m}$ ) up to 57.84  $\mu\text{m}$  above the glass surface. Images for overlay (A), platelets (B), fibrin (C), and annexin V (D) are included.



**A****B**

**Supplemental Figure S4-3. Quantitative analysis of confocal images at different heights in the z-direction.**

Images from the same clot in Supp. Fig. S4-2 were quantitatively analyzed for the fluorescence intensity for platelets (blue), fibrin (orange), and annexin V (grey) at different heights in the z-direction (A). Fluorescence values in each data set in (A) were divided by the respective maximum value in each individual data set to yield a normalized fluorescence intensity among the different fluorophore labels (B). (A.U.= arbitrary units)

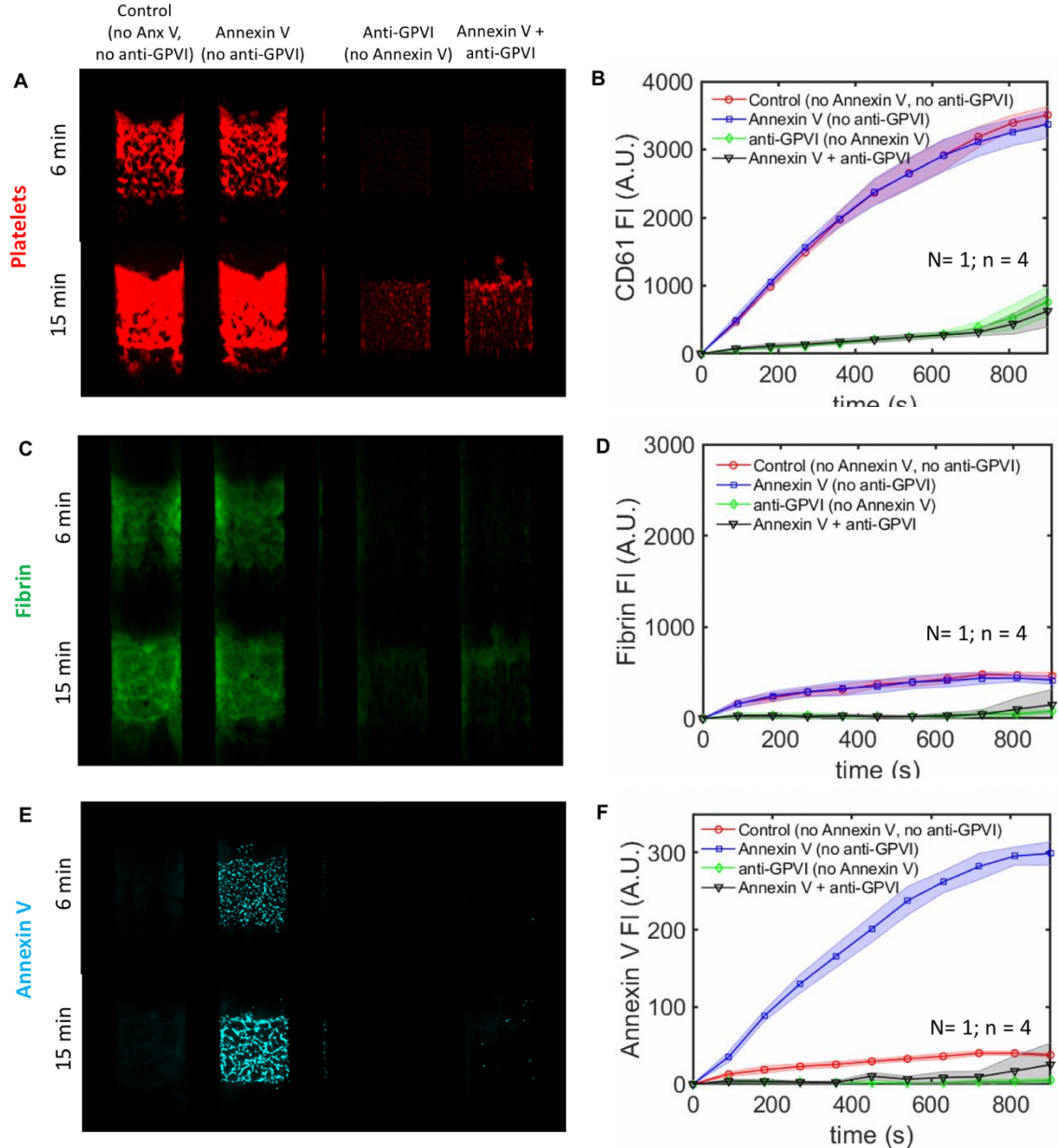


**Supplemental Figure S4-4. P-selectin staining of platelets treated with GR-144053.**

High CTI WB with or without GR-144053 was perfused over collagen/TF at  $100 \text{ s}^{-1}$  for 15 minutes. CD61, fluorescent fibrinogen, and P-selectin fluorophores were added to label platelets (A), fibrin (B), and alpha-granule release (C), respectively, with images taken at 270s and 630s. Fluorescence intensities for platelets (D), fibrin (E), and P-selectin (F) were measured throughout the course of the experiments. Representative data are from 1 individual donor ( $N = 1$ ) and 8 individual clots ( $n = 8$ ). (A.U. = arbitrary units)



# PPACK WB $\pm$ anti-GPVI $\pm$ Annexin V $\rightarrow$ collagen ( $100 \text{ s}^{-1}$ )



**Supplemental Figure S4-5. With thrombin inhibited, anti-GPVI strongly inhibits platelet deposition regardless of annexin V presence.**

PPACK-treated WB, with and without annexin V and anti-GPVI, was perfused over collagen at  $100 \text{ s}^{-1}$  with CD61, fluorescent fibrinogen, and annexin V fluorophores added for platelets (A), fibrin (C), and annexin V (E). Fluorophores were measured throughout the course of the experiment for platelet fluorescence (B), fibrin fluorescence (D), and annexin V fluorescence (F). Representative data are from 1 individual donor (N = 1) and 4 individual clots (n = 4). (A.U. = arbitrary units).

## BIBLIOGRAPHY

1. Tutwiler V, Litvinov RI, Lozhkin AP, Peshkova AD, Lebedeva T, Ataullakhanov FI, et al. Kinetics and mechanics of clot contraction are governed by the molecular and cellular composition of the blood. 2016;**127**:149–59.
2. Stalker TJ, Welsh JD, Tomaiuolo M, Wu J, Colace T V., Diamond SL, et al. A systems approach to hemostasis: 3. Thrombus consolidation regulates intrathrombus solute transport and local thrombin activity. *Blood*. 2014;**124**:1824–31.
3. Carr ME. Development of platelet contractile force as a research and clinical measure of platelet function. *Cell Biochem Biophys*. 2003;**38**:55–78.
4. Lam WA, Chaudhuri O, Crow A, Webster KD, Li T De, Kita A, et al. Mechanics and contraction dynamics of single platelets and implications for clot stiffening. *Nat Mater*. 2011;**10**:61–6.
5. Muthard RW, Diamond SL. Blood clots are rapidly assembled hemodynamic sensors: Flow arrest triggers intraluminal thrombus contraction. *Arterioscler Thromb Vasc Biol*. 2012;**32**:2938–45.
6. Leon C, Eckly A, Aleil B, Freund M, Ravanat C, Jourdain M, et al. Megakaryocyte-restricted MYH9 inactivation dramatically affects hemostasis while preserving platelet aggregation and secretion. *Blood*. 2007;**110**:3183–91.
7. Versteeg HH, Heemskerk JWM, Levi M, Reitsma PH. New Fundamentals in hemostasis. *Physiol Rev*. 2013;**93**:327–58.
8. Lentz BR. Exposure of platelet membrane phosphatidylserine regulates blood coagulation. *Prog Lipid Res*. 2003;**42**:423–38.
9. Suzuki J, Umeda M, Sims PJ, Nagata S. Calcium-dependent phospholipid scrambling by TMEM16F. *Nature*. 2010;**468**:834–40.
10. Baig AA, Haining EJ, Geuss E, Beck S, Swieringa F, Wanitchakool P, et al. TMEM16F-Mediated Platelet Membrane Phospholipid Scrambling Is Critical for Hemostasis and Thrombosis but not Thromboinflammation in Mice - Brief Report. *Arterioscler Thromb Vasc Biol*. 2016;**36**:2152–7.
11. Bevers EM. To the editor : Compound heterozygosity for 2 novel TMEM16F mutations in a patient with Scott syndrome. *Blood*. 2015;**117**:4399–401.
12. Emeis JJ, Jirouskova M, Muchitsch EM, Shet AS, Smyth SS, Johnson GJ. A guide to murine coagulation factor structure, function, assays, and genetic alterations. *J Thromb Haemost*. 2007;**5**:670–9.
13. Maloney SF, Brass LF, Diamond SL. P2Y<sub>12</sub> or P2Y<sub>1</sub> inhibitors reduce platelet

- deposition in a microfluidic model of thrombosis while apyrase lacks efficacy under flow conditions. *Integr Biol*. 2010;**2**:183–92.
14. Zhu S, Herbig BA, Li R, Colace T V., Muthard RW, Neeves KB, et al. In microfluidico: Recreating in vivo hemodynamics using miniaturized devices. *Biorheology*. 2015;**52**:303–18.
  15. Heemskerk JWM, Bevers EM, Lindhout T. Platelet Activation and Blood Coagulation. 2002;**88**:186–93.
  16. Stalker TJ, Traxler EA, Wu J, Wannemacher KM, Cermignano SL, Voronov R, et al. Hierarchical organization in the hemostatic response and its relationship to the platelet-signaling network. *Blood*. 2013;**121**:1875–85.
  17. Heemskerk JWM, Mattheij NJA, Cosemans JMEM. Platelet-based coagulation: Different populations, different functions. *J Thromb Haemost*. 2013;**11**:2–16.
  18. Briedé JJ, Heemskerk JWM, Hemker HC, Lindhout T. Heterogeneity in microparticle formation and exposure of anionic phospholipids at the plasma membrane of single adherent platelets. *Biochim Biophys Acta - Mol Cell Res*. 1999;**1451**:163–72.
  19. Pang A, Cui Y, Chen Y, Cheng N, Delaney MK, Gu M, et al. Shear-induced integrin signaling in platelet phosphatidylserine exposure, microvesicle release, and coagulation. *Blood*. 2018;**132**:533–43.
  20. Leventis PA, Grinstein S. The Distribution and Function of Phosphatidylserine in Cellular Membranes. *Annu Rev Biophys*. 2010;**39**:407–27.
  21. Agbani EO, Van Den Bosch MTJ, Brown E, Williams CM, Mattheij NJA, Cosemans JMEM, et al. Coordinated membrane ballooning and procoagulant spreading in human platelets. *Circulation*. 2015;**132**:1414–24.
  22. Berny MA, Munnix ICA, Auger JM, Schols SEM, Judith MEM, Panizzi P, et al. Spatial Distribution of factor Xa , thrombin , and fibrin(ogen) on thrombi at venous shear. *PLoS One*. 2010;**5**:e10415.
  23. Eckly A, Mangin PH, Obydennyi SI, Kotova YN, Gachet C, Nechipurenko DY, et al. Coagulation factors bound to procoagulant platelets concentrate in cap structures to promote clotting. *Blood*. 2016;**128**:1745–55.
  24. Liu J, Shen B, Zheng Y, Cho J, Du X, Stojanovic-Terpo A, et al. Agonist-induced platelet procoagulant activity requires shear and a Rac1-dependent signaling mechanism. *Blood*. 2014;**124**:1957–67.
  25. Munnix ICA, Cosemans JMEM, Auger JM, Heemskerk JWM. Platelet response heterogeneity in thrombus formation. *Thromb Haemost*. 2009;**102**:1149–56.

26. Cosemans JMEM, Iserbyt BF, Deckmyn H, Heemskerk JWM. Multiple ways to switch platelet integrins on and off. *J Thromb Haemost*. 2008;**6**:1253–61.
27. Munnix ICA, Kuijpers MJE, Auger J, Thomassen CMLGD, Panizzi P, van Zandvoort MAM, et al. Segregation of Platelet Aggregatory and Procoagulant Microdomains in Thrombus Formation. *Arterioscler Thromb Vasc Biol*. 2007;**27**:2484–90.
28. Nechipurenko DY, Receveur N, Yakimenko AO, Shepelyuk TO, Yakusheva AA, Kerimov RR, et al. Clot Contraction Drives the Translocation of Procoagulant Platelets to Thrombus Surface. *Arterioscler Thromb Vasc Biol*. 2019;**39**:37–47.
29. Chen Z, Lu J, Zhang C, Hsia I, Yu X, Marecki L, et al. Microclot array elastometry for integrated measurement of thrombus formation and clot biomechanics under fluid shear. *Nat Commun*. 2019;**10**:2051.
30. Samson AL, Alwis I, Maclean JAA, Priyananda P, Hawke B, Schoenwaelder SM, et al. Endogenous fibrinolysis facilitates clot retraction in vivo. *Blood*. 2017;**130**:2453–62.
31. Petersen N, Hddelius PL, Wiseman PW, Seger O. Quantitation of Membrane Receptor Distributions by Image Correlation Spectroscopy : Concept and Application. *Biophys J*. 1993;**65**:1135–46.
32. Nohe A, Petersen NO. Image Correlation Spectroscopy INTRODUCTION MATERIALS. *Sci STKE*. 2007;**2**:1–17.
33. Hagen N, Dereniak EL. Gaussian profile estimation in two dimensions. *Appl Opt*. 2008;**47**:6842–51.
34. Robertson C, George SC. Theory and practical recommendations for autocorrelation-based image correlation spectroscopy autocorrelation-based image correlation spectroscopy. *J Biomed Opt*. 2012;**17**:080801.
35. Mohapatra S, Weisshaar JC. Modified Pearson correlation coefficient for two-color imaging in spherocylindrical cells. *BMC Bioinformatics*. 2018;**19**:428.
36. Manders EMM, Stap J, Brakenhoff GJ, Driel RVAN, Aten JA. Dynamics of three-dimensional replication patterns during the S-phase, analysed by double labelling of DNA and confocal microscopy. *J Cell Sci*. 1992;**103**:857–62.
37. Vyavahare Scott, N., Hanson, S.R., Kohn, J. N. In vitro and in vivo evaluation of the site-specific administration of the thrombin inhibitor PPACK. *J Control Release*. 1993;**27**:165–73.
38. Yamazumi K, Doolittle RF. The synthetic peptide Gly-Pro-Arg-Pro-amide limits the plasmic digestion of fibrinogen in the same fashion as calcium ion. *Protein Sci*. 1992;**1**:1719–20.

39. Lance MD, Lionikiene AS, Heemskerk JWM, van der Meijden PEJ, Whyte CS, Mastenbroek TG, et al. Plasminogen associates with phosphatidylserine-exposing platelets and contributes to thrombus lysis under flow. *Blood*. 2015;**125**:2568–78.
40. Tutwiler V, Litvinov RI, Lozhkin AP, Peshkova AD, Lebedeva T, Ataullakhanov FI, et al. Kinetics and mechanics of clot contraction are governed by the molecular and cellular composition of the blood. *Blood*. 2016;**127**:149–59.
41. Tutwiler V, Wang H, Litvinov RI, Weisel JW, Shenoy VB. Interplay of Platelet Contractility and Elasticity of Fibrin / Erythrocytes in Blood Clot Retraction. *Biophysj*. 2017;**112**:714–23.
42. Aleman MM, Byrnes JR, Wang J-G, Tran R, Lam WA, Paola J Di, et al. Factor XIII activity mediates red blood cell retention in venous thrombi. *J Clin Invest*. 2014;**124**:3590–600.
43. Byrnes JR, Wang Y, Hansen CE, Ahn B, Mooberry MJ, Clark MA, et al. Factor XIIIa-dependent retention of red blood cells in clots is mediated by fibrin  $\alpha$ -chain crosslinking. *Blood*. 2015;**126**:1940–8.
44. Geffen JP Van, Swieringa F, Heemskerk JWM. Platelets and coagulation in thrombus formation : aberrations in the Scott syndrome. *Thromb Res*. 2016;**141**:S12–6.
45. Zhu S, Lu Y, Sinno T, Diamond SL. Dynamics of thrombin generation and flux from clots during whole human blood flow over collagen/tissue factor surfaces. *J Biol Chem*. 2016;**291**:23027–35.
46. Yu X, Diamond SL. Fibrin Modulates Shear-Induced NETosis in Sterile Occlusive Thrombi Formed under Haemodynamic Flow. *Thromb Haemost*. 2019;**119**:586–93.
47. Zhu S, Chen J, Diamond SL. Establishing the transient mass balance of thrombosis: From tissue factor to thrombin to fibrin under venous flow. *Arterioscler Thromb Vasc Biol*. 2018;**38**:1528–36.
48. Kim O V., Litvinov RI, Alber MS, Weisel JW. Quantitative structural mechanobiology of platelet-driven blood clot contraction. *Nat Commun*. 2017;**8**:1–10.
49. Ting LH, Feghhi S, Taparia N, Smith AO, Karchin A, Lim E, et al. Contractile forces in platelet aggregates under microfluidic shear gradients reflect platelet inhibition and bleeding risk. *Nat Commun*. 2019;**10**:1–10.
50. Cines DB, Lebedeva T, Nagaswami C, Hayes V, Massefski W, Litvinov RI, et al. Clot contraction: Compression of erythrocytes into tightly packed polyhedra and redistribution of platelets and fibrin. *Blood*. 2014;**123**:1596–603.

51. Tutwiler V, Mukhitov AR, Peshkova AD, Le Minh G, Khismatullin RR, Vicksman J, et al. Shape changes of erythrocytes during blood clot contraction and the structure of polyhedrocytes. *Sci Rep*. 2018;**8**:1–14.
52. Trigani KT, Diamond SL. Intrathrombus Fibrin Attenuates Spatial Sorting of Phosphatidylserine Exposing Platelets during Clotting under Flow. *Thromb Haemost*. 2021;**121**:46–57.
53. Peshkova A, Malyasyov D, Bredikhin R, Le Minh G, Andrianova I, Tutwiler V, et al. Reduced Contraction of Blood Clots in Venous Thromboembolism Is a Potential Thrombogenic and Embologenic Mechanism. *TH Open*. 2018;**02**:e104–15.
54. Evtugina NG, Peshkova AD, Pichugin AA, Weisel JW, Litvinov RI. Impaired contraction of blood clots precedes and predicts postoperative venous thromboembolism. *Sci Rep*. 2020;**10**:1–11.
55. Tutwiler V, Peshkova AD, Andrianova IA, Khasanova DR, Weisel JW, Litvinov RI. Contraction of blood clots is impaired in acute ischemic stroke. *Arterioscler Thromb Vasc Biol*. 2017;**37**:271–9.
56. Calaminus SDJ, Thomas S, McCarty OJT, Machesky LM, Watson SP. Identification of a novel, actin-rich structure, the actin nodule, in the early stages of platelet spreading. *J Thromb Haemost*. 2008;**6**:1944–52.
57. Ono A, Westein E, Hsiao S, Nesbitt WS, Hamilton JR, Schoenwaelder SM, et al. Identification of a fibrin-independent platelet contractile mechanism regulating primary hemostasis and thrombus growth. *Blood*. 2008;**112**:90–9.
58. Cohen I, De Vries A. Platelet contractile regulation in an isometric system. *Nature*. 1973;**246**:36–7.
59. Jen CJ, McIntire L V. The structural properties and contractile forces of a clot. *Cell Motil*. 1982;**2**:445–55.
60. Carr ME, Zekert SL. Measurement of platelet-mediated force development during plasma clot formation. *Am J Med Sci*. 1991;**302**:13–8.
61. Jackson SP. The growing complexity of platelet aggregation. *Blood*. 2007;**109**:5087–95.
62. Maxwell MJ, Westein E, Nesbitt WS, Giuliano S, Dopheide SM, Jackson SP. Identification of a 2-stage platelet aggregation process mediating shear-dependent thrombus formation. *Blood*. 2007;**109**:566–76.
63. Sakariassen KS, Orning L, Turitto VT. The impact of blood shear rate on arterial thrombus formation. *Futur Sci OA*. 2015;**1**:4.

64. Zhu S, Travers RJ, Morrissey JH, Diamond SL. FXIa and platelet polyphosphate as therapeutic targets during human blood clotting on collagen/tissue factor surfaces under flow. *Blood*. 2015;**126**:1494–502.
65. Welsh JD, Stalker TJ, Voronov R, Muthard RW, Tomaiuolo M, Diamond SL, et al. A systems approach to hemostasis: 1. The interdependence of thrombus architecture and agonist movements in the gaps between platelets. *Blood*. 2014;**124**:1808–15.
66. Peshkova AD, Le Minh G, Tutwiler V, Andrianova IA, Weisel JW, Litvinov RI. Activated Monocytes Enhance Platelet-Driven Contraction of Blood Clots via Tissue Factor Expression. *Sci Rep*. 2017;**7**:1–9.
67. Khismatullin RR, Nagaswami C, Shakirova AZ, Vrtková A, Procházka V, Gumulec J, et al. Quantitative Morphology of Cerebral Thrombi Related to Intravital Contraction and Clinical Features of Ischemic Stroke. *Stroke*. 2020;**51**:3640–50.
68. Maly M, Reidel T, Stikarova J, Suttner J, Kotlin R, Hajsl M, et al. Incorporation of Fibrin, Platelets, and Red Blood Cells into a Coronary Thrombus in Time and Space. *Thromb Haemost*. 2021;
69. Tutwiler V, Litvinov RI, Protopopova A, Nagaswami C, Villa C, Woods E, et al. Pathologically stiff erythrocytes impede contraction of blood clots. *J Thromb Haemost*. 2021;**19**:1990–2001.
70. Litvinov RI, Peshkova AD, Le Minh G, Khaertdinov NN, Evtugina NG, Sitdikova GF, et al. Effects of hyperhomocysteinemia on the platelet-driven contraction of blood clots. *Metabolites*. 2021;**11**:354.
71. Le Minh G, Peshkova AD, Andrianova IA, Sibgatullin TB, Maksudova AN, Weisel JW, et al. Impaired contraction of blood clots as a novel prothrombotic mechanism in systemic lupus erythematosus. *Clin Sci*. 2018;**132**:243–254.
72. Alshehri OM, Hughes CE, Montague S, Watson SK, Frampton J, Bender M, et al. Fibrin activates GPVI in human and mouse platelets. *Blood*. 2015;**126**:1601–8.
73. Lee MY, Verni CC, Herbig BA, Diamond SL. Soluble fibrin causes an acquired platelet glycoprotein VI signaling defect: implications for coagulopathy. *J Thromb Haemost*. 2017;**15**:2396–407.
74. Nieswandt B, Schulte V, Bergmeier W, Mokhtari-Nejad R, Rackebrandt K, Cazenave JP, et al. Long-term antithrombotic protection by in vivo depletion of platelet glycoprotein VI in mice. *J Exp Med*. 2001;**193**:459–69.
75. Schuhmann MK, Kraft P, Bieber M, Kollikowski AM, Schulze H, Nieswandt B, et al. Targeting platelet GPVI plus rt-PA administration but not  $\alpha 2\beta 1$ -mediated collagen binding protects against ischemic brain damage in mice. *Int J Mol Sci*.

2019;**20**:1–7.

76. Zhang D, Ebrahim M, Adler K, Blanchet X, Jamasbi J, Megens RTA, et al. Glycoprotein VI is not a Functional Platelet Receptor for Fibrin Formed in Plasma or Blood. *Thromb Haemost.* 2020;**120**:977–93.
77. Rayes J, Watson SP, Nieswandt B. Functional significance of the platelet immune receptors GPVI and CLEC-2. *J Clin Invest.* 2019;**129**:12–23.
78. Onselaer M, Hardy AT, Wilson C, Sanchez X, Babar AK, Miller JLC, et al. Fibrin and D-dimer bind to monomeric GPVI. *Blood Adv.* 2017;**1**:1495–504.
79. Massberg S, Gawaz M, Grüner S, Schulte V, Konrad I, Zohlnhöfer D, et al. A crucial role of glycoprotein VI for platelet recruitment to the injured arterial wall in vivo. *J Exp Med.* 2003;**197**:41–9.
80. Ahmed MU, Kaneva V, Loyau S, Nechipurenko D, Receveur N, Le Bris M, et al. Pharmacological Blockade of GPVI Promotes Thrombus Disaggregation in the Absence of Thrombin. *Arterioscler Thromb Vasc Biol.* 2020;**40**:2127–42.
81. Munnix ICA, Strehl A, Kuijpers MJE, Auger JM, Van Der Meijden PEJ, Van Zandvoort MAM, et al. The glycoprotein VI-phospholipase Cy2 signaling pathway controls thrombus formation induced by collagen and tissue factor in vitro and in vivo. *Arterioscler Thromb Vasc Biol.* 2005;**25**:2673–8.
82. Van Der Meijden PEJ, Munnix ICA, Auger JM, Govers-Riemslog JWP, Cosemans JMEM, Kuijpers MJE, et al. Dual role of collagen in factor XII-dependent thrombus formation. *Blood.* 2009;**114**:881–90.
83. Mangin PH, Onselaer MB, Receveur N, Le Lay N, Hardy AT, Wilson C, et al. Immobilized fibrinogen activates human platelets through glycoprotein VI. *Haematologica.* 2018;**103**:898–907.
84. Lehmann M, Schoeman RM, Krohl PJ, Wallbank AM, Samaniuk JR, Jandrot-Perrus M, et al. Platelets drive thrombus propagation in a hematocrit and glycoprotein VI-dependent manner in an in vitro venous thrombosis model. *Arterioscler Thromb Vasc Biol.* 2018;**38**:1052–62.
85. Reininger AJ, Bernlochner I, Penz SM, Ravanat C, Smethurst P, Farndale RW, et al. A 2-Step Mechanism of Arterial Thrombus Formation Induced by Human Atherosclerotic Plaques. *J Am Coll Cardiol.* 2010;**55**:1147–58.
86. Clarke AS, Rousseau E, Wang K, Kim JY, Murray BP, Bannister R, et al. Effects of GS-9876, a novel spleen tyrosine kinase inhibitor, on platelet function and systemic hemostasis. *Thromb Res.* 2018;**170**:109–18.
87. Zhang Y, Diamond SL. Src family kinases inhibition by dasatinib blocks initial and subsequent platelet deposition on collagen under flow, but lacks efficacy with



- thrombin generation. *Thromb Res.* 2020;**192**:141–51.
88. Dubois C, Panicot-Dubois L, Merrill-Skoloff G, Furie B, Furie BC. Glycoprotein VI-dependent and -independent pathways of thrombus formation in vivo. *Blood.* 2006;**107**:3902–6.
  89. Mangin P, Yap CL, Nonne C, Sturgeon SA, Goncalves I, Yuan Y, et al. Thrombin overcomes the thrombosis defect associated with platelet GPVI/FcR $\gamma$  deficiency. *Blood.* 2006;**107**:4346–53.
  90. Nagy M, Perrella G, Dalby A, Becerra MF, Quintanilla LG, Pike JA, et al. Flow studies on human GPVI-deficient blood under coagulating and noncoagulating conditions. *Blood Adv.* 2020;**4**:2953–61.
  91. Spalton JC, Mori J, Pollitt AY, Hughes CE, Eble JA, Watson SP. The novel Syk inhibitor R406 reveals mechanistic differences in the initiation of GPVI and CLEC-2 signaling in platelets. *J Thromb Haemost.* 2009;**7**:1192–9.
  92. Van Eeuwijk JMM, Stegner D, Lamb DJ, Kraft P, Beck S, Thielmann I, et al. The novel oral Syk inhibitor, B11002494, protects mice from arterial thrombosis and thromboinflammatory brain infarction. *Arterioscler Thromb Vasc Biol.* 2016;**36**:1247–53.
  93. Dobie G, Kuriri FA, Omar MMA, Alanazi F, Gazwani AM, Tang CPS, et al. Ibrutinib, but not zanubrutinib, induces platelet receptor shedding of GPIIb-IX-V complex and integrin  $\alpha$ IIb $\beta$ 3 in mice and humans. *Blood Adv.* 2019;**3**:4298–311.
  94. Senis YA, Mazharian A, Mori J. Src family kinases: At the forefront of platelet activation. *Blood.* 2014;**124**:2013–24.
  95. Vielreicher M, Harms G, Butt E, Walter U, Obergfell A. Dynamic interaction between Src and C-terminal Src kinase in integrin  $\alpha$ IIb $\beta$ 3-mediated signaling to the cytoskeleton. *J Biol Chem.* 2007;**282**:33623–31.
  96. Perrella G, Nagy M, Watson SP, Heemskerk JWM. Platelet gpvi (glycoprotein vi) and thrombotic complications in the venous system. *Arterioscler Thromb Vasc Biol.* 2021;**41**:2681–92.
  97. DeCortin ME, Brass LF, Diamond SL. Core and shell platelets of a thrombus: A new microfluidic assay to study mechanics and biochemistry. *Res Pract Thromb Haemost.* 2020;**4**:1158–66.
  98. Colace T V., Diamond SL. Direct observation of von Willebrand factor elongation and fiber formation on collagen during acute whole blood exposure to pathological flow. *Arterioscler Thromb Vasc Biol.* 2013;**33**:105–13.
  99. Boilard E, Ducheze AC, Brisson A. The diversity of platelet microparticles. *Curr Opin Hematol.* 2015;**22**:437–44.

100. Reutelingsperger CPM, Van Heerde WL. Annexin V, the regulator of phosphatidylserine-catalyzed inflammation and coagulation during apoptosis. *Cell Mol Life Sci.* 1997;**53**:527–32.
101. Stuart MC, Bevers EM, Comfurius P, Zwaal RF, Reutelingsperger CP, Frederik PM. Ultrastructural detection of surface exposed phosphatidylserine on activated blood platelets. *Thromb Haemost.* 1995;**74**:1145–51.
102. Majumder R, Weinreb G, Lentz BR. Efficient thrombin generation requires molecular phosphatidylserine, not a membrane surface. *Biochemistry.* 2005;**44**:16998–7006.
103. Straight AF, Cheung A, Limouze J, Chen I, Nick WJ, Sellers JR, et al. Dissecting Temporal and Spatial Control of Cytokinesis with a Myosin II Inhibitor. *Science.* 2003;**299**:1743–7.
104. Kovács M, Tóth J, Hetényi C, Málnási-Csizmadia A, Seller JR. Mechanism of blebbistatin inhibition of myosin II. *J Biol Chem.* 2004;**279**:35557–63.